Thermal Analysis of Unglazed Transpired Solar Collectors

by

Hani Abulkhair

A thesis
presented to University of Waterloo
in fulfillment of the
thesis requirement for the degree of
Master of Applied Science
in
Mechanical Engineering

Waterloo, Ontario, Canada, 2011

I hereby declare that I am the sole author of this thesis. This is a true copy of the thesis, including any required final revisions, as accepted by my examiners.

I understand that my thesis may be made electronically available to the public.

Abstract

Unglazed transpired solar collectors (UTSCs) preheat makeup ventilation air for buildings, thereby reducing energy used for heating. The performance of the UTSC is dependent on the heat loss from the absorber plate, which is strongly affected by the wind speed. To date, correlations to determine UTSC heat loss are limited to flat or sinusoidal plate corrugations. In reality, trapezoidal corrugations have been added to UTSCs to provide them with structural stiffness. These corrugations prevent the attachment of the flow to the absorber plate and cause flow separation which increases the heat loss.

In this study, a numerical simulation of a UTSC with trapezoidal shape corrugation has been performed to investigate the heat loss in the developing region due to wind on the UTSCs. It has been found that heat loss from new configuration is up to three times greater than the heat loss from a perforated flat absorber plate. A correlation of heat loss due to the wind speed and suction velocity was developed.

This study also includes an evaluation of the effectiveness in the asymptotic region. In this case, wind speed had no effect. A correlation was derived in terms of suction velocity.

Acknowledgments

"Bear in mind that the wonderful things that you learn in your school are the work of many generations, produced by enthusiastic effort and infinite labour in every country in the world. All this is put into your hands as your inheritance in order that you may receive it, honor it, add to it, anode day hand it on to your children. Thus, do we mortals achieve immortality in the permanent things we create in the common." Albert Einstein, 1934.

This thesis could not have been completed without the effort and the help of some people who I am grateful to. Therefore, I would like to take the opportunity to express my gratitude to those who have had a direct influence in helping me finish this study.

First, I would like to thank my thesis supervisor Dr. Collins for his effort and time. The help I received from him was really helpful, valuable, and appreciated. I would like to thank him that he has been very generous of his time throughout the different stages of the research.

Second, I would like to acknowledge my friend Dr. Abu-Ramadan for his help in building my componential model. I would like to thank him for assistance, time and advices.

Finally, I would like to thank my wife Ghayda for her motivation and emotional support. Because of her, I found the encouragement to complete this work.

Table of Contents

List of Tables

List of Figures

Nomenclature

A	Amplitude, m
A	Area, m^2
C_p	Specific heat of air, J/kgK
D	Diameter or hydraulic diameter of the perforation, m
F	View factor, *dim*
g	Gravity acceleration, m/s^2
h	Heat transfer coefficient, W/m^2K
k	Thermal conductivity of air, W/mK
L	Length, m
L_e	Heat Loss starting length, m
L_s	Velocity starting length, m
Nu	Nusselt number, *dim*
Nu_{att}	Nusselt number for attached flow, *dim*
Nu_{flat}	Nusselt number over a flat plate with suction, *dim*
Nu_{sep}	Nusselt number for separated flow, *dim*
Nu_D	Nusselt number based on hydraulic diameter, *dim*
P	Pitch, *m*
Pr	Prandtl number of air, *dim*
q	Heat flux, W
q'	Heat flux per unit width, $/mW$
$q^{"}$	Solar heat flux, W/m^2
Re	Reynolds number, *dim*
Re_c	Critical Reynolds number, *dim*
Re_D	Reynolds number based on hydraulic diameter, *dim*
Re_s	Suction parameter, *dim*
t	Thickness, *m*
T	Temperature, *K*
u	Velocity in x-direction, m/s
U	Heat transfer coefficient, W/m^2K
U	Velocity, m/s
U_∞	Wind velocity, m/s
v	Velocity in y-direction, m/s
V_o	Suction velocity, m/s
w	Velocity in z-direction, m/s
W	Width of the test plate
x	x-direction, m
y	y-direction, m
z	z-direction, m

Greek Characters

α	Thermal diffusivity of air, m^2/s
α_p	Absorbtivity of the plate, *dim*
β	Inclination angle (from horizontal), *deg*
β	Thermal expansion coefficient, *1/K*
δ	Boundary layer thickness, m
Δ	Difference, m
ε	Emissivity, *dim*
ε	Effectiveness, *dim*
ν	Kinematic viscosity of air, m^2/s
μ	Dynamic viscosity of air, kg/ms
ρ	Density of air, kg/m^3
σ	Porosity ratio, *dim*
σ_{SB}	Stefan Boltzmann constant, $5.67 \times 10^{-8}\ W/m^2K^4$

Subscripts

abs	Absorber
att	Attached flow
b	Back
c	Critical
$conv$	Convective
dev	Developing region
e	Equivalent
f	Front
flat	Flat
grd	Ground
h	Hole
in	In plenum
mid	After hole
nat	Natural convection
o	Suction
out	Outlet
p	Plate
rad	Radiative
s	Starting
sep	Separated flow
sky	Sky
∞	Free stream

Chapter 1

Introduction

1.1 Energy and Environmental Concerns

The majority of global energy requirements are met through the combustion of fossil fuels. For space and water heating, people burn a variety of fuels such as natural gas, propane, fuel oil, coal and wood. Even if electric-based heating sources are used, much of that energy ultimately is produced from power plants that burn fossil fuels. This energy demand is ever increasing. According to BP's Statistical Review of World Energy (2009), global electrical demand increased by 66% between 1990 and 2008.

The combustion of fossil fuels from any source has a number of negative consequences. First and foremost, it results in a release of chemicals into the air and water, such as hydrochloric and sulfuric acids. These chemicals can be harmful to human health and to the environment. For humans, pollution causes respiratory diseases, cardiovascular diseases, and skin irritations. In China, an estimated 656,000 people die prematurely each year because of air pollution (The New York Times 2007). With respect to the environment, sulfur dioxide causes acid rain, which

lowers the PH value of the soil, and creates smog and haze that obscures sunlight. An additional concern related to fossil fuel combustion, is Green House Gas emissions (GHGs) and the climate change that GHGs are causing. The increase in human activities since pre-industrial times is one of the major causes of GHGs. The International Panel on Climate Change (IPCC 2007) reported that GHGs increased 70% due to human activities between 1970 and 2007. Carbon dioxide (CO_2) is the predominant GHG, and its emissions increased by 80% during that period. According to the IPCC (2007), the resulting warming of the climate is unequivocal because evidence from other countries shows that oceans and forests are being affected by the temperature increase. Many adverse effects will result from a global temperature rise. 20% to 30% of animals and plants will face the danger of extinction if the global temperature increases by 1.5 to 2.5 ^{o}C above 1990 levels. The risks of extreme weather events such as heat waves and floods will also increase as well as their negative impacts (IPCC 2007).

In Canada, a lot of effort has been made to measure the amount of GHGs resulting from space heating, since it accounts for the largest amount of consumed energy. Figure 1.1 shows the total amount of energy used and GHGs produced in the residential and commercial institutional sectors (Statistics Canada 2007). Since the amount of usage accounts for approximately 50% of the total demand, efficient use of energy in this sector will make a significant contribution towards alleviating our energy and GHG problems.

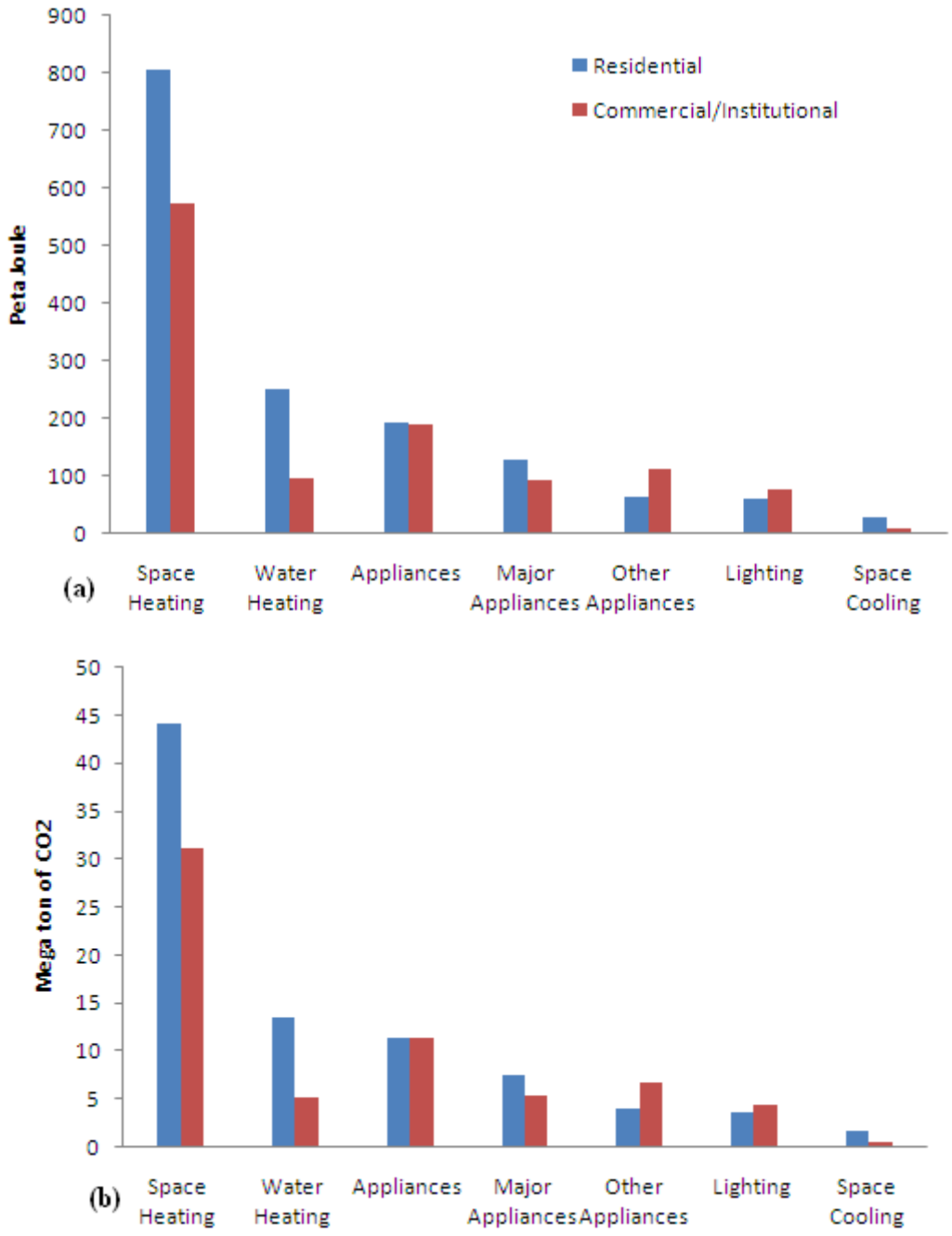

Figure 1.1: Energy Consumed (a) and GHG Emissions (b) in Canadian Residential and Institutional Sectors (Statistics Canada 2007).

1.2 Solutions

Solutions that lead to reductions in the production of GHGs related to space heating are divided into two groups: those that reduce heating demand, and those that replace heating energy supplies with less polluting sources. Reducing the amount of energy used for space heating can be accomplished through the use of better insulating materials and practices in buildings, the sealing of air gaps inside the walls, and through the use of high performance HVAC equipment. Replacing energy sources with something less polluting generally leads to the use of renewable sources. These include wind, geothermal, and solar. Solar energy in particular is an excellent alternative. The Earth receives a significant amount of solar energy every day which is available everywhere, and solar thermal heating systems offer a cost effective and efficient means of collecting it.

1.3 Background

1.3.1 Availability of Solar Energy

Earth receives around 174 PW of solar energy radiation each year with a mean extraterrestrial irradiance of 1.36 kW/m^2 (Duffie and Beckman 2006). Roughly 52% of this radiation reaches the surface of the earth (land and sea). The other portions are reflected or absorbed by the atmosphere. A world population of 10 billion with a total personal need of 10 kW per capita would require 10^{11} kW. Just 1% of the available solar energy collected at an efficiency of 10% will fulfill these needs (Goswami and Kreider 2000).

1.3.2 Solar Energy Technologies and Applications

Solar energy applications transform solar radiation into useful energy. This energy could be heat or electricity. Applications of solar energy include (Garg 1982):

- Water heating for domestic, commercial and industrial usage.
- Residential and institutional outdoor pool heating
- Agricultural product drying
- Ventilation air pre-heating
- Mechanical power production
- Solar refrigeration
- Electricity production

The general classifications of solar technologies are:

- ***Passive Thermal Systems*** are those systems that require little or no active mechanical device for operation. Examples include Trombe Walls, windows and shades, and sunspaces.
- ***Active Thermal Systems*** are solar heaters and coolers that involve the use of a mechanical device such as a pump or fan. Examples include solar domestic water and air heaters, and solar assisted chiller systems
- ***Photovoltaic cells*** convert sunlight directly to electricity. Typical commercially available systems have efficiencies ranging between 6% - 15%, depending on the type of the cell (Duffie and Beckman 2006).

Of particular interest to the present work are active thermal systems. These include concentrating collectors, evacuated tube collectors, flat plate collectors (glazed and unglazed), and transpired air collectors. Each is discussed.

Concentrating Collectors

Concentrating collectors are designed to deliver energy at high temperatures. These collectors usually have a parabolic shape to reflect the solar energy and concentrate it to a certain point (focusing) or area (non-imaging). They are often designed to produce steam used to run an electric generator or electricity, and the receiver is. usually a pipe containing a heat transfer fluid, a photovoltaic cell, or both. Manufacturing these collectors is expensive and they very often must be designed to track the sun. Figure 1.2 is a photo of a typical concentrating collector.

Figure 1.2: A Concentrating Collector (Sandia 2007).

Evacuated Tube Solar Collectors

Evacuated tube collectors are constructed from a number of evacuated glasses that have an absorber plate within the glass. This evacuation provides excellent insulation which allows high temperatures to be achieved in the absorber. These collectors are better than flat plates in colder weather due to their lower heat loss, but worse during the summer months due to lower optical efficiency (Ramlow and Nusz 2006). Figure 1.3 is a photo of this kind of absorber.

Figure 1.3: An Evacuated Tube Solar Collector (Green Terra Firma 2007).

Glazed Flat Plate Collectors

Flat plate collectors are generally of two types: Solar Water Heaters (SWHs), and Solar Air Heaters (SAHs). Both types generally consist of a frame, insulated back, and absorber plate, and many also have a glazing cover. The absorber plate is usually a finned heat exchanger which facilitates transfer of solar energy to the working fluid. It is located beneath the glazing and

usually has two manifolds for the fluid inlet and outlet. A glazing is used in many collectors to minimize the heat loss to the environment, where glass is the most common material used in covering since its lower transmittance in longer wavelength solar radiation (Goswami and Kreider 2000). Figures 1.4 and 1.5 show photos of a typical SWH system and SAH system, respectively.

Figure 1.4: A Flat Plate Solar Water Heater (Solar Panels Plus, 2007).

SAHs come in many forms depending on their application. They are commonly used for space heating and drying applications. For crop drying, their basic advantages appear to be their low sensitivity to leakage and that they do not need external drying equipment.

Flat plate collectors have many advantages over concentrating or evacuated tube collectors. They have no requirement for tracking, are simpler in design and cheaper to construct, and have little need for maintenance (Duffie and Beckman 2006).

Figure 1.5: A Flat Plate Solar Air Heater (AltE Store 2010).

Unglazed Transpired Solar Collectors

The use of Unglazed Transpired Solar Collectors (UTSCs) is considered to be one of the most effective methods of reducing HVAC loads in buildings. They provide high efficiency and low cost preheated air.

This technology is relatively simple. Generally, a perforated black painted metal sheet (absorber plate) is placed on a southern building facade. As air is sucked through perforations in the

absorber plate and into the plenum, and heat energy from the absorber is transferred to it. The plenum is a gap of 15 -20 cm behind the absorber plate. This pre-warmed air makes a significant contribution towards decreasing the energy used for heating. Figures 1.6 is a photo of a typical UTSC. Figure 1.7 shows a UTSC in operation.

Figure 1.6: An Unglazed Transpired Solar Collector (NRCan 2009).

The main advantage of this type of solar collector is twofold. The air is sucked directly through the perforations which make the surface of the absorber operate at a relatively low temperature. Consequently, heat loss will be decreased. Moreover, because there is no need for a glazing cover, its cost and installation is easier than other types of solar heaters.

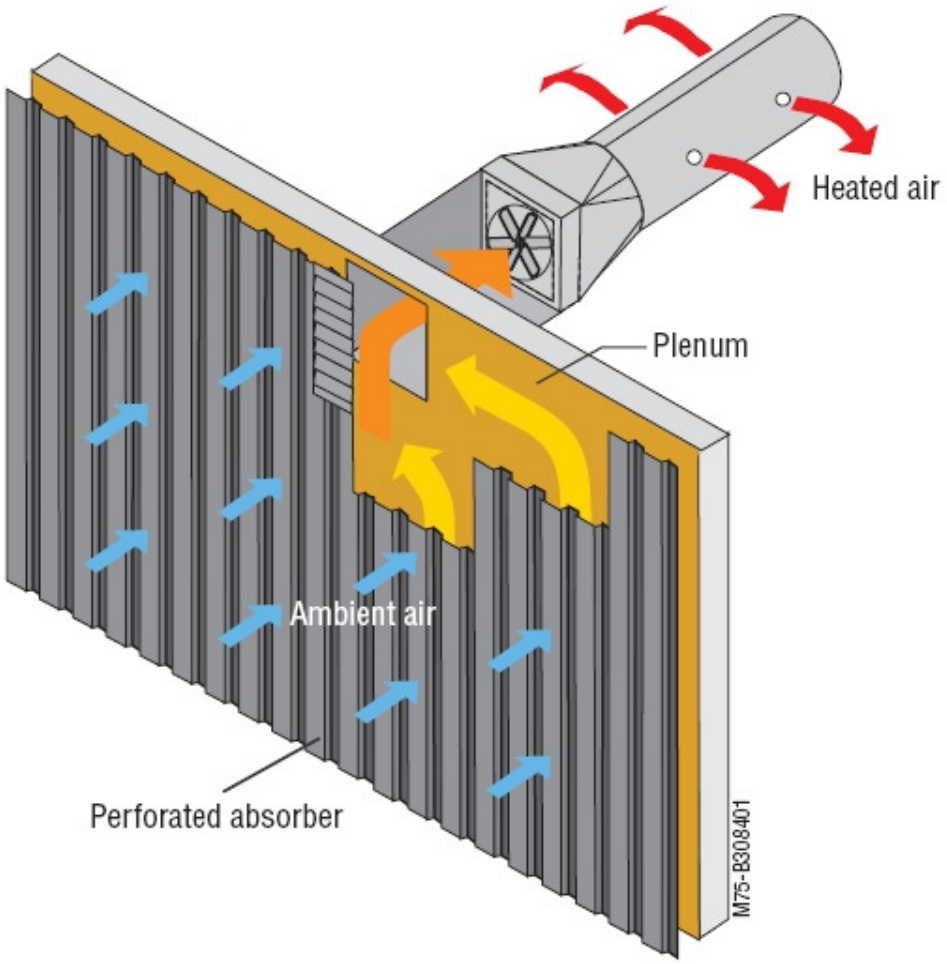

Figure 1.7: An Unglazed Transpired Solar Collector (Sustainable Design Update 2008).

One commercially available version of these collectors is made by Conserval Engineering. This system, called Solarwall™, has been installed in more than 25 countries. Many studies have been made on UTSCs. These studies include calculating collector effectiveness, flow distribution, heat transfer coefficient and plate shape effect.

1.4 Motivation and Objective of the Thesis

All previous studies on UTSCs were based on flat plates or plates with sinusoidal corrugations. Commercially available products, and in particular, SolarWall™, have a trapezoidal design to provide structural stiffness. Evaluating the heat transfer coefficient and the wind heat loss will assist in better design of systems that use these collectors.

The objective of the current work is to:

- Determine the average heat transfer coefficient between the absorber and the intake air;
- Determine the heat loss due to wind, and;
- Compare the results with the previous experimental and numerical results.

The study will be performed numerically.

1.5 Thesis Outline

This thesis is divided in 5 chapters;

- Chapter 1 is an introduction and background information.
- Chapter 2 contains a literature review of previous studies. First, studies related to flow characteristics and heat transfer on perforated absorber plates will be examined. Secondly, a review is performed of the previous studies on UTSC's in terms of their convective heat loss and effectiveness.
- Chapter 3 describes the computational model that has been developed for this simulation.
- Chapter 4 shows and discusses the simulation results.
- Chapter 5 contains the conclusions and recommendations resulting from this work.

Chapter 2

Literature Review

2.1 Introduction

Since the design of UTSCs consist of both perforations and corrugations, it is vital to study the effect of both features on the air flow and heat transfer. This chapter reviews previous studies related to these geometric aspects of UTSC design.

Section 2.2 will present the governing physical equations and theory of perforated plates and the effect of perforations on the temperature and velocity profiles. Section 2.3 presents the previous studies conducted on perforated plates, while Section 2.4 and 2.5 present previous experimental and numerical studies conducted on corrugated plates and on backward facing steps, respectively. Studies that focused specifically on UTSC performance are of particular interest. These studies will be reviewed in Section 2.6.

2.2 Flow and Heat Transfer Theory Over Perforated Plates

2.2.1 Velocity Profile and the Starting Length

When considering forced flow over a flat plate (without suction), velocity boundary layer growth can be characterized generally. At the fluid-plate interface, the fluid is assumed to have zero velocity. This fluid layer restricts fluid motion in the adjacent layer through shear stresses. Therefore, the fluid velocity increases as one moves away from the plate to such a point where the plates influence is negligible, and the free stream velocity is attained. The point at which the fluid velocity reaches 99% of the free stream velocity defines the velocity boundary layer. Initially, the boundary flow exhibits laminar behavior, and the velocity boundary layer growth is proportional to $x^{\frac{1}{2}}$ where x is the distance from the leading edge of the plate. Transition to turbulence occurs further downstream, depending on the flow velocity and fluid properties, at which point the velocity boundary layer grows proportional to $x^{\frac{4}{5}}$ (Bejan 1984).

The situation where there is homogenous suction at the fluid-plate interface was studied analytically by Schlichting (1979). When homogenous suction occurs, the velocity boundary layer is 'sucked' through the plate. As a result, the velocity boundary layer thickness is decreased depending on the ratio of free stream velocity to suction velocity. If the suction velocity is great enough, the transition to turbulence will not occur and boundary layer growth stops completely (called the asymptotic region). Schlichting defined the critical Reynolds number for transition, Re_c, based on the boundary layer thickness at transition, $\delta(x_c)$, and free stream velocity, U_∞, to be:

$$Re_c = \frac{\rho U_\infty \delta(x_c)}{\mu} \tag{2.1}$$

where ρ and μ are the fluid density and dynamic viscosity, respectfully. He showed the minimum suction velocity, V_o, for asymptotic behavior to occur to be:

$$V_0 = 1.24 \times 10^{-4} U_\infty \quad (2.2)$$

where the suction velocity is the average velocity of air flowing through the plate in relation to its entire surface area, and not the velocity through any particular hole. He showed that Re_c increased by a factor of 130 for cases where the minimum suction velocity was applied. Figure 2.1 shows the velocity boundary layer over a flat plate with suction.

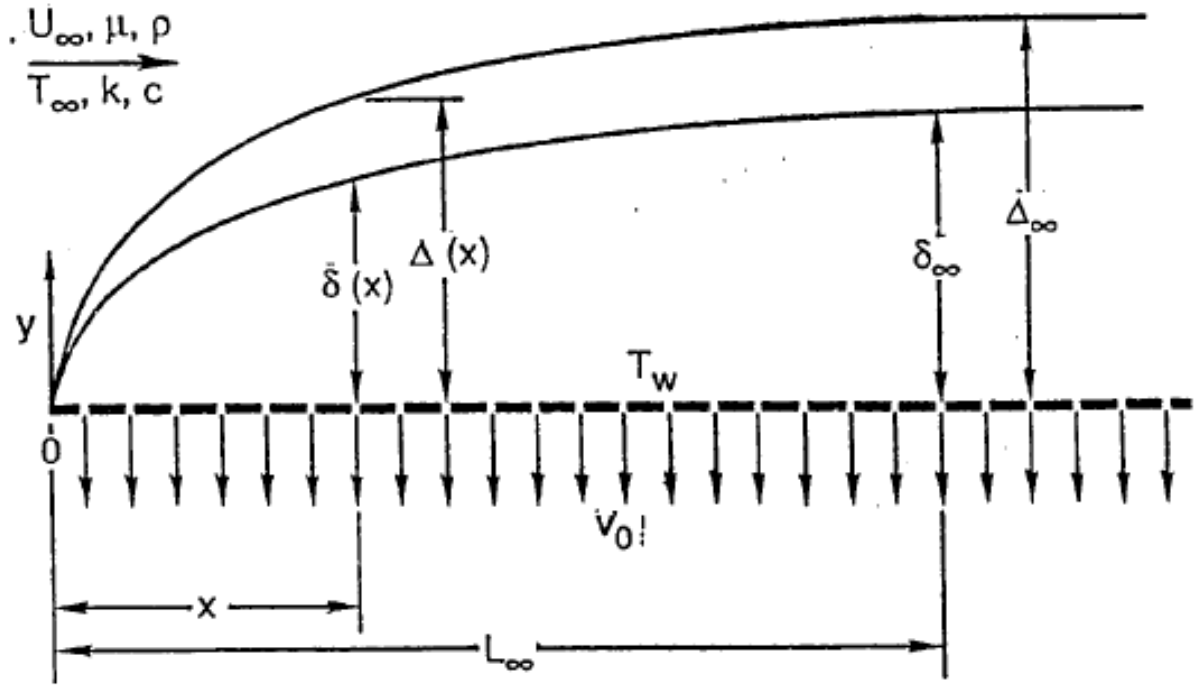

Figure 2.1: Thermal and Velocity Boundary Layer Development over a Perforated Plate (Kutscher et al. 1993).

Schlichting (1979) was also able to develop an equation for the velocity profile. By assuming a relatively small suction velocity and relatively large distance downstream of the plates' leading edge, the momentum equation becomes:

$$-V_0 \frac{du}{dy} = \nu \frac{d^2u}{dy^2} \tag{2.3}$$

where $u = u(y)$ is the velocity profile for fluid flowing in the x-direction, y is the distance perpendicular from the plate, and ν is the kinematic viscosity. Applying the boundary conditions of $u = 0$ at the wall ($y = 0$) and a free stream velocity of $u = U_\infty$ at $y = \infty$, and integrating Eqn. 2.3, the flow velocity profile becomes:

$$u(y) = U_\infty(1 - e^{\frac{-V_o y}{\nu}}) \tag{2.4}$$

Schlichting's (1979) analysis was based on the assumption of uniform or homogenous suction at the plate. In difference to this, discrete suction is said to occur when the perforation spacing of the plate is larger than the boundary layer thickness (Arulanandam et al. 1999). When discrete suction exists, the velocity boundary layer thickness will vary near to the locations of the perforations, and appear 'dimpled' in nature. It is likely that the situation studied in this work will classify as discrete suction. This point will be revisited in Chapter 3.

Arpaci and Larson (1984) also analytically examined flow over a perforated plate with suction. By assuming a parabolic velocity profile in the momentum equation, they found that the velocity boundary layer thickness in the asymptotic region, δ_∞, was given by:

$$\delta_\infty = \frac{2\nu}{V_0} \tag{2.5}$$

Using this, Kutscher (1992) showed that flow over a plate will reach the asymptotic region after a specific velocity starting length, L_s , given by:

$$L_s = 0.96 \frac{U_\infty v}{V_0^2} \cong \frac{U_\infty v}{V_0^2} \quad (2.6)$$

This starting length corresponds to the point where the boundary layer has reached 87% of δ_∞.

2.2.2 Temperature Profile and the Equivalent Starting Length

If a temperature difference exists between a flat plate (without suction) and the fluid flowing over it, then a thermal boundary layer will also develop. Heat transfer is via conduction at the surface (where the fluid is assumed to be stationary), and via conduction and advection as one moves further from the plate surface. The point at which the temperature ratio $(T_p - T)/(T_p - T_\infty)$ reaches 99%, defines the thermal boundary layer. Here T_∞ is the free stream or wind temperature, and T_p is the plate temperature. The nature of the flow will have a significant impact on the heat transfer rate and temperature distribution within this boundary layer. In the turbulent regime, mixing is enhanced, and boundary layer growth occurs more quickly than it does in the laminar regime.

As was previously mentioned, the situation where there is homogenous suction at the fluid-plate interface was studied analytically by Kutscher et al. (1993). When homogenous suction occurs, the thermal boundary layer is also 'sucked' through the plate. As a result, the thermal boundary layer thickness is decreased depending on the ratio of stream velocity to suction velocity. As was also mentioned, since the flow is less likely to change to turbulence, boundary growth is significantly retarded. Kutscher assumed that if asymptotic behavior existed with the flow, then it also existed with the thermal boundary layer.

Kutscher et al. (1993) developed an equation for the thermal profile. By assuming a relatively small suction velocity and relatively large distance downstream of the plate leading edge, the energy equation becomes:

$$V_0 \frac{dT}{dy} = \alpha \frac{d^2T}{dy^2} \tag{2.7}$$

where $T = T(y)$ is the temperature profile at some distance x from the plate leading edge, and α is the thermal diffusivity of the fluid. This equation can be integrated after the application of constant heat flux boundary condition ($dT/dy = q''/k$) on the wall ($y = 0$), and free stream boundary condition, $T = T_\infty$ at y = ∞. Here q'' is the radiant heat flux to the plate, and k is the thermal conductivity of air. The integration yields the temperature profile:

$$T(y) = T_\infty + \frac{\alpha q''}{kV_o} e^{-\frac{V_0}{\alpha}y} \tag{2.8}$$

Kutcsher et al. (1993) followed an equivalent procedure to that used by Arpci and Larson (1984) to determine a thermal starting length for asymptotic behavior in the thermal boundary layer. By assuming the thermal boundary layer thickness to be equivalent to velocity boundary layer, the thermal boundary layer thickness Δ_∞ will be:

$$\Delta_\infty = 2\frac{\alpha}{V_0} = \frac{\delta_\infty}{Pr} \tag{2.09}$$

where Pr is the Prandtl number and is given by:

$$Pr = \frac{\nu}{\alpha} \tag{2.10}$$

The equivalent heat loss starting length L_e is approximated by:

$$L_e = \frac{L_s}{Pr+Pr^2} \tag{2.11}$$

2.3 Previous Studies on Perforated Plates

Literature related to the characterization of heat loss from a perforated plate is limited, and only considered heat loss from perforated flat plates.

Iglish (1944) gives an explanation of the flow behavior of a flat plate with homogenous suction in the developing region, and determined the point at which the flow could be assumed to be asymptotic. His model was improved by Maddaeus (1983), who developed a 3-D solution for the boundary layer, and a series solution for the boundary layer in the asymptotic region.

One of the earliest experimental studies of heat loss from a perforated plate was performed by Sparrow and Ortiz (1982). They tested a number of perforated plates consisting of a hexagonal area containing 19 holes in a staggered pattern. They then filled this area with naphthalene, and used a sleeve to protect the naphthalene edges. The plate was weighed at this stage, and then exposed the plate to air flow for a period of time. During this time, the weight of naphthalene decreased due to sublimation. Finally, the plate was weighed again to find the amount of naphthalene lost. By knowing the amount of naphthalene loss, the relationship between the Nusselt, *Nu*, number and Prandtl number could be determined.

Sparrow and Ortiz (1982) produced an expression of Nusselt number for two hole pitch to hole diameter ratios. The best fit of Nusselt number from their experiments was:

$$Nu = 0.881 Re^{0.476} Pr^{1/3} \tag{2.12}$$

where:

$$Nu = \frac{hP}{k} \tag{2.13}$$

Here, h is the heat transfer coefficient, and P is the hole pitch. Sparrow and Ortiz's experiment was performed on Reynolds numbers (based on the hole diameter) ranging from between 2000 and 20000, and porosity ratios between 14% and 22%. It is noted that these porosity ratios are much higher than the ones considered in the present study, which are in the range of 0.5 and 2%.

2.4 Previous Studies on Corrugated Plates

The main purpose of using corrugations in plates is to enhance the structural stiffness of the plate. These corrugations, however, also serve to enhance the convective heat transfer between the plate and the fluid in that they result in interruptions in the viscous sub-layer. The flow over a plate with corrugations is characterized by the extent of the recirculation zone upstream and downstream of the obstacle (Abdalla et al. 2009). Separation and reattachment enhances heat transfer between the plate and the fluid flow and increases mixing of the fluid particles.

Corrugated plates have been extensively reported on in the literature. Previous studies cover the effect of corrugation shape and their arrangement on the plate, Reynolds number, and channel height. Since this area is very broad, only studies related to solar air heaters and early numerical simulations will be discussed in this chapter.

Prasad (1983) experimentally studied solar air heaters used for drying purposes. He used wires on the underside of the absorber plate to trip the turbulent boundary layer and significantly enhance the convective heat transfer coefficients. Following his earliest experiment, he studied the effect of roughness and pitch (Prasad and Saini 1988). He found that increased roughness resulted in an increase in convective heat transfer and friction factor. Increasing the pitch resulted in a decrease in the heat transfer rate and friction factor.

Sunden and Trollheden (1989) performed a numerical investigation of laminar flow in two dimensional channels. He developed a 2D model for a channel with stream-wise periodic variation at different cross sectional areas. The channel wall was exposed to a uniform heat flux and the simulation was performed at Reynolds numbers (based on the maximum distance between the upper and lower walls) between 50 and 1250, and Prandtl numbers between 0.7 and 5. The simulation resulted in lower heat transfer rates for low Prandtl numbers, and higher heat transfer for higher Prandtl numbers, when compared to smooth channels. He theorized that these phenomena likely occurred due to the low intensity of the recirculation zone between corrugations.

Karwa et al. (1999) performed comprehensive experimental studies on the effects of rib roughness on surfaces. He used a rectangular duct with repeated chamfered ribs on the horizontal surfaces of the duct. The ranges of parameters for his experiment were: Reynolds numbers (based on the duct hydraulic diameter) between 3000 and 20,000, relative roughness heights from 0.041 to 0.0328, relative roughness pitch to the duct hydraulic diameter ratios of 4.5, 5.8. 7 and 8.5, and rib chamfer angles of -15, 0, 5, 10, 15 and 18 deg. Figure 2.2 shows the arrangement of these ribs on the plate.

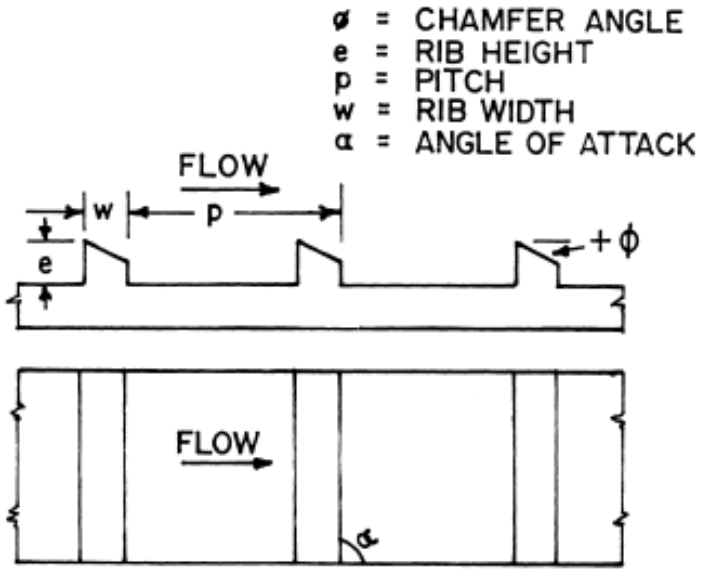

Figure 2.2: Rib Shape on the Test Plate used in the Experimental Study by Karwa et al. (1999).

The goal of the experiment of Karwa et al. (1999) was to find the effect of these ribs on the friction factor and heat transfer. He found that at low Reynolds numbers, the friction factors and Stanton number (the ratio between the heat transfer to the fluid to the heat capacity of the fluid) for a roughened surface were close to those found for smooth surfaces. It was surmised that this occurred because the roughed elements lay within the laminar sub-layer. When Reynolds numbers increased, however, these roughed elements interrupt this layer, which in turn enhanced the convective heat transfer rate. However, this increase in friction factor and heat transfer reached a maximum value in spite of increasing Reynolds numbers. This happens because the thickness of laminar boundary sub layer becomes quite small, and the energy loss due to vortices became constant. He also found that increasing the chamfers angle and rib height enhanced the heat transfer and friction factor while increasing the pitch decreased them (confirming the conclusions of Prasad (1983)). Based on this result, Karwa et al. (2001) performed further studies. Of the chamfer angles tested, 15^{o} had the best performance. He developed a mathematical model and performed experimental studies on a wider range of parameters using

this chamfer angle. The thermal efficiency of solar collectors was enhanced by up to 40% with this roughness in comparison to smooth plates, while friction increased by as much as 29%.

Lee and Abdelmoneim (2001) developed a 2D CFD model for predicting the turbulent heat transfer coefficient over a surface which has ribs with different pitch to height ratios. This simulation was performed for wind velocities of 27 m/s and 30 m/s with pitch to height ratios of 21.33 and 53.33. Figure 2.3 shows a schematic of the ribbed plate used in Lee's model. The goal of the study was to estimate the extent of the recirculation zone behind the rib, and to estimate the heat transfer coefficient over the plate.

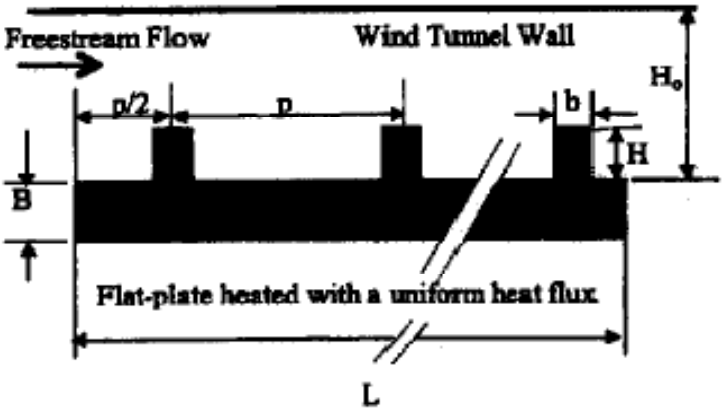

Figure 2.3: Schematic of the Test Plate used in the Numerical Study by Lee and Abdelmoneim (2001).

Chaube et al. (2006) developed a 2D CFD model of a surface mounted with artificial roughness to find the best turbulent model for numerical simulation. The numerical results were compared with the experimental results of Karwa et al. (2003). Reasonable agreement was found by using the standard $k - \omega$ model.

2.5 Previous Studies on Backward Facing Steps

Since the corrugations of the absorber plate considered in the present work has a shape (Figure 2.4), literature related to flow over backward facing step is considered. Literature related to this problem is extensive. As such, only a brief overview will be considered here.

Figure 2.4: Corrugation Shape of the Plate Examined in the Current Study.

One of the earliest studies on this topic was performed by Armaly et al. (1983) who used a laser doppler anemometry to measure the velocity distribution over accounted with vertical step. His experimental setup ran at Reynolds numbers (based on the height of the step) between 100 and 10000. It showed the three kinds of flow behavior and the Reynolds numbers at which they occurred: laminar ($\mathrm{Re} < 1200$), transition ($1200 < \mathrm{Re} < 6600$), and turbulent ($\mathrm{Re} > 6600$). Several numerical and experimental studies followed this work. Of note, Chiang and Sheu (1999) studied the geometry examined by performing a 2D numerical simulation. They worked with the assumption of laminar flow, and only considered Reynolds numbers ranging from 100 to 1000. They found a good agreement with the experimental results.

The only study that was found on inclined backward steps was by Chen et al. (2006). They performed 3D numerical simulation to test the effect of the inclination of the step on the flow behavior. Figure 2.5 shows the domain of the numerical model. Four inclination angles were tested: 15^{o}, 30^{o}, 45^{o} and 90^{o}. The Reynolds number used in this study was 343 for all the tested

angles. Separation and recirculation zones were observed in all angles testes except 15^{o} (Figure 2.6). It is noted that in difference to the current work, surface z/L = 0 is a wall. Still, surface z/L = 0.5 might offer insight into flow behavior at low suction velocities.

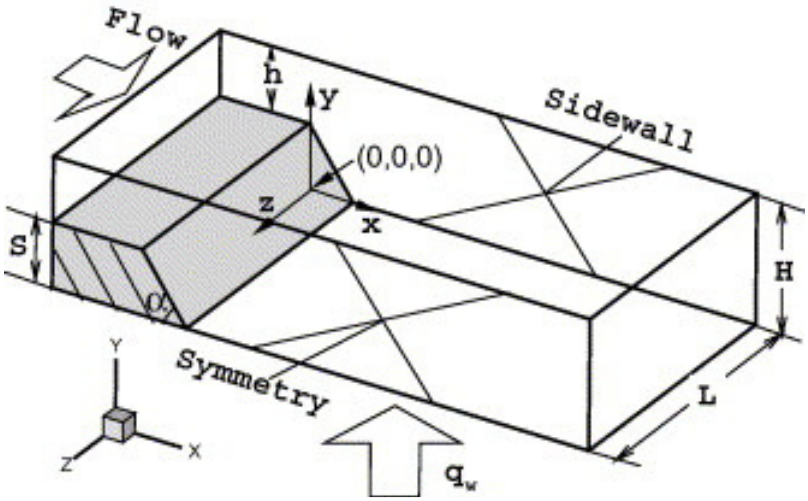

Figure 2.5: Domain of the Numerical Model Studied by Chen et al. (2006).

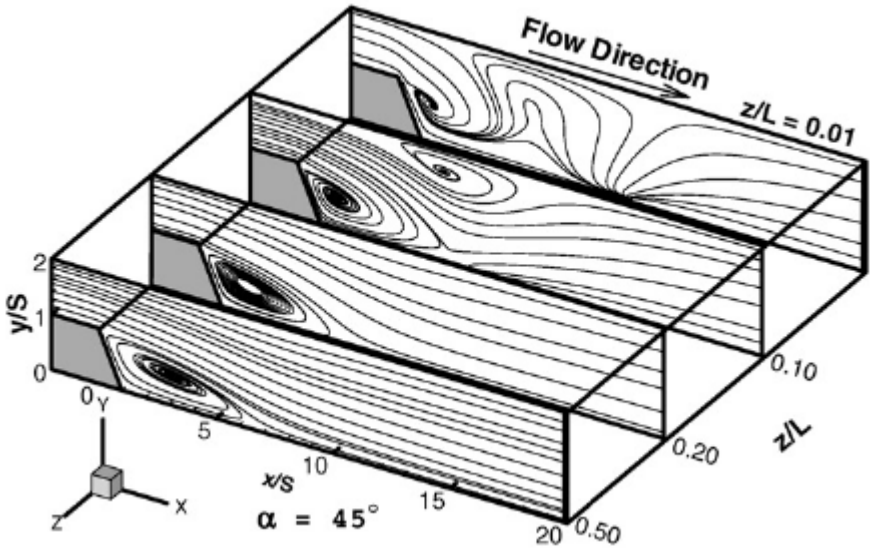

Figure 2.6: Results for Flow over a Backward Facing Sloped Surface (Chen et al. 2006).

2.6 Previous Studies on UTSCs

As was previously noted, studies that specifically examined UTSC performance have been reviewed separately due to their obvious relevance to the current work. The first work that focused specifically on UTSCs was performed by Kutscher et al. (1991, 1993), Kutscher (1992, 1994), Dymond and Kuscher (1997), Gawlik and Kuscher (2002), and Gawlik et al. (2005). This work was both experimental and numerical in nature, and considered system aspects such as geometry, absorber porosity, and wind and suction velocity. Subsequently, studies were conducted at the University of Waterloo by Cao et al. (1993), Golneshan (1994), Gunnewiek et al. (1996), Arulanandam et al. (1999), and Van Decker et al. (2001). Again, these studies were both experimental and numerical in nature, and focused on the design and development of the SolarWall transpired air collector (Conserval 2010). The only other study found was an analytical model developed by Summers (1995).

The aforementioned research will be divided into two sections. First, studies which considered radiative and convective heat loss from UTSC's will be reviewed. Then, those studies that examine plate effectiveness will be considered.

2.6.1 UTSC Heat Loss

Kutscher (1992), Kutscher, Christensen, and Barker (1993)

Kutscher was the first to develop heat loss theory for UTSC's (Kutscher 1992, Kutscher et al. 1993). By considering a flat plate absorber with homogenous suction, the basic heat transfer equation of the unglazed transpired solar collector was given by:

$$\rho C_p V_o A_{abs}(T_{out} - T_\infty) = q^{"} A_{abs}\alpha_{abs} - q_{conv} - q_{rad} \quad (2.14)$$

where C_p is the specific heat of air, A_{abs} is the absorber surface area, T_{out} is the outlet temperature from the absorber (temperature entered to the space), T_∞ is the ambient temperature, and α_{abs} is the absorber absorptance.

Radiation heat loss from the absorber plate, q_{rad}, can occur from both sky and ground, depending on the tilt of the absorber plate. By assuming an adiabatic wall behind the absorber plate (the other side of the Plenum), and that the absorber is grey and diffuse, radiation heat losses become:

$$q_{rad} = \varepsilon_{abs}\sigma_{SB}A_{abs}\left(T_{abs}^4 - F_{sky}T_{sky}^4 - F_{grd}T_{grd}^4\right) \quad (2.15)$$

where ε_{abs} is the emissivity of the absorber, σ_{SB} is the Stefan Boltzmann constant, T_{abs}, T_{sky} and T_{grd} are the collector, sky and ground temperatures respectively, F_{sky} and F_{grd} are viewfactors expressed as a function of collector slope and given as:

$$F_{sky} = \frac{1+cos\beta_{abs}}{2} \quad (2.16)$$

$$F_{grd} = \frac{1-cos\beta_{abs}}{2} \quad (2.17)$$

where β_{abs} is the inclination angle of the absorber .

Kutscher initially considered convective heat loss, q_{conv}, from the UTSC under no wind (natural convection) conditions (Kutscher et al. 1993). To do so, he applied the same procedure used by Arpaci (1984) for determining the velocity and thermal boundary layers, as outlined in Section 2.2.1. The momentum equation for the natural convection is:

$$-V_o\frac{du}{dy} = \beta g(T - T_\infty) + \nu\frac{d^2u}{dy^2} \quad (2.18)$$

where β is the thermal expansion coefficient, and g is the acceleration due to gravity. The boundary conditions for this equation are: at $y = 0$, $u = 0$ and $dT/dy = q''/k$. At $y = \infty$, $u = U_\infty$, $T = T_\infty$. The temperature profile is the same for the forced convection Figure 2.7. Thus, the velocity profile for the free convection will be:

$$u = \frac{\beta g \alpha^2 q''}{V_o^3 k(Pr-1)} \left(e^{\frac{-V_0 y}{Pr\ \alpha}} - e^{\frac{V_0 y}{\alpha}} \right) \quad (2.19)$$

Using the known profiles for the velocity and boundary layers, the equation for the heat loss for the natural convection will be Kutscher et al. (1993) found:

$$q_{nat} = \frac{\beta g \alpha^3 q''^2 W}{V_o^5 k(Pr-1)} \left(\frac{Pr}{Pr+1} - \frac{1}{2} \right) \quad (2.20)$$

where q_{nat} is the that loss due to natural convection, and W is the width of the plate. For the suction velocity of 0.01 m/s, a radiant heat flux of $1000\ W/m^2$, and air properties at 27 C^o, heat loss due to natural convection will be less that 1 W/m. Therefore, the heat loss due to natural convection will be negligible.

Kutscher also considered heat losses as a result of wind (Kutscher et al. 1993). Based on an assumption of homogenous suction and laminar flow over the absorber, they showed analytically that the flow over the absorber plate should become asymptotic after a certain starting length. In the asymptotic region, there is no net convective heat flux because the boundary layer is sucked through the perforations, stopping the growth of the boundary layer, and so convective heat losses occur in the starting length only. Kutscher et al. (1991) derived an expression for the convective heat loss to the ambient to be:

$$h_{conv} = \frac{U_\infty \nu\ \rho C_p}{L_{abs} V_0} \quad (2.21)$$

where L_{abs} is the length of the absorber plate.

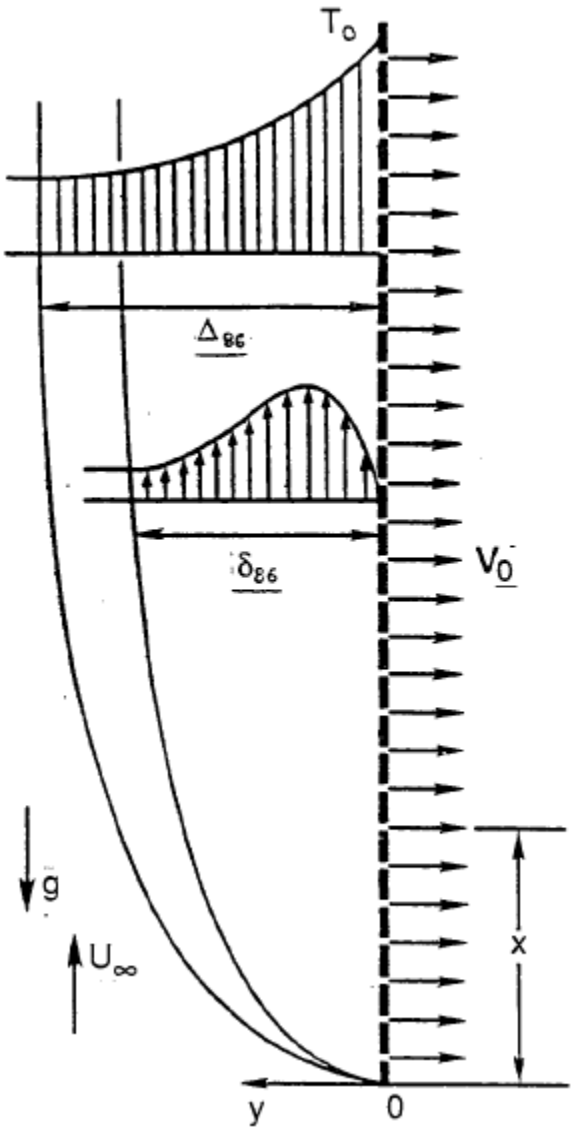

Figure 2.7: Velocity and Thermal Boundary Layer Profiles for Natural Convection (Kutscher et al. 1993).

Gawlik and Kutscher (2002)

The previous analysis was performed on a flat plate absorber. Commercially available products, however, are not flat. They contain some corrugations to provide structural stiffness. The presence of this corrugation changes the flow behavior over the plate, and typically creates a turbulent recirculation region.

Gawlik and Kutscher (2002) performed both experimental and numerical investigations of UTSCs with sinusoidal corrugations. Experimentally, they used hot wire anemometry to calculate the heat transfer from four sinusoidal shaped plates with a variety of aspect ratios (i.e. the ratio of pitch to amplitude). They used out numerical investigations to cover wider aspect ratios. Figure 2.8 shows a diagram of their test plate with amplitude and pitches of the corrugations.

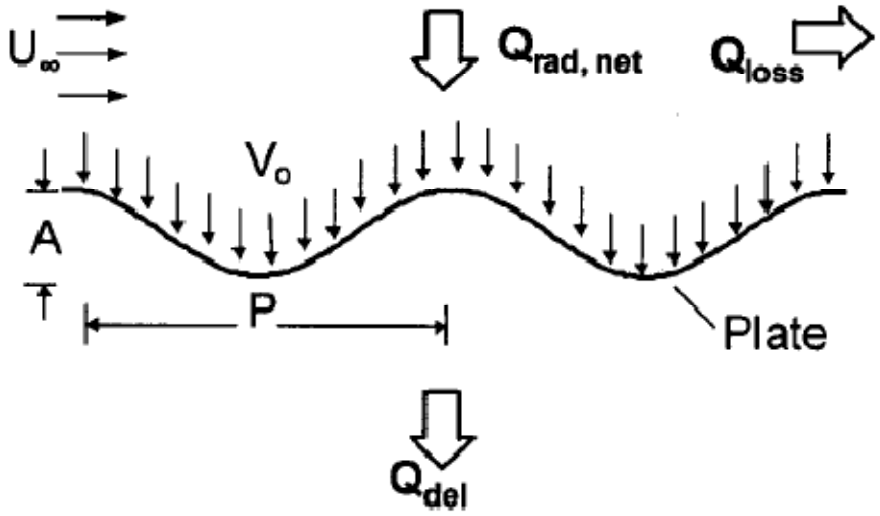

Figure 2.8: Diagram of the Sinusoidal Plate used by Gawlik and Kutscher (2002).

By assuming a uniform suction and wind velocity over the plate, Gawlik and Kutscher (2002) found that an asymptotic boundary layer still developed after a certain distance, depending on the ratio between the wind and suction velocity, and that this starting length was greater than those found for a flat plate absorber exposed to the same flow and suction conditions. They assumed that the flow could be attached or separated, and that the expression for heat loss could be built on the aspect ratio. For the attached flow they used:

$$Nu_{att} = Nu_{flat}\left[1 + 0.81\left(\frac{A}{P}\right)^{0.5}\right] \tag{2.22}$$

where A is the amplitude of corrugation, and P is the pitch. Nu_{att} is the Nusselt number for the attached flow, and Nu_{flat} is the Nusselt Number for the flat plate. For separated flow:

$$Nu_{sep} = 2.05\left(\frac{A}{P}\right)^{1.4} Re_s^{1.63} \tag{2.23}$$

Here, Re_s is the suction parameter which is given by

$$Re_s = \frac{U_\infty}{V_0} \tag{2.24}$$

2.6.2 UTSC Effectiveness

Kutscher (1994)

The first experimental works on UTSCs were performed by Kutscher (1994) in an effort to determine the heat exchanger effectiveness. He designed a number of plates with circular perforations arranged in a triangular pattern (Figure 2.9). The plates were placed in a wind tunnel and exposed to arrays of heat lamps. The asymptotic region was examined at air speeds of 1, 2 and 4 m/s, and suction velocities between 0.02 and 0.08 m/s. A correlation for Nusselt number was found to be:

$$Nu = 2.75\left[\left(\frac{P}{D}\right)^{-1.2} Re_D^{0.43} + 0.011\sigma Re_D \left(\frac{U_\infty}{V_o}\right)^{0.48}\right] \tag{2.25}$$

where Re_D is the Reynolds number based on the suction velocity and perforation diameter, D is the hole (hydraulic) diameter, σ is the porosity of the plate (the ratio between the area of the holes and the total area of the plate). This Nusselt number takes into account heat transfer from all three regions of the hole: the front, sides, and back. The correlation is valid for Re_D from100 to 2000 and σ from 0.1% to 5%.

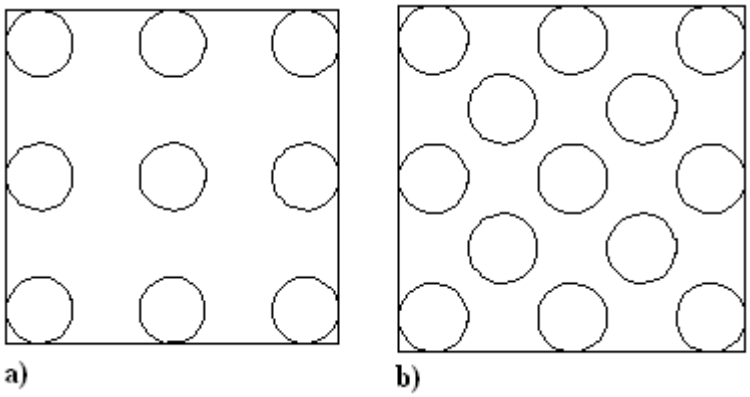

Figure 2.9: a) Square Pattern Studied by Arulanandam et al. (1999) b) Triangular Pattern Studied by Kutscher (1992).

In that same work, Kutscher also numerically modeled the flow through a single perforation of a UTSC (Kutscher 1994). He assumed the perforation could be treated as an orifice if the air flow was perpendicular to the plate. This assumption was limited to zero wind conditions. He modeled 5 plates; different in their pitch to diameter ratio. He chose the laminar model since it better handled the boundary layer near to the perforation. A schematic of the stream lines from his model is shown in Figure 2.10.

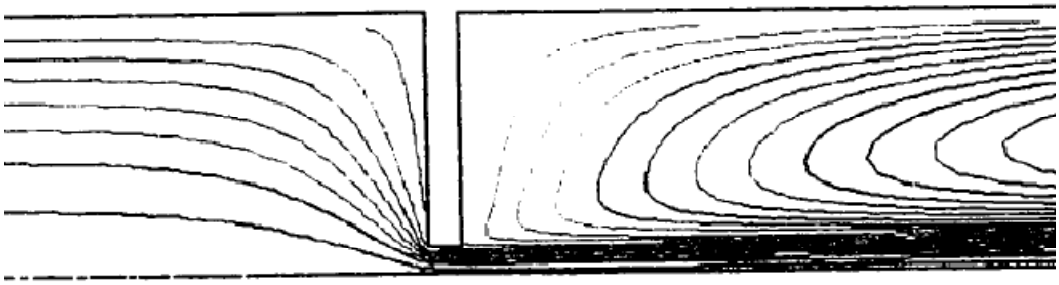

Figure 2.10: Streamlines of Flow Through a Perforation (Kutscher 1992).

To model the heat transfer, the perforation was assumed to have a uniform temperature, and the regions of heat transfer were divided into front, back and perforation. The effect of each region was simulated separately, and then combined into one relation to be:

$$Nu = 9.075\left(\frac{P}{D}\right)^{-1.304} Re_D^{0.2523} \tag{2.26}$$

Kutscher combined his numerical results with experiential data from his previous research (Kutscher 1992). He found that the numerical results under predicted the effectiveness for high suction flow rates, and that he had better agreement for high porosity plates.

Cao, Hollands, and Brundrett (1993), Golneshan (1994)

Several studies conducted in the Solar Thermal Research Lab at the University of Waterloo followed the work done by Kutscher and investigated effectiveness for different plate designs. Cao et al. (1993) and Golneshan (1994) studied plates perforated with long narrow rectangular perforations.

Cao et al. (1993) conducted a two-dimensional numerical analysis. They assumed the flow to be transverse to the perforations but parallel to the absorber. They found the velocity and temperature at the entrance of a perforation and expressed the plate effectiveness as a combination of the heat transfer occurring at the front and in the holes (they neglected heat transfer from the back). Their results showed that 20% of the total heat transfer occurred in the perforation.

Golneshan (1994) studied the same geometry both analytically and experimentally. The analytical work was performing using a two dimensional momentum integral analysis. Experimentally, he tested four different absorber plates in the asymptotic region. He found a relation between the absorber effectiveness and six dimensionless parameters.

Arulanandam, Hollands and Brundrett (1999), Van Decker, Hollands and Brunger (2001)

Arulanandam et al. (1999) and Van Decker et al. (2001) used CFD and experiments, respectively, to extend the work of Kutscher (1994).

Arulanandam et al. (1999) developed a 3D model to examine the effectiveness on a plate with circular holes in a square array (Figure 2.9). The work covered a wider range of parameters than those previously investigated such as plate thickness and thermal conductivity. They considered only the heat transfer occurring at the front of the plate and in the hole, modeling the back of the plate as adiabatic, and did not take the wind into account. The relation obtained was in agreement with Kutscher's work for the same conditions.

Van Decker et al. (2001) used experiments to cover a wider range of parameters. They tested nine different plates of varied porosity, thickness and materials, using the same experimental setup used by Golneshan (1994). Using their experimental data and the previous work of Arulanandam et al. (1999) and Golneshan (1994), a correlation for the effectiveness of UTSCs with holes laid out on a square pitch was developed by splitting the total effectiveness into three parts: the effectiveness at the front face, ε_f , at the sides of the holes, ε_h, and at the back face, ε_b.

$$\varepsilon_{HX} = 1 - \left(1 - \varepsilon_f\right)(1 - \varepsilon_h)(1 - \varepsilon_b) \tag{2.27}$$

where

$$\varepsilon_f = \left(\frac{1}{1+Re_s \min\left(1.72Re_\infty^{-0.5}, 0.0654\right)}\right) \tag{2.28}$$

$$\varepsilon_b = 1 - \frac{1}{1+3.4Re_b^{-1/3}} \tag{2.29}$$

$$\varepsilon_h = 1 - exp\left(-0.0204\frac{P}{D} - \frac{20.62t}{Re_h D}\right) \tag{2.30}$$

and

$$Re_\infty = \frac{U_\infty P}{v} \qquad Re_s = \frac{V_o P}{v} \qquad Re_b = \frac{V_o P}{v\sigma} \qquad Re_h = \frac{V_o D}{v\sigma}$$

where t_{abs} and k_{abs} are the absorber thickness and thermal conductivity. They found that their model could also be applied to plates with a triangular pitch by multiplying P by a scaling factor

corresponding to 1/1.6. Using this factor, they were able to compare their model to the one of Kutscher (1994) and found that both models were giving similar results for the same conditions and plate geometry. Van Decker's model was, however, applicable for a wider number of plates, being valid for the following ranges of variables: $0.028 \leq V_o \leq 0.083$ m/s, $0 \leq U_\infty \leq 5$ m/s, $7 \leq P \leq 24$ mm, $0.8 \leq D \leq 3.6$ mm, $0.6 \leq t_{abs} \leq 6.5$ mm, $0.15 \leq k_{abs} \leq 200$ W/mK.

2.6.3 Other UTSC Studies

Gawlik, Christensen and Kutscher (2005)

The research conducted on UTSCs heat exchange effectiveness by Golneshan and Hollands (1998), Arulanandam et al. (1999) and Van Decker et al. (2001) demonstrated that plate conductivity had an important effect on the effectiveness, but only slightly influenced the collector efficiency. The effect of the plate conductivity was studied in depth by Gawlik et al. (2005) who compared numerically and experimentally the performance of a plate of high-conductivity (aluminum) and a plate of low-conductivity (styrene). Both panels were flat and perforated with holes on a triangular layout. The two plates showed comparable efficiencies under similar conditions. This result was explained by the fact that the holes on the plate are so close to each other that a large temperature gradient between the perforations cannot be supported. They extended their result to corrugated plates, by suggesting that the plate conductivity would not affect the performance of these kinds of panels since the height of a corrugation and the distance between two corrugations were much larger than the hole pitch. This was of great interest, because using materials of low conductivity could significantly decrease the cost of UTCs.

Gunnewiek, Brundrett and Hollands (1996)

Gunnewiek et al. (1996) numerically modeled flow in the plenum behind the UTSC, and considered the effect of six dynamic and geometrical parameters. The wall of the absorber plate was modeled as having homogenous suction. He found that a significant amount of heat transfer occurred in the plenum, and at low suction flow velocities, reverse flow could occur. The minimum suction velocity needed for preventing the reverse flow was studied by Gunnwiek (2002). He found that the suction velocity should increase in the presence of wind from 0.0125 m/s to 0.02 m/s.

Dymond and Kutscher (1997)

Dymond and Kutscher (1997) designed a computer model to find the effectiveness and the flow distribution for UTSCs using the pipe network analogy. The computer model they made allowed the designer to change the geometric parameters for the required design. The model included the friction pressure drop through the system, friction across the collector, friction in the plenum, and the acceleration of the fluid in the plenum. For the energy balance, they included solar radiation, convection heat loss, radiation heat loss to the sky and ground and the energy delivered to the air. They called their computer model TCflow and it was used by Conserval Engineering for their design of the solar wall.

Summers (1995)

Other studies were performed using other commercial software like TRNSYS (SEL 2005), such as the model developed by Summers (1995). His model solves a set of energy balance equations to predict the collector performance and to find the optimal amount of auxiliary energy needed for air going into the collector.

Chapter 3

Computational Domain Description

3.1 Introduction

In this chapter, the development of a numerical model of an actual Unglazed Transpired Solar Collector (UTSC) is described and validated. Initially, a general description of the problem to be studied is explained, followed by a description of the componential domain and boundary conditions. Then, a description of the meshing procedure is presented. The chapter also contains a study of mesh independence and initial comparisons to related studies.

3.2 Problem Description

The system which will be discussed here is a representation of the UTSC system Solarwall^{TM}; produced by Conserval Engineering Inc (2010). Figure 3.1 shows the whole UTSC system, which consists of a perforated and blackened absorber plate and a plenum (the area between the back wall and the plate).

The system operation of the UTSC is relatively simple. The absorber plate is installed in a location where it is exposed to solar radiation; heating the plate and surrounding air. This air is sucked through the perforations, through the plenum, and into the HVAC system where it is delivered to a traditional HVAC system before being supplied to the internal space. The flow is usually driven by a fan that is already a part of the existing HVAC system.

The present research is focused on examination of the flow and heat transfer around the front and the back sides of the absorber plate, with the intention of developing better models to be used for system design. The absorber is to be examined at different wind speeds and suction flow velocities to evaluate absorber plate heat losses in the entry region, and effectiveness in the asymptotic region. The wind is assumed to flow horizontally and parallel to the plate. Analysis of flow in the plenum is outside of the scope of this work.

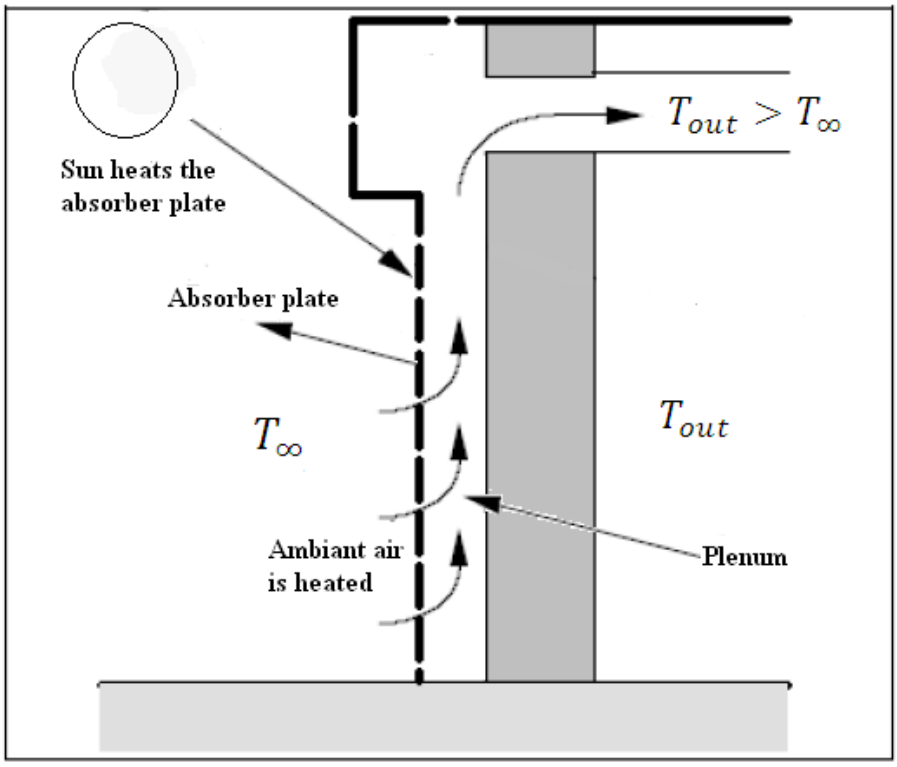

Figure 3.1: An Unglazed Transpired Solar Collector System in Operation.

3.3 Absorber Plate Geometry

As was previously mentioned, the geometry to be studied here reflects the Solarwall™ product produced by Conserval Engineering Inc (2010). Figure 3.2 shows a photo drawing of the geometry to be studied. To analyze this system, a CFD model was developed. Figure 3.3 is a rendering of the computation domain to be studied. Perforations were placed in an aligned position; three on the bottom plate and one on each side of the corrugation. As can be seen, the perforations consist of a semi-circular piece that is open on both ends. The arrangement of the perforations and their dimensions are presented in Figure 3.4.

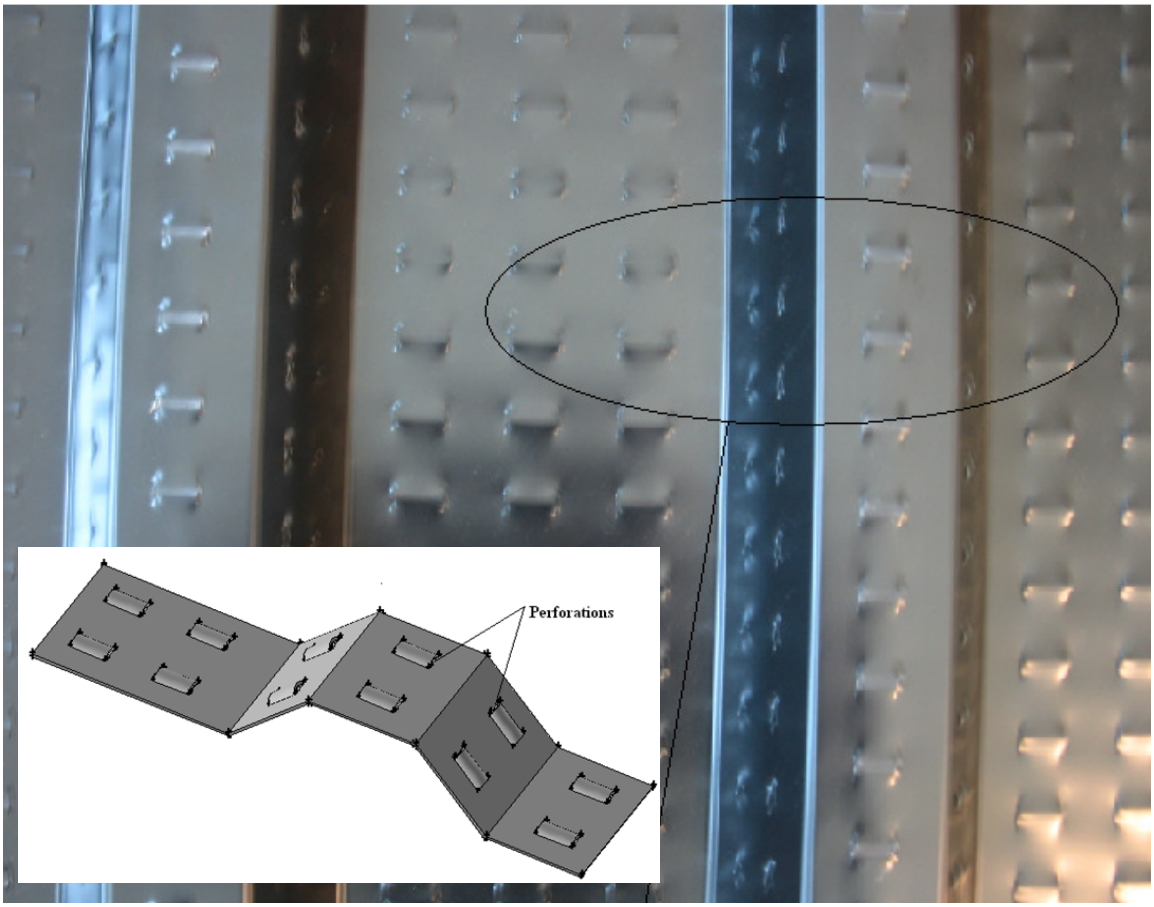

Figure 3.2: Photo and Rendering of Current Solarwall™ System.

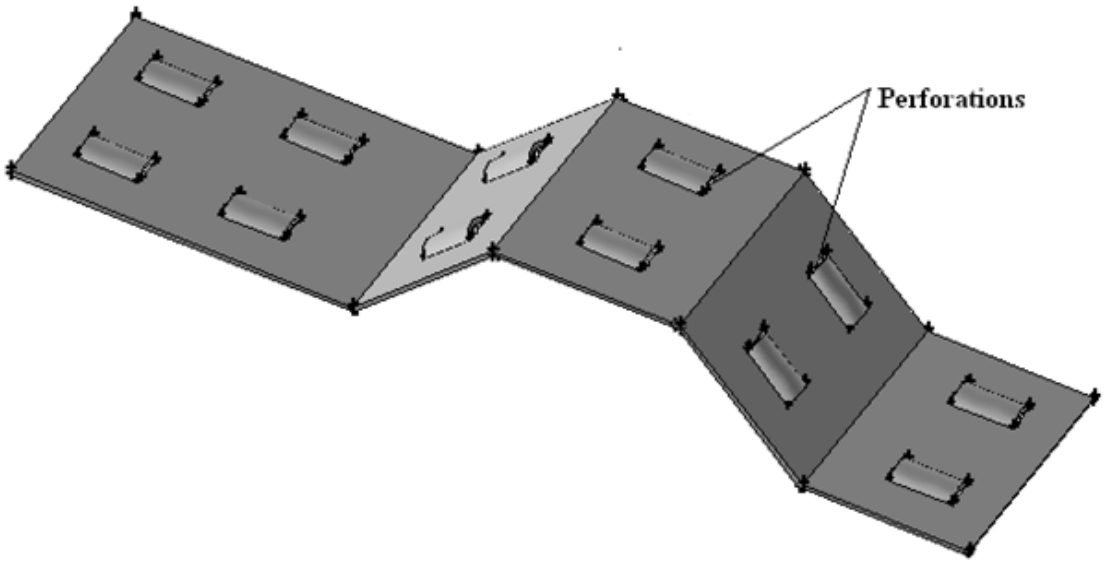

Figure 3.3: Rendering of Solarwall^{TM} System.

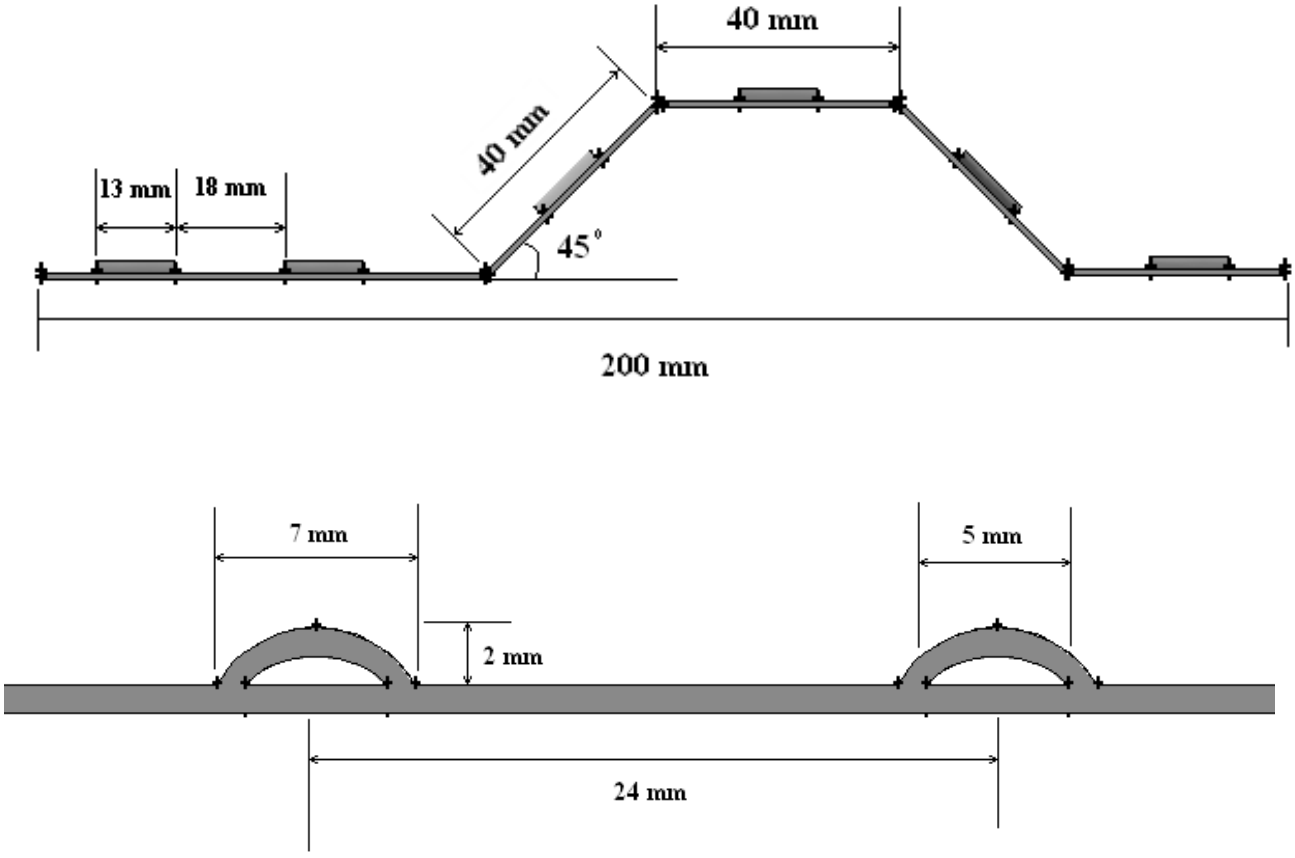

Figure 3.4: Horizontal (top) and Vertical (bottom) Cross Sections of Solarwall^{TM} System.

3.4 Numerical Model

3.4.1 Governing Equations

The governing equations used in the numerical simulation are the steady-state conservation of mass equation (Eqn. 3.1), momentum equations (Eqns. 3.2 to 3.4), and energy equation (Eqn. 3.5).

$$\frac{\partial}{\partial x}(\rho u) + \frac{\partial}{\partial y}(\rho v) + \frac{\partial}{\partial z}(\rho w) = 0 \tag{3.1}$$

$$\frac{\partial}{\partial x}(\rho uu) + \frac{\partial}{\partial y}(\rho uv) + \frac{\partial}{\partial z}(\rho uw) = -\frac{\partial p}{\partial x} + \mu\left(\frac{\partial^2 u}{\partial x^2} + \frac{\partial^2 u}{\partial y^2} + \frac{\partial^2 u}{\partial z^2}\right) \tag{3.2}$$

$$\frac{\partial}{\partial x}(\rho uv) + \frac{\partial}{\partial y}(\rho vv) + \frac{\partial}{\partial z}(\rho vw) = -\frac{\partial p}{\partial y} + \mu\left(\frac{\partial^2 v}{\partial x^2} + \frac{\partial^2 v}{\partial y^2} + \frac{\partial^2 v}{\partial z^2}\right) \tag{3.3}$$

$$\frac{\partial}{\partial x}(\rho uw) + \frac{\partial}{\partial y}(\rho vw) + \frac{\partial}{\partial z}(\rho ww) = -\frac{\partial p}{\partial z} + \mu\left(\frac{\partial^2 w}{\partial x^2} + \frac{\partial^2 w}{\partial y^2} + \frac{\partial^2 w}{\partial z^2}\right) \tag{3.4}$$

$$\frac{\partial}{\partial x}\left(\rho C_p uT\right) + \frac{\partial}{\partial y}\left(\rho C_p vT\right) + \frac{\partial}{\partial z}\left(\rho C_p wT\right) = k\left(\frac{\partial^2 T}{\partial x^2} + \frac{\partial^2 T}{\partial y^2} + \frac{\partial^2 T}{\partial z^2}\right) \tag{3.5}$$

Through the absorber plate itself, heat transfer is via conduction, so the governing equation is:

$$\frac{\partial T_{abs}}{\partial x^2} + \frac{\partial T_{abs}}{\partial y^2} + \frac{\partial T_{abs}}{\partial z^2} = 0 \tag{3.6}$$

Here, u, v, and w represent the fluid velocities in the x, y, and z directions respectively. *P* is the pressure.

A number of assumptions were made in formulating this model. It was assumed that the flow was laminar, air properties were constant, the viscous dissipation terms could be neglected, and that gravity could be neglected since the heat loss due to natural convention is very small as stated in Section 2.6.1.

Laminar Flow: The assumption of laminar flow was justified in two ways. First, as was discussed in Section 2.2.1, the work of Schlichting (1979) suggested that given sufficient suction, turbulent transition would not occur, and the flow would achieve asymptotic behavior. He derived Eqn. 2.2 to find the minimum suction velocity required to achieve these conditions. Considering the maximum wind velocity considered in this study (2.0 m/s), the minimum suction velocity needed to stabilize the flow would be $2.48 \times 10^{-4}\, m/s$. This is well below the minimum suction velocity considered of 0.01 m/s. It is noted that Schlichting's analysis was for homogenous suction through a flat plate; neither of which exists for the system being considered. More important are the previous experimental studies which showed that laminar and asymptotic behavior occurs (discussed in Section 2.6). In particular, the study conducted on sinusoidal plates by Gawlik and Kutscher (2002), observed that the flow followed a linear pattern of separation and reattachment (asymptotic flow). When they compared their results with numerical simulation, turbulent assumptions did not replicate flow behavior, while laminar assumptions did. It is noted that the models from the present work were also run using k-ω and k-ε models. Those models did not replicate the expected flow behavior either.

Constant Fluid Properties: The maximum temperature differences experienced in the system was on the order of 15-25^{o}C. Differences in air properties within this range were considered to be negligible.

Viscous Dissipation: The flow velocities considered in this work were small, and viscous dissipation terms were 2nd order. These terms were therefore deemed to have negligible impact on the model results.

3.4.2 Solution Domain and Boundary Conditions

The domain of the numerical simulation had two regions (Figure 3.5). Region (1) is the upper region where the plate was exposed to the environment, while Region (2) (Plenum) is located under the plate. Both regions were divided into a set of virtual volumes to facilitate the use of a structured mesh. Separating these two regions was the absorber plate. The absorber is a solid region of 1 mm thickness with a thermal conductivity equivalent to aluminum ($k = 202\ W/m.k$). Air is sucked through the perforations in the absorber plate from Region (1) to Region (2).

Two versions of the numerical simulation were used in the present analysis. The first was used to consider heat loss and effectiveness when wind was present (Figure 3.5). To get an accurate indication of the flow behavior before and after the corrugations, one of the perforations was placed before the corrugation, and the other two were placed after. The second was used to evaluate effectiveness under no-wind conditions (Figure 3.6). In this situation, the corrugation would have a negligible effect, and the solution domain could be simplified.

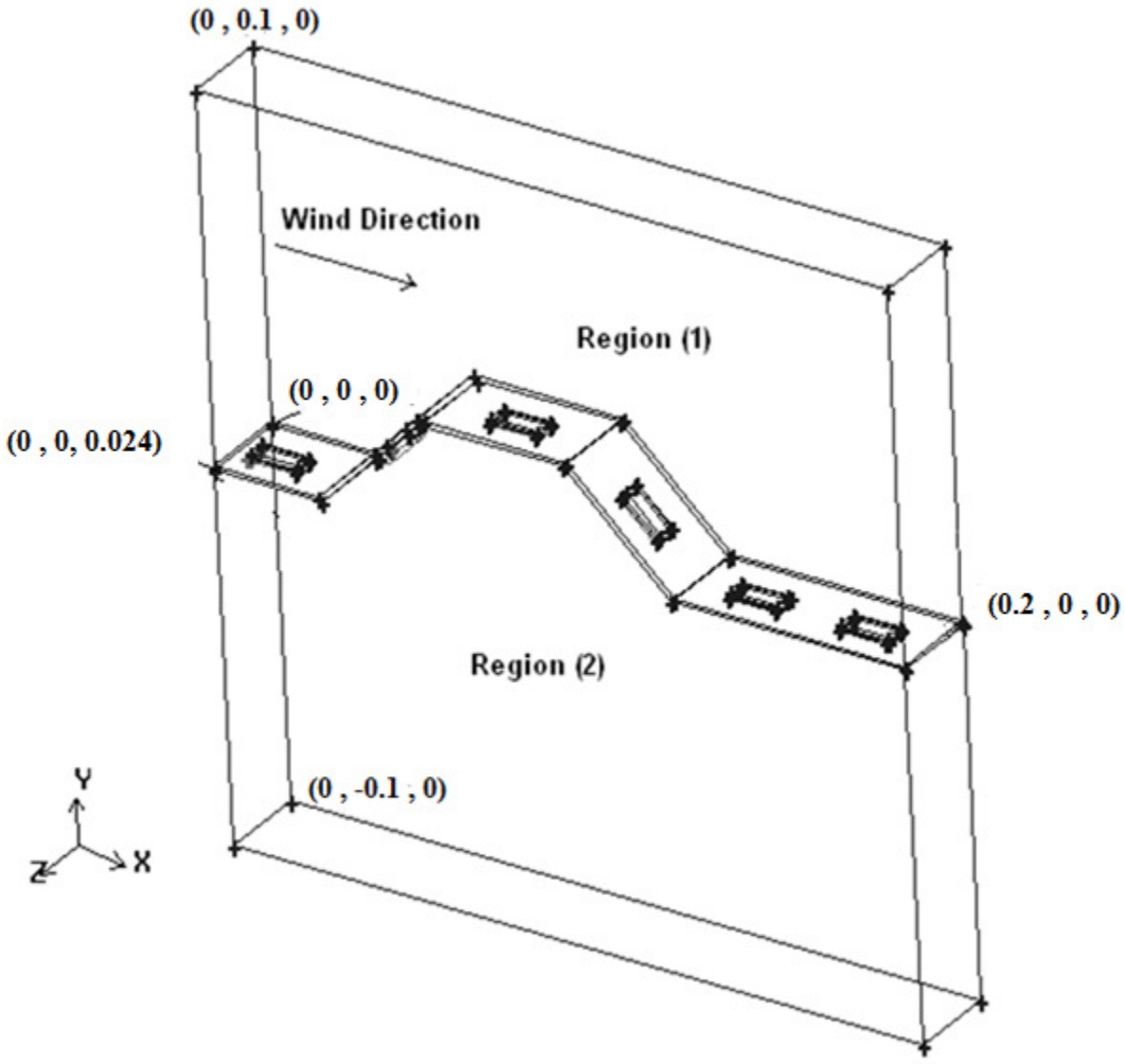

Figure 3.5: Solution Domain of the Numerical Model for Cases where Wind was Present.

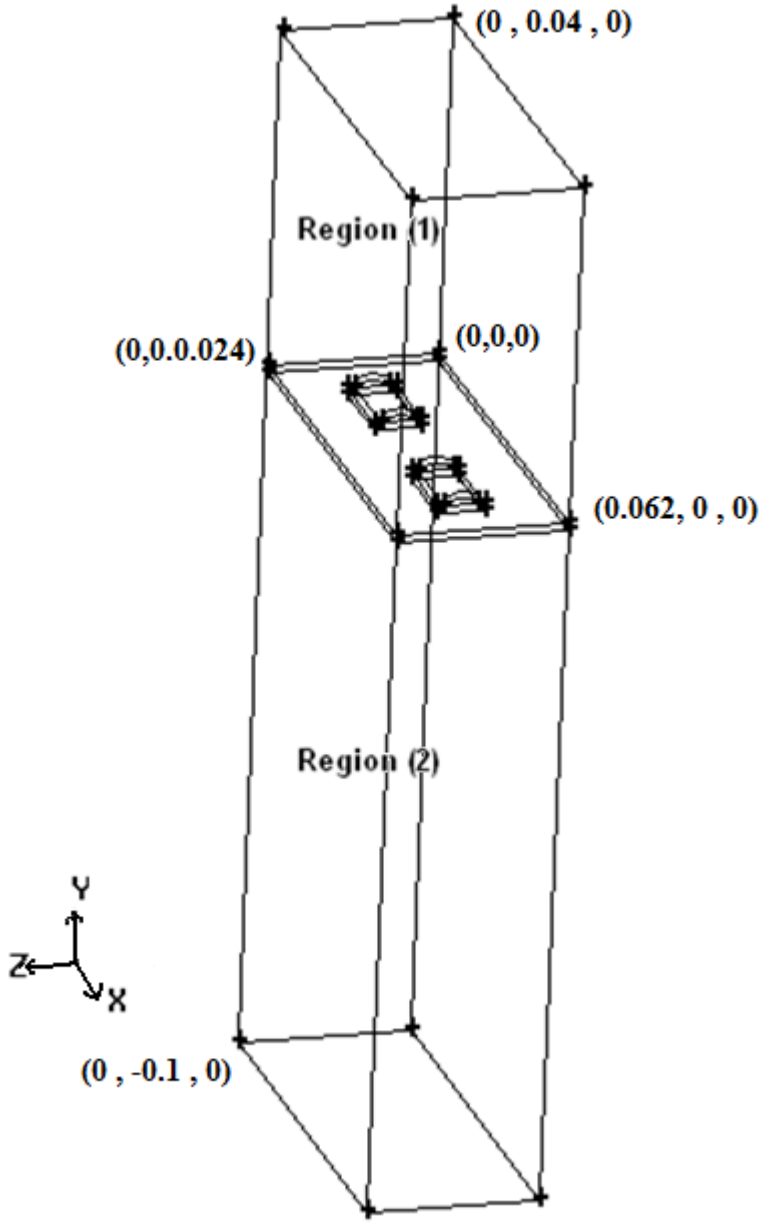

Figure 3.6: Solution Domain of the Numerical Simulation for Cases where No Wind was Present.

3.4.2.1 Boundary Conditions: Wind

Referring to Figure 3.5, the boundary conditions for analyzing heat loss and effectiveness when wind was present are as follows:

- Planes x=0 and x=0.2 in Region 1 are assigned periodic boundaries. This means that the inlet and outlet temperature and velocity profiles must be the same. This allows for simulation of the asymptotic region. This option requires that the user set the mass flow rate between the periodic boundaries. This was done and adjusted to achieve the desired ambient flow velocity. In Region 2, these planes are specified as symmetry. This means that there is no heat transfer or fluid flow across these boundaries.
- At plane y=0.1, an ambient pressure inlet boundary is used to allow for the entrainment of ambient air at a specified temperature of 300K. It is noted, as discussed in Section 2.2.1, that the work of Arpaci and Larson (1984) can be used to estimate the velocity boundary layer thickness in the asymptotic region (i.e. its maximum thickness). Using Eqn. 2.5 with the minimum suction velocity considered of 0.01 m/s shows that the boundary layer thickness would be less than 1 mm. This was, however, for a flat plate. If the 'hump' in the absorber is considered, the boundary layer would protrude as much as 7 cm above y = 0. The outer domain of 10 cm was set ensure that the upper boundary did not interfere with the numerical solution.
- Plane y=-0.1 is modeled as a velocity outlet with the velocity set to match the desired suction velocity.
- Planes z=0 and z=0.024 are specified as symmetry.
- The absorber plate is modeled as a solid with a heat generation rate of 500 W/m^3.
- The surfaces of the absorber plate are modeled as no slip walls.

3.4.2.2 Boundary Conditions: No-Wind

Referring to Figure 3.6, the boundary conditions for analyzing effectiveness from the absorber when no wind is present are as follows:

- Planes x=0 and x=0.062 in Regions 1 and 2 are specified as symmetry.
- At plane y=0.1, an ambient pressure inlet boundary is used to allow for the entrainment of ambient air at a specified temperature of 300K.
- Plane y=-0.1 is modeled as a velocity outlet with the velocity set to match the desired suction velocity.
- Planes z=0 and z=0.024 are specified as symmetry.
- The absorber plate is modeled as a solid with a heat generation rate of 500 W/m^3.
- The surfaces of the absorber plate are modeled as no slip walls.

3.4.3 Meshing Procedure

The grid generation software (Gambit 2005) was used to mesh the solution domain.

Originally, an unstructured mesh was used with the application of a size function. This approach, however, was problematic. If the mesh was refined to provide adequate detail inside and around the perforations, the resulting mesh density elsewhere would result in too many mesh elements to allow reasonable run times.

Body Fitted Co-ordinates (BFC) was used to produce the mesh. The method of using BFC depends on splitting the domain into hexagonal volumes, and then mapping the surfaces of these volumes. This approach allows for good geometric representation, the possibility of refinement study near surfaces and high gradient places (like perforations), and appropriate meshing of curved surfaces and boundary layers with wall functions.

Discretization of the numerical simulation can result in errors in the model results. Too course a mesh, can result in lack of convergence or inaccurate solutions, while too fine a mesh results in excessive solution times. To determine an adequate mesh density, therefore, a mesh refinement study is required. Often, this study is performed by doubling number of grids repeatedly until such time that further grid refinements produce no appreciable change in simulation results. For the current work, however, this procedure was found to be prohibitive. For the three dimension domain, the number of grids will be doubled in three directions. In this case, however, the refinement was performed in high gradient flow regions such as perforations and at fluid-solid interfaces.

To evaluate the required mesh density for heat loss analysis, a high wind velocity (2 m/s) and low suction velocity (0.01 m/s) was chosen. This case should result in separated flow, and a fairly complex flow structure. The average temperature and heat losses across the periodic boundaries were compared. Table 3.1 shows these parameters as a function of the mesh density.

Table 3.1: Heat Loss and Wind Outlet Temperature versus Mesh Density.

Number of grid elements	Wind temperature (K)	Heat loss (W/m)
1041379	300.73	349
1972139	300.92	463
2489851	300.96	490

As can be seen, the calculated heat loss is very sensitive to minute changes in outlet temperature. As such 1972139 elements were chosen. This mesh was also applied to the effectiveness models.

The same mesh densities were used to compare the calculated effectiveness in the no-wind model. In case, a suction velocity of 0.01 m/s was used. Table 3.2 shows the results of this analysis.

Table 3.2: Calculated Effectiveness versus Mesh Density.

Number of grid elements	Effectiveness
181440	84.2
316480	85.1
488960	85.3

Figures 3.7 and 3.8 show the final mesh at the absorber surface for the periodic boundaries and over the perforations. Black lines show the fluid regions (ambient flow and perforation), while. gray regions represent the absorber surface.

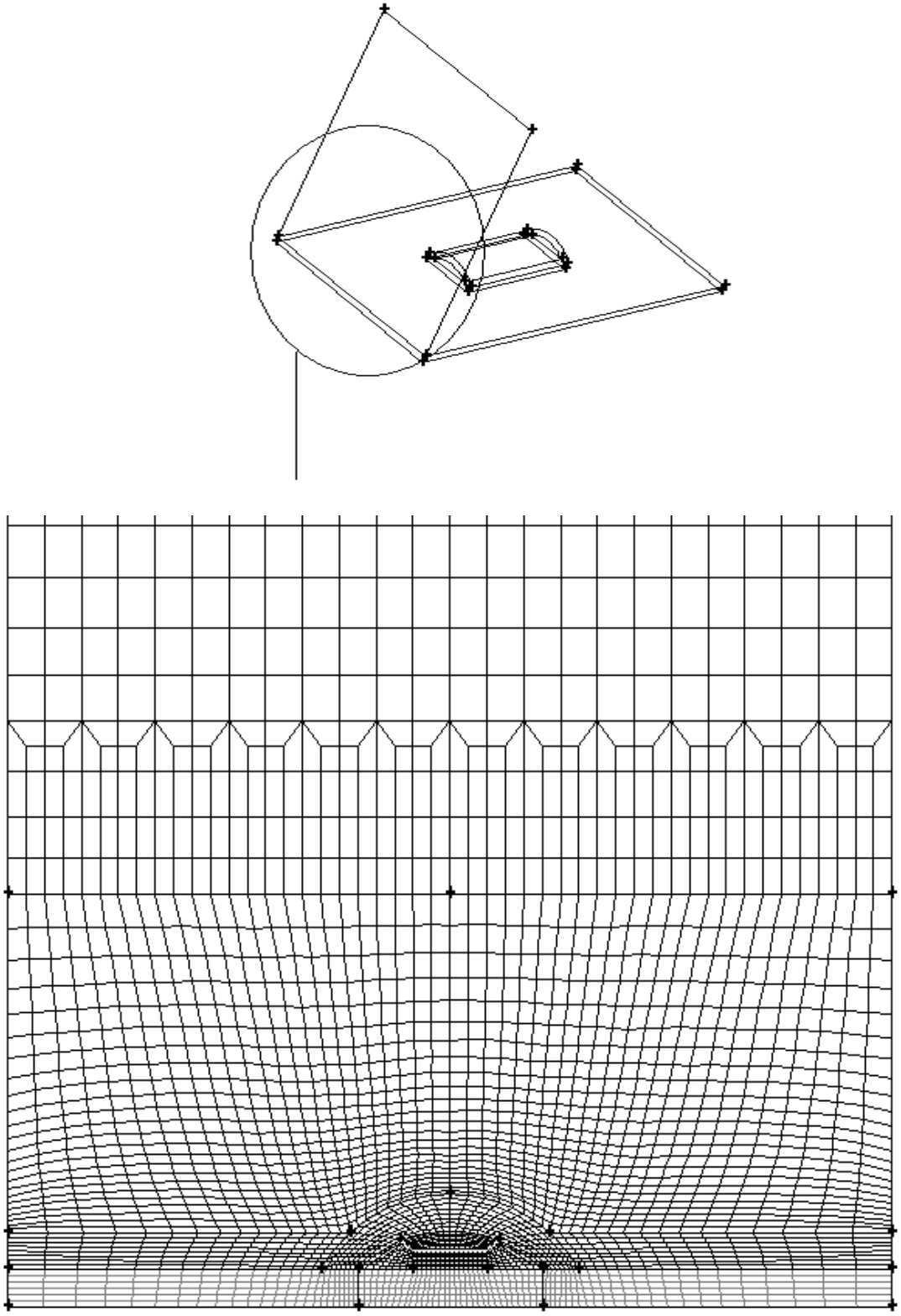

Figure 3.7: Meshing Scheme at the Absorber Surface for the Periodic Boundaries.

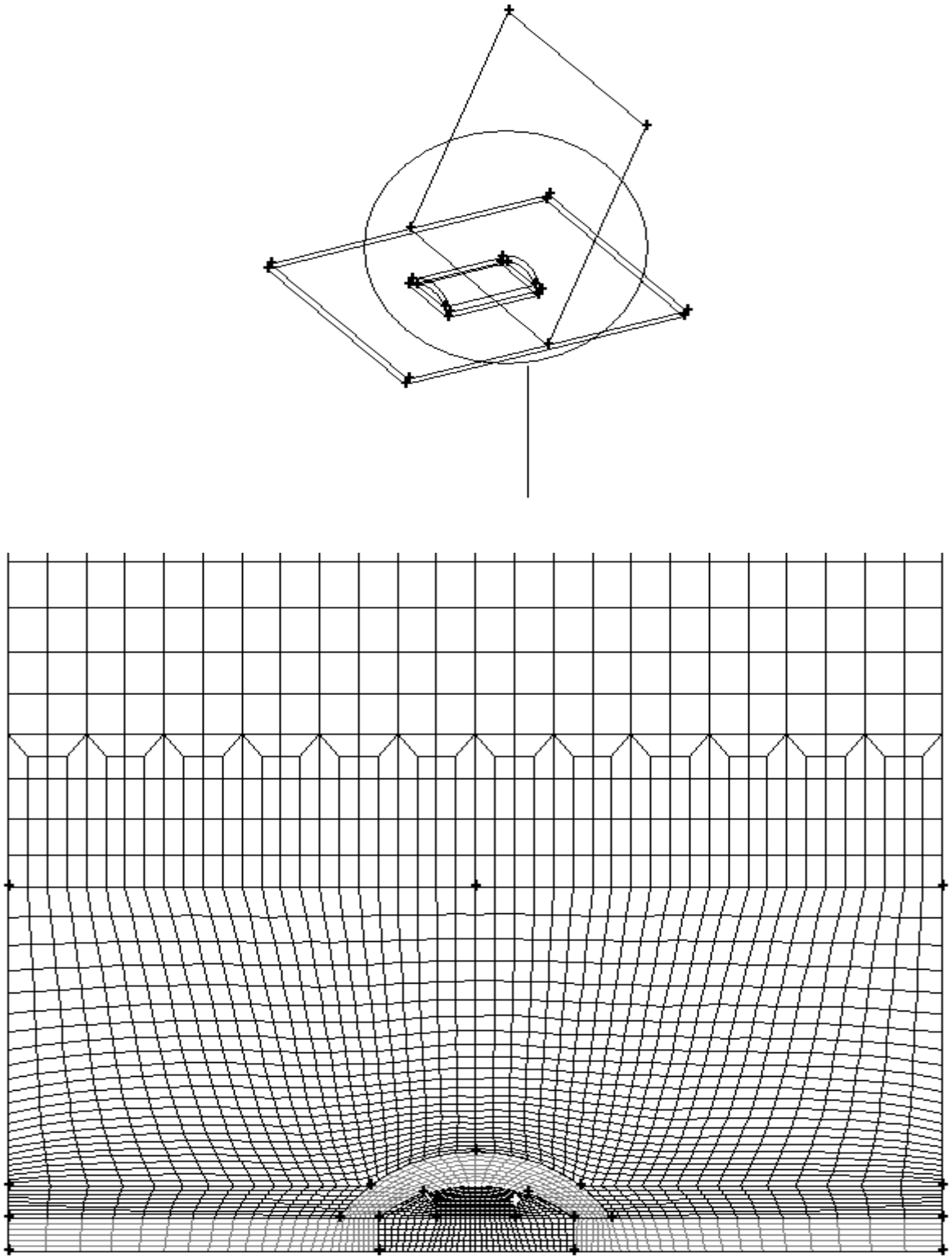

Figure 3.8: Meshing Scheme at the Absorber Surface over the Perforation.

3.4.4 Solution Methodology

The governing equations were solved numerically with the specified boundary conditions using Fluent software (FLUENT 2005). The numerical model was executed using the following steps

- Build the solution domain as per Section 3.4.2.
- Generate the mesh as per Section 3.4.3.
- Set the fluid and solid properties. All properties were taken at 300 K.
- Selection of laminar flow behavior as justified in Section 3.4.1.
- Selection of the method of accuracy for the discretization. For all of the simulations, a second order upwind scheme was chosen.
- Selection of the solution tolerance. The convergence criteria was set to be 10^{-3} for the mass and momentum equations, and 10^{-6} for the energy equation. Fluent States these values are sufficient for most of the fluid problems (FLUENT 2005).

Appendix A describes the procedure for solving the numerical domain used in FLUENT.

Both heat loss in the entry region, and effectiveness in the asymptotic region, were determined from these results. Heat loss can be determined by considering the thermal energy contained in the boundary layer. Convective heat loss will contribute to thermal boundary layer growth. Therefore, with reference to Figure 3.9, the difference in the energy at the start of the asymptotic region, and at the leading edge of the absorber plate, will be the heat loss. These numbers can be obtained directly from the results using the FLUENT post processing software (FLUENT 2005). This heat loss was assumed to occur over the same starting length given by Kutscher (1992) in Eqn. 2.6.

Effectiveness was easily determined from the numerical simulation. It was calculated using:

$$\varepsilon = \frac{T_{out} - T_\infty}{T_{abs} - T_\infty} \tag{3.7}$$

where T_{out} is the air temperature leaving the plenum.

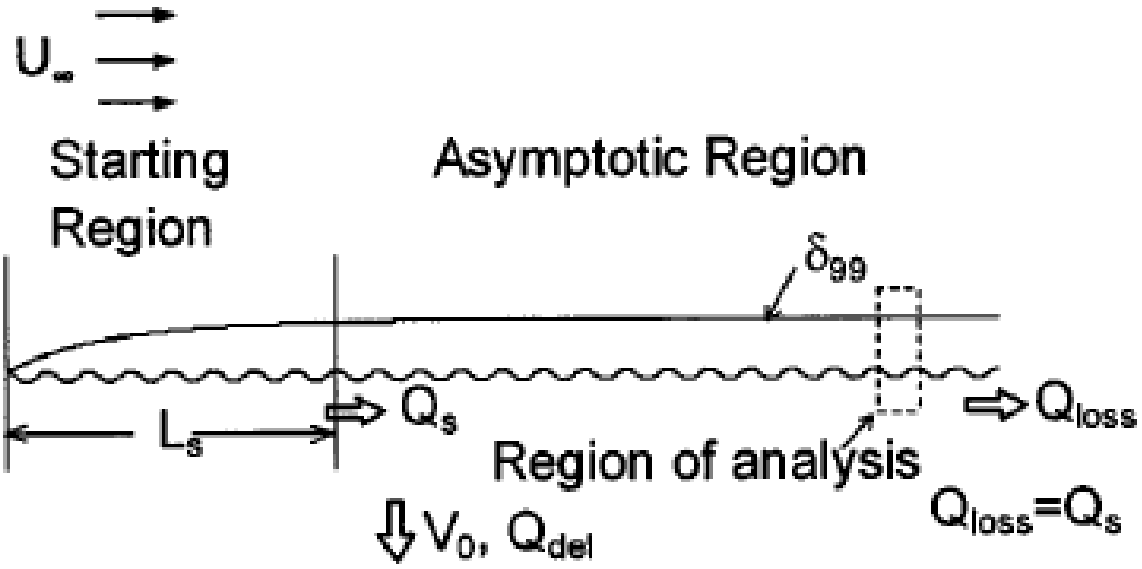

Figure 3.9: Boundary Layer Developing over a Sinusoidal Absorber Plate (Gawlik and Kutscher 2002).

3.5 Model Validations

To create confidence in the numerical simulation, numerical output was compared to similar studies found in the literature. A comparison with experimental studies of effectiveness (Kutscher 1992) and wind heat loss (Gawlik and Kutscher 2002) were selected. Further, flow structures produced could be compared to the work of Chen et al. (2006) for flow over a backward facing step.

3.5.1 Comparisons to Kutscher (1992)

Kutscher's (1992) experimental study of USTC effectiveness was described in Section 2.6.1. In that work, he tested flat UTSCs with circular perforations with porosities from 0.5% to 2%. The absorber plate modeled in the present work has a porosity of 1%. Hence, a comparison at the same porosity could be made. The comparison was limited to the no wind condition because the modeled absorber was corrugated. In the absence of wind, the corrugation should not play any role. The only difference between the numerical and experimental results is in the shape of the perforations.

The comparison of effectiveness is shown in Figure 3.10. The results from the current numerical simulation slightly underestimate the effectiveness of the absorber plate with around 3%. Given the difference in perforation shape, however, this was deemed acceptable.

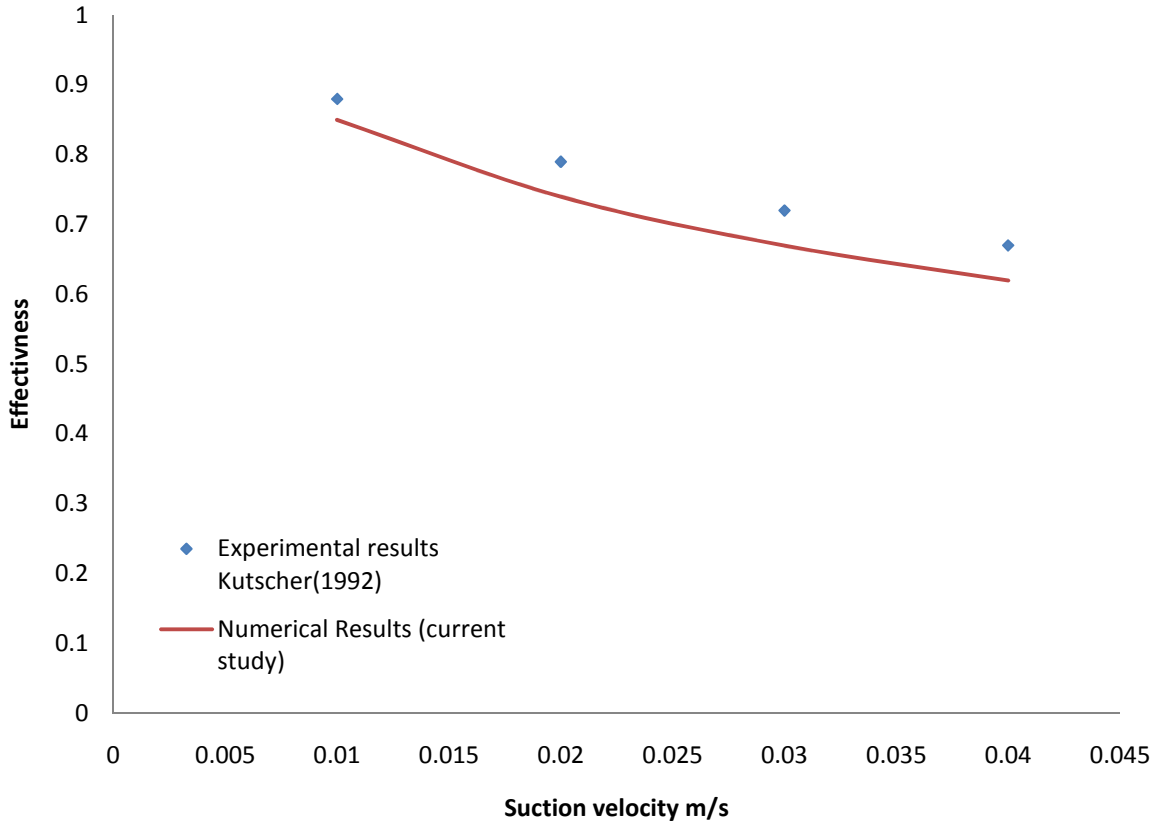

Figure 3.10: Effectiveness Comparison Between Present Numerical Analysis and the Experimental Results of Kutscher (1992).

3.5.2 Comparisons to Gawlik and Kutscher (2002)

Gawlik and Kutscher's (2002) experimental study of UTSC heat loss was described in Section 2.6.1. They evaluated heat loss from a sinusoidally corrugated absorber plate, and produced a correlation that included the pitch and amplitude of the corrugation. Their correlation was also a function of the heat loss from a flat and corrugated plate, which includes porosity, wind speed, and suction velocity.

Numerical results were obtained for the following conditions:

- porosity of 1%
- pitch of 200 mm
- amplitude of 28.3 mm
- a wind speed of 2 m/s
- suction velocity of 0.01 m/s

The only difference in the comparison, therefore, is the shape of the corrugation (Figure 3.11).

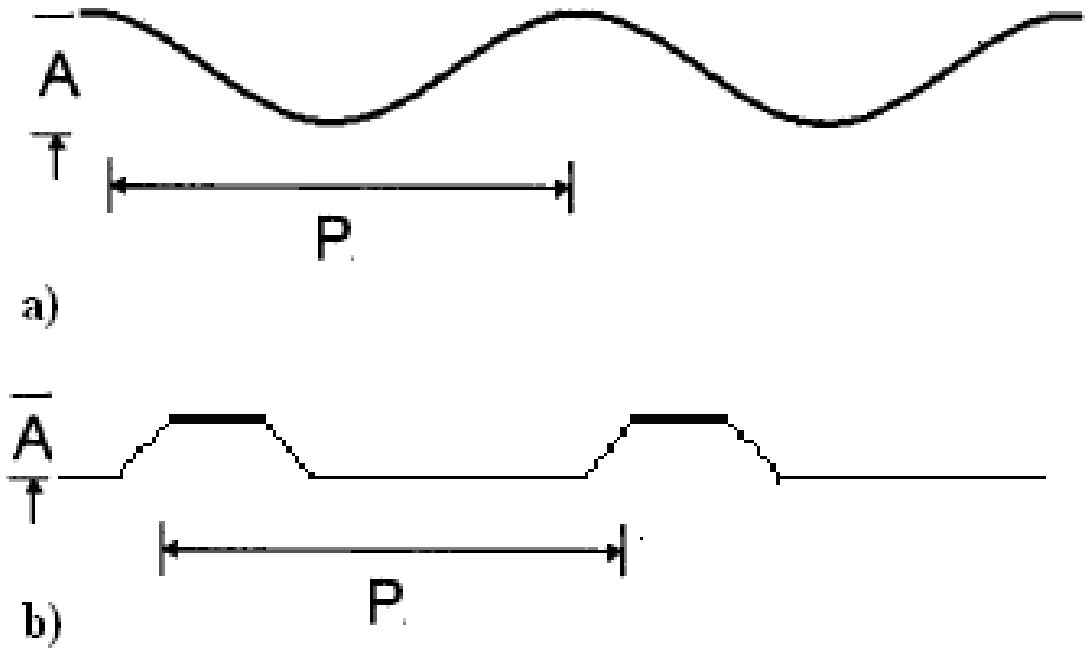

Figure 3.11: Corrugation Shape (a) Gawlik and Kutscher (2002) (b) Present Study.

Using the given conditions, wind heat loss from the numerical work is 488 W/m, compared to 432 W/m from Gawlik and Kutscher's (2002) model. Given the difference in geometry, however, this was deemed acceptable.

3.5.3 Comparisons to Chen et al. (2006)

Chen et al. (2006) numerically simulated flow over backward facing steps; including one at a 45 deg tilt (see Section 2.5). There are significant differences between the present work and the work of Chen et al. (2006). They did not examine a perforated surface with suction, and their flow was ducted. Further, in the current system, the will flow up a forward facing step, and therefore have some vertical momentum at the top of the step. Still, if the numerical model is run without suction, and with an imposed uniform velocity profile at the entrance, similar flow structures should result.

Figure 3.12 shows the numerical results for a wind speed of 2 m/s and without suction. The results are qualitatively comparable.

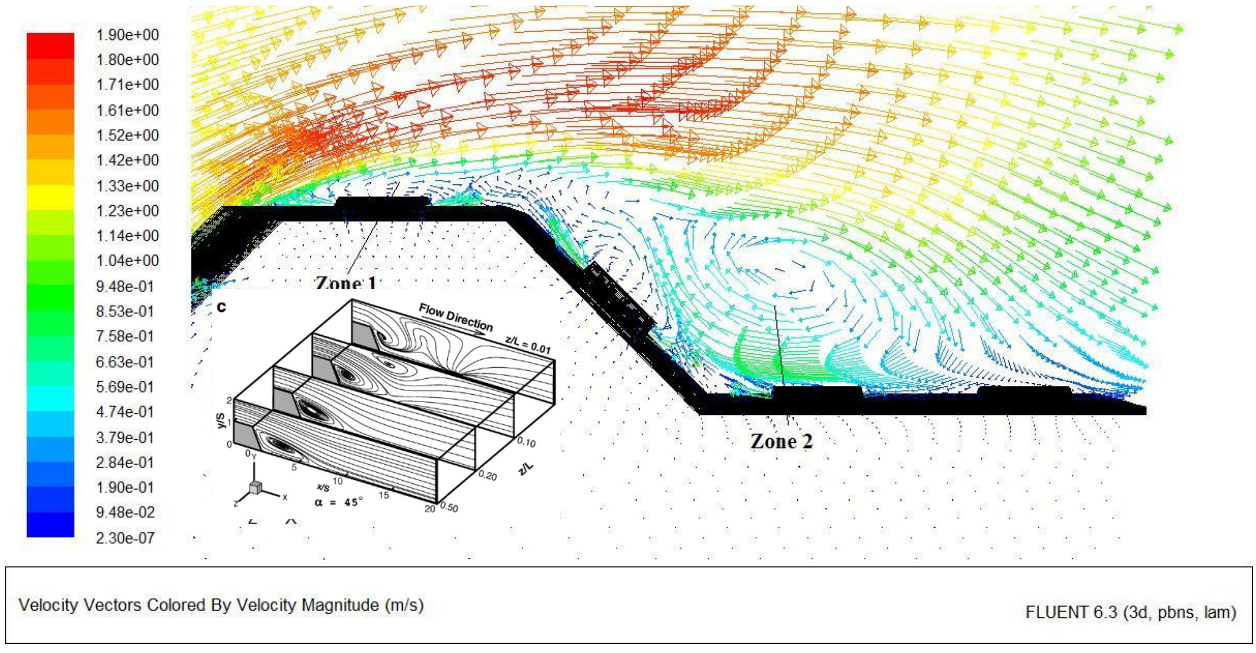

Figure 3.12: Velocity Vectors for 2 m/s Wind Velocity without Suction. Inset shows the results from Chen et al. (2006)

Chapter 4

Results and Discussion

4.1 Introduction

In this chapter, the numerical model developed in Chapter 3 will be used to examine UTSC performance. Initially, a general analysis of the effects of the corrugation and suction velocity or flow characteristics will be considered. These comparisons mainly focus on the formation of separated or attached flows, and the conditions at which they occur. Next, heat loss in the entry region (when wind is present) will be examined. Finally, the effectiveness of the absorber for a number of flow and suction conditions will be considered. A correlation for heat exchanger effectiveness is developed and presented. The correlation is compared to the accepted correlation of Van Decker et al. (2001).

UTSC performance is considered under realistic operating conditions. Wind velocities of 0, 0.5, 1 and 2 m/s, and suction velocities of 0.01, 0.02, 0.03, and 0.04 m/s were chosen to represent the typical values found in a real installation.

4.2 Attached and Separated Flows

One of the main issues observed in the flow behavior is the occurrence of separation and reattachment of the flow. The extent of the separation and reattachment, and its effect, depends on the wind and suction velocities, and the absorber plate geometry.

To examine the extent at which separation might occur, a no-suction case was first examined. It is noted that this condition is purely for comparative purposes, and the situation where no suction is present in the plate is of no value to typical UTSC operation. Furthermore, under these circumstances the flow will constantly develop as it flows over the absorber, and it will eventually transition to turbulence. As such, uniform wind velocity profiles of 0.5, 1 and 2 m/s were considered at the absorbers leading edge (i.e. the periodic boundaries described in Section 3.4.2.2 were not used), and laminar flow behavior was used. These velocities correspond to Reynold's numbers (based on wind speed and corrugation height) of 878, 1756, and 3513. Figures 4.1 to 4.3 show the velocity vectors predicted by the numerical model.

At all three of the tested wind speeds, separation of the flow occurred downstream of the corrugation. As would be expected, the recirculation zone varied in shape and size. At a wind speed of 0.5 m/s (Figure 4.1), a small recirculation zone occurs at the point where the flow leaves the peak of the corrugation (Zone 1). At a wind speed of 1 m/s (Figure 4.2), the same phenomena takes place, and a small recirculation zone occurs at the point where the flow leaves the peak of the corrugation (Zone 1). Moreover, a second recirculation zone is seen to occur just above the surface of the absorber plate (Zone 2). This recirculation zone occurs due to the velocity gradient

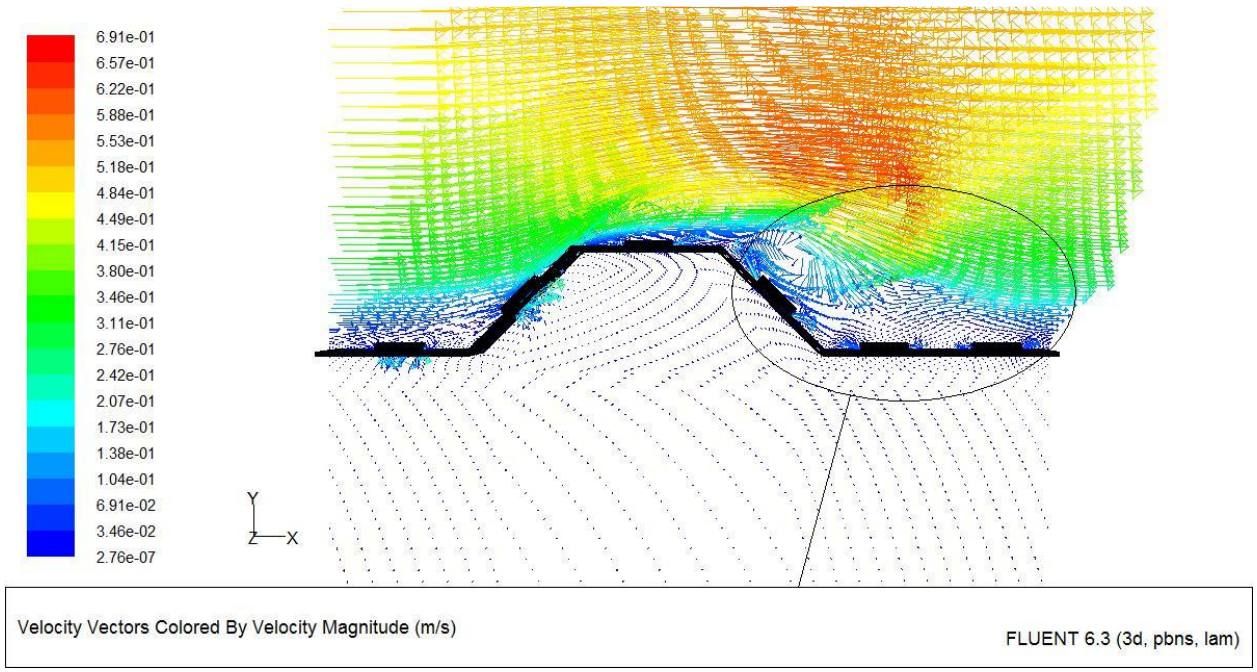

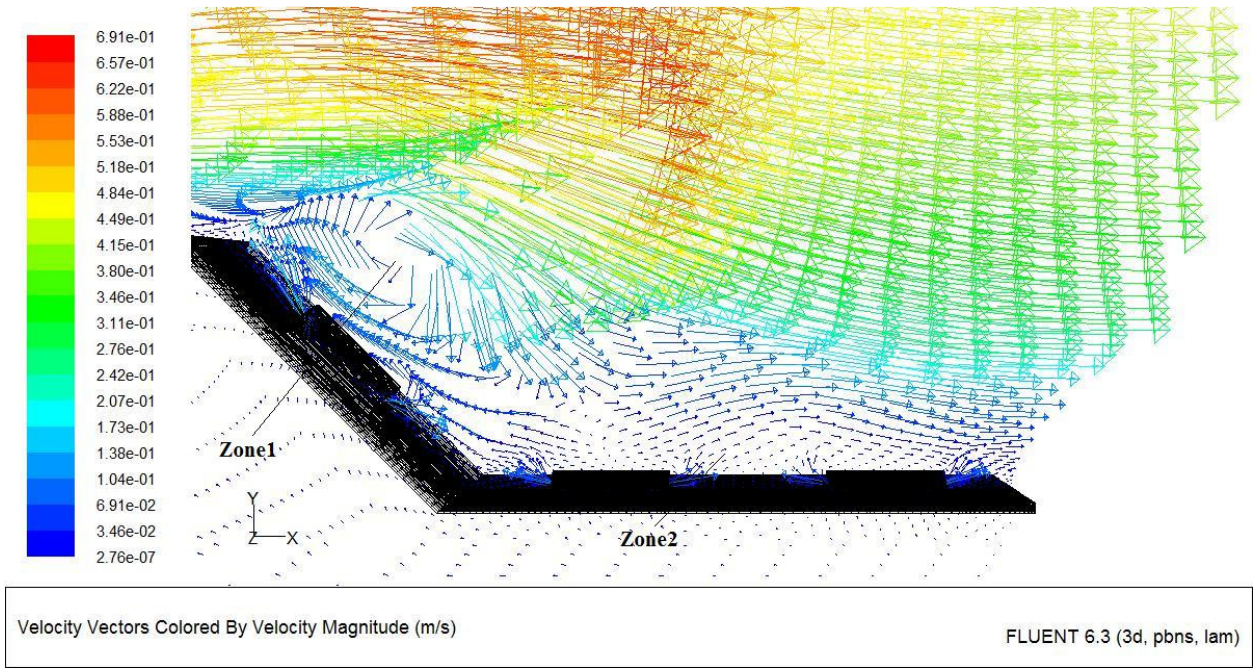

Figure 4.1: Flow Behavior at a Wind Speed of 0.5 m/s and with No Suction.

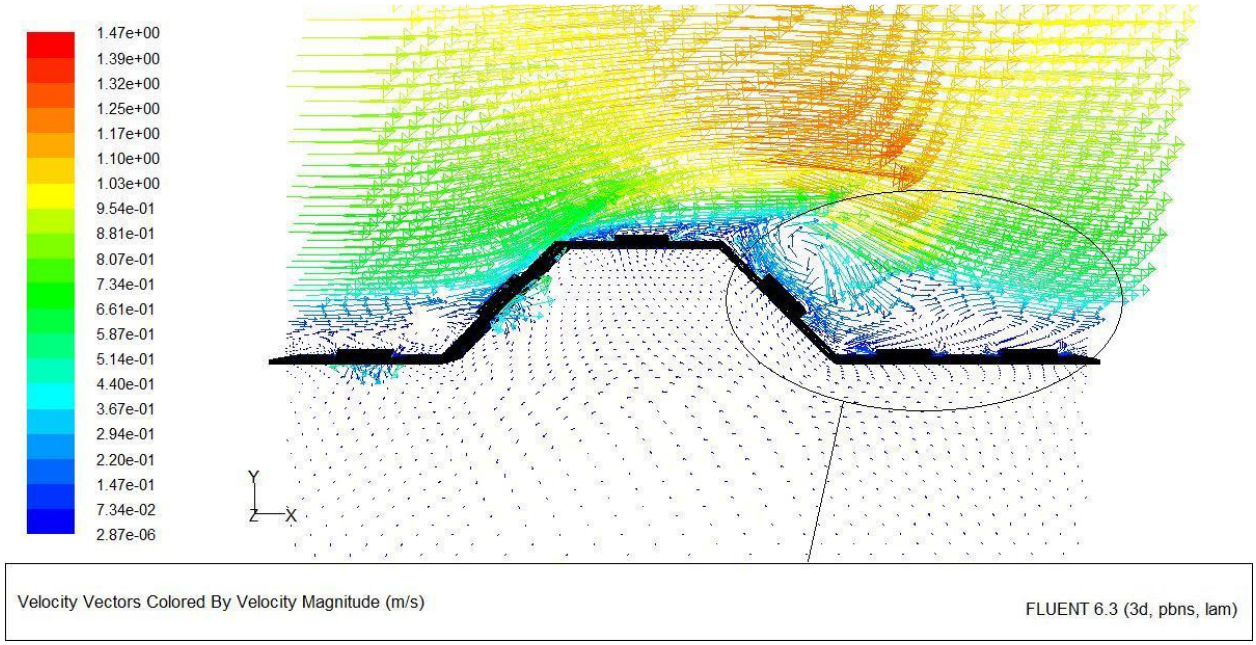

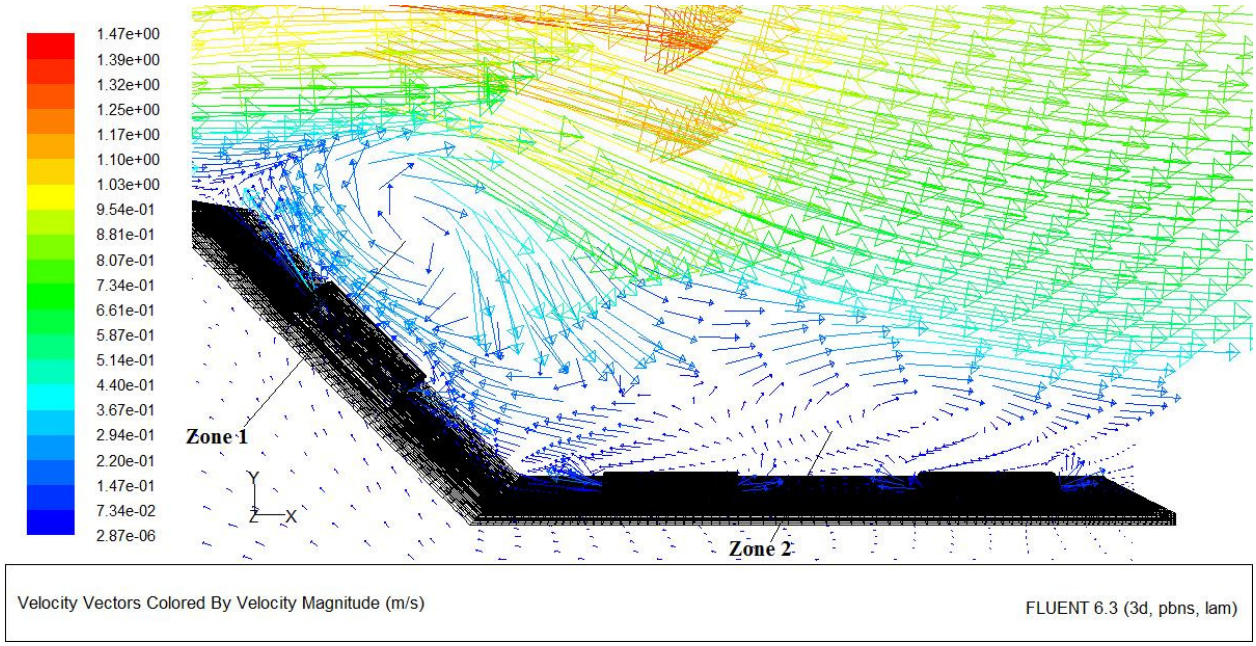

Figure 4.2: Flow Behavior at a Wind Speed of 1.0 m/s and with No Suction.

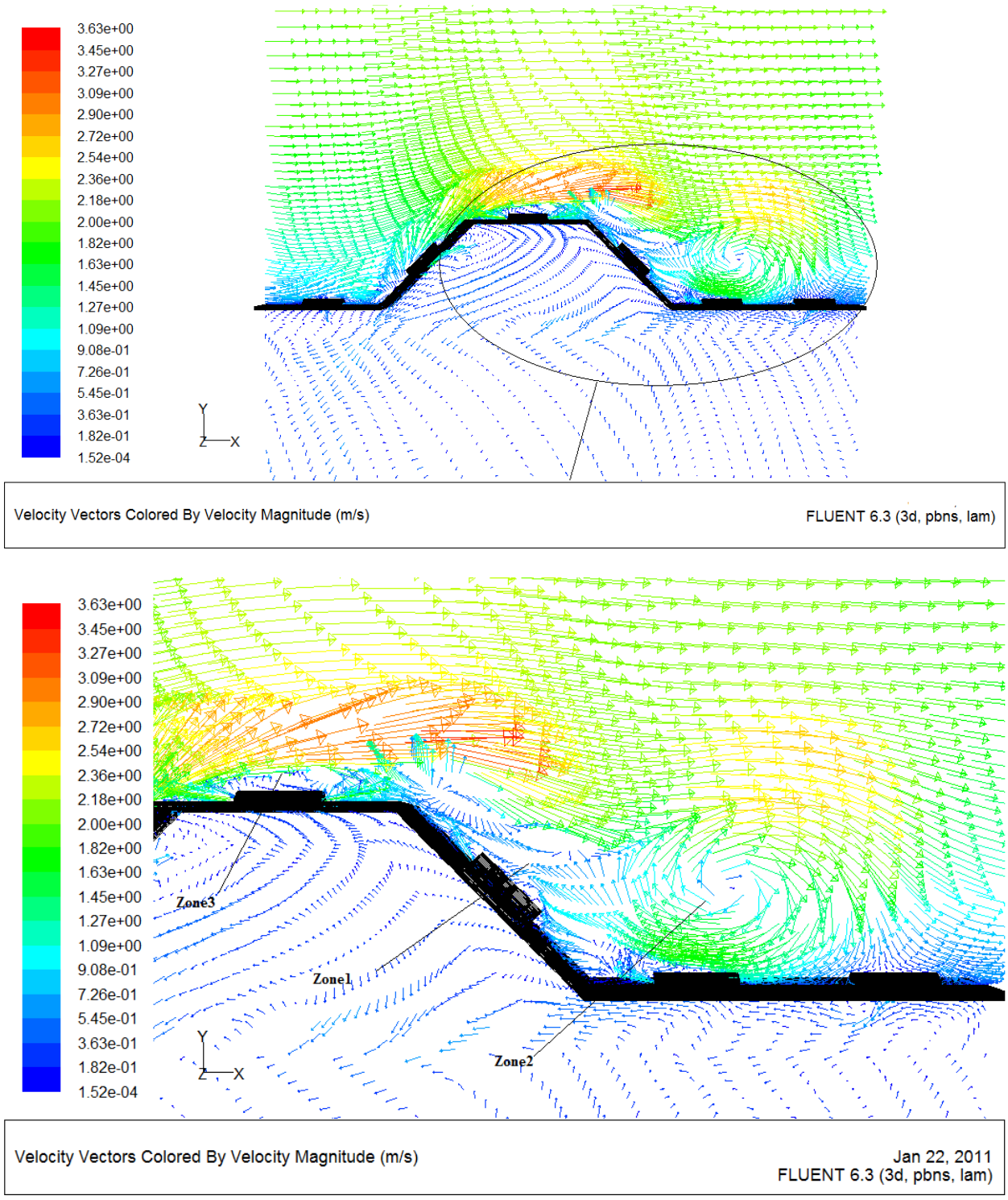

Figure 4.3: Flow Behavior at a Wind Speed of 2.0 m/s and with No Suction.

near to the surface of the absorber plate. At a wind speed of 2 m/s (Figure 4.3), three recirculation zones are seen to develop. The recirculation zones located behind the corrugation (Zones 1 and 2) were again seen to develop, where the recirculation at Zone 2 has increased in size due to the higher gradient of velocity that exists near to the absorber plate. In addition, a third separation occurs at the peak of the corrugation (Zone 3).

The application of suction on corrugated surfaces should have a stabilizing effect on the flow. The work of Gawlik and Kutscher (2002), however, showed that while laminar behavior was present, flow separation could still occur. As such, wind velocities of 0.5, 1 and 2 m/s were considered in the asymptotic region at suction velocities of 0.01, 0.02, 0.03, ad 0.04 m/s.

Figures 4.4 to 4.7 show examples of the difference in the recirculation zones at various suction velocities and wind speeds. A complete set of vector plots are given in Appendix B. Table 4.1 summarizes separated versus attached behavior.

Table 4.1: Observation of Attached and Separated Flow Regimes.

	Suction Velocity			
Wind Speed	0.01 m/s	0.02 m/s	0.03 m/s	0.04 m/s
0.5 m/s	Separated	Separated	Attached	Attached
1.0 m/s	Separated	Separated	Separated	Separated
2.0 m/s	Separated	Separated	Separated	Separated

In difference to the observations of Gawlik and Kutscher (2002), separated flow is the norm for the conditions studied. Only at the lowest wind speed, in combination with the two highest suction velocities, was attached flow seen to occur. When separation did occur, the size and position of the recirculation region was consistent between flow cases.

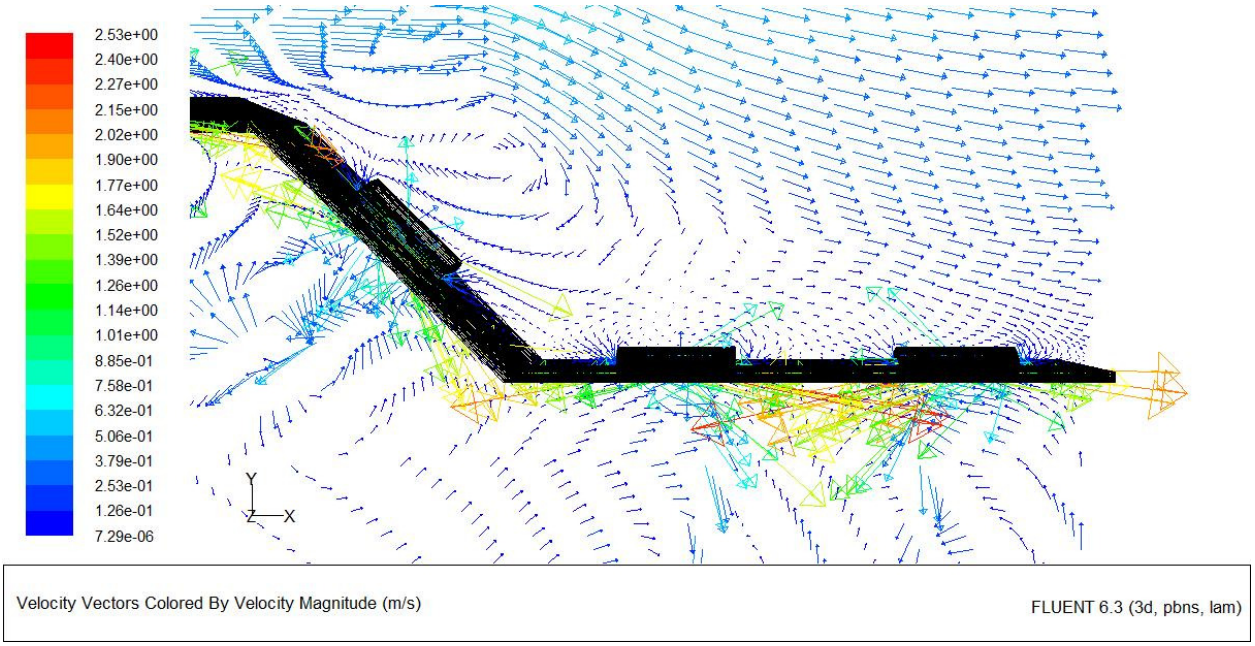

Figure 4.4: Flow Behavior at a Wind Speed of 0.5 m/s and Suction Velocity of 0.01 m/s.

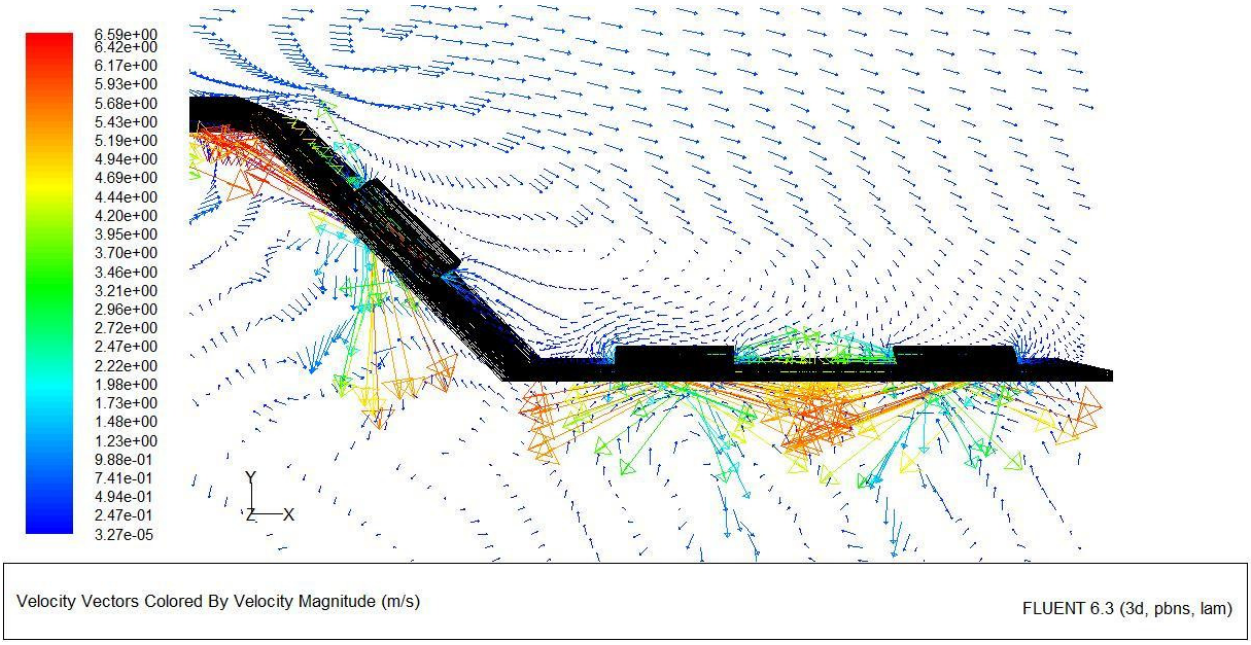

Figure 4.5: Flow Behavior at a Wind Speed of 0.5 m/s and Suction Velocity of 0.04 m/s.

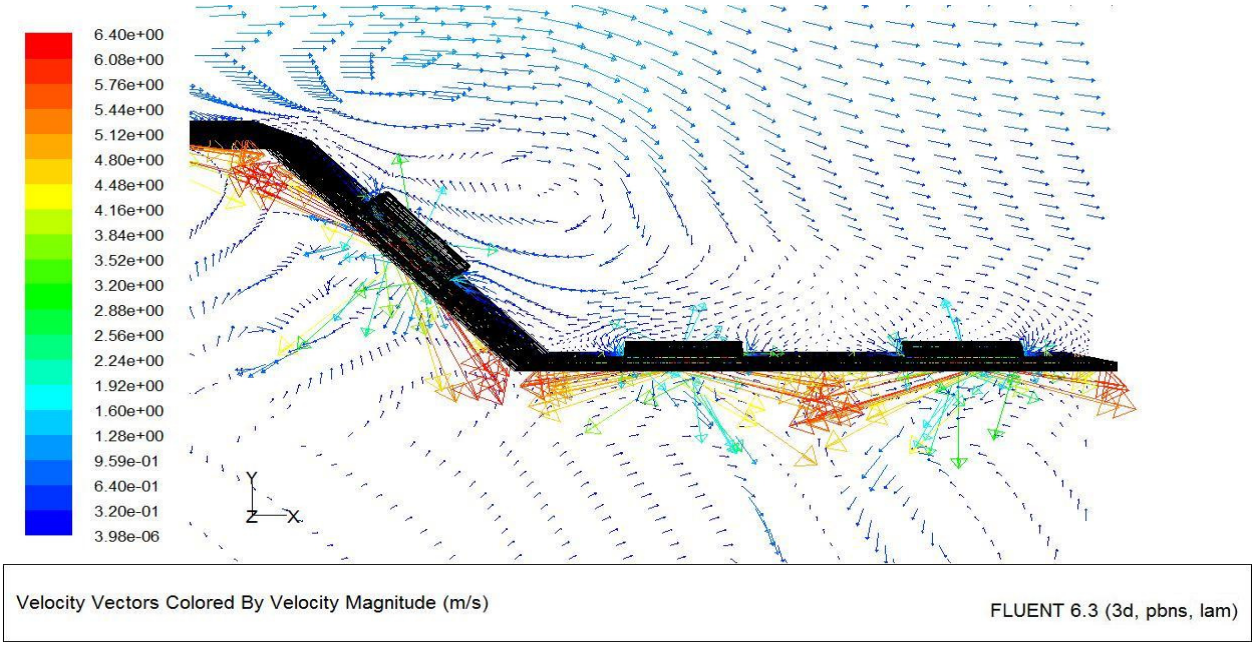

Figure 4.6: Flow Behavior at a Wind Speed of 1.0 m/s and Suction Velocity of 0.04 m/s.

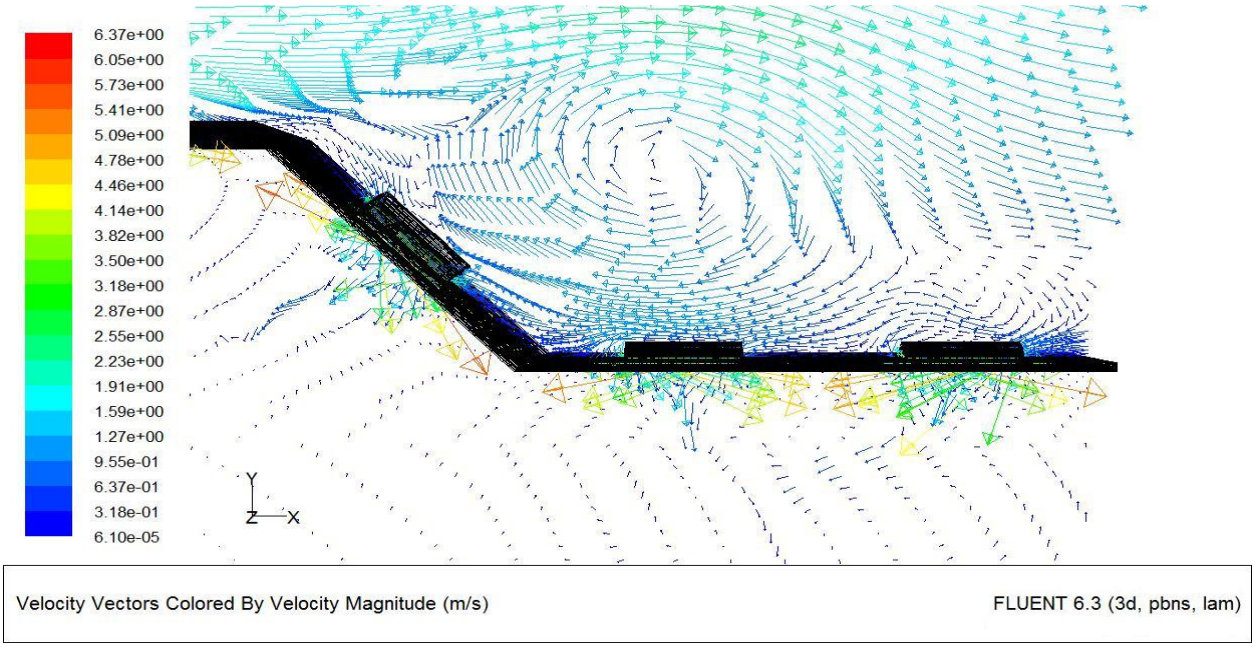

Figure 4.7: Flow Behavior at a Wind Speed of 2.0 m/s and Suction Velocity of 0.04 m/s.

4.3 Wind Heat Loss

As was discussed in Section 2.2, heat loss from the absorber plate occurs only in the entrance region where the velocity and thermal boundaries are developing. When the velocity boundary layer reaches the asymptotic region, there is no net convective heat loss from the absorber plate to the ambient, as indicated by the fact that the boundary layer is no longer increasing in size, and the free stream air temperatures entering and leaving the section have the same velocity and temperature profiles. Wind heat loss is a function of wind speed and suction velocity.

It is this later fact that allows for the estimation of heat loss in the entry region. By comparing the energy, q, in the flow that crosses the boundaries in the asymptotic region (perpendicular to the absorber and wind), to the energy crossing the ambient boundary at the leading edge, the energy loss can be determined. In both cases, this calculation is performed automatically by the Fluent Software (Fluent 2005) using:

$$q = \rho C_p W \int_0^{0.05} V(y)T(y)dy \tag{4.1}$$

Therefore, the energy loss in the developing region, q_{dev}, is given by:

$$q_{dev} = \rho C_p W \left(\int_0^{0.05} V(y)T(y)dy_{asymptotic} - \int_0^{0.05} V(y)T(y)dy_{leading\ edge} \right) \tag{4.2}$$

In terms of the unit absorber width, the wind induced heat loss is expressed as:

$$q'_{dev} = \frac{q_{dev}}{W} \tag{4.3}$$

It is assumed that this heat loss occurs over the same distance predicted by the equation of Kutscher (1992):

$$L_s \cong \frac{U_\infty v}{V_0^2} \tag{2.6}$$

Figures 4.8 and 4.9 are contour plots of heat loss per unit width for a flat perforated plate, and for the corrugated perforated plate, respectively. Both have been presented as a function of wind speed and suction velocity. The plot for the flat plate has been produced using a correlation produced by Kutscher (1992).

$$q'_{dev,flat} = \frac{\rho C_p \Delta T U_\infty}{V_0}\left[\frac{\upsilon}{Pr+Pr^2}\right] \tag{4.4}$$

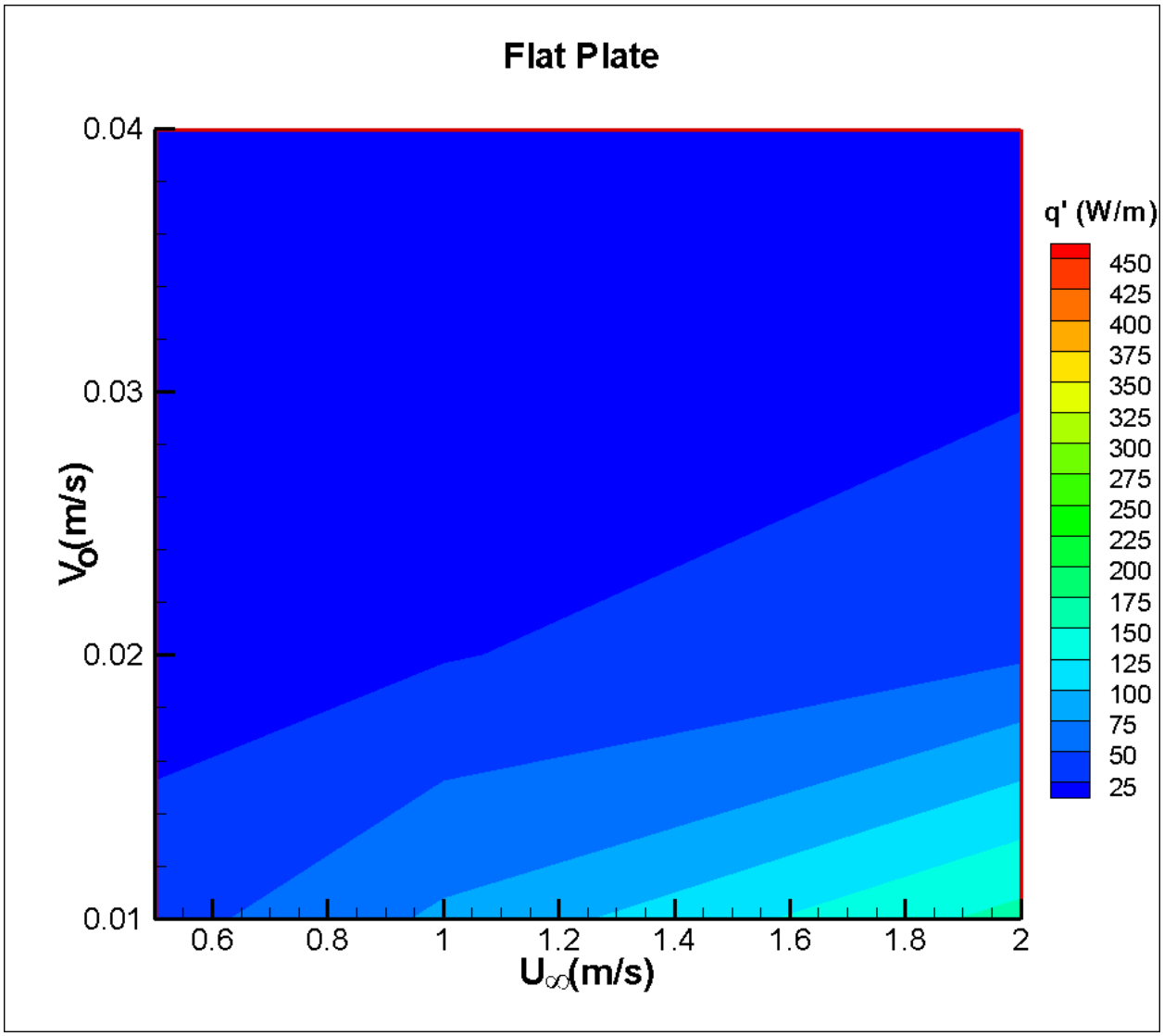

Figure 4.8: Contour Plot for Heat Loss from a Perforated Flat Plate in the Developing Region. (adapted from Kutscher 1992).

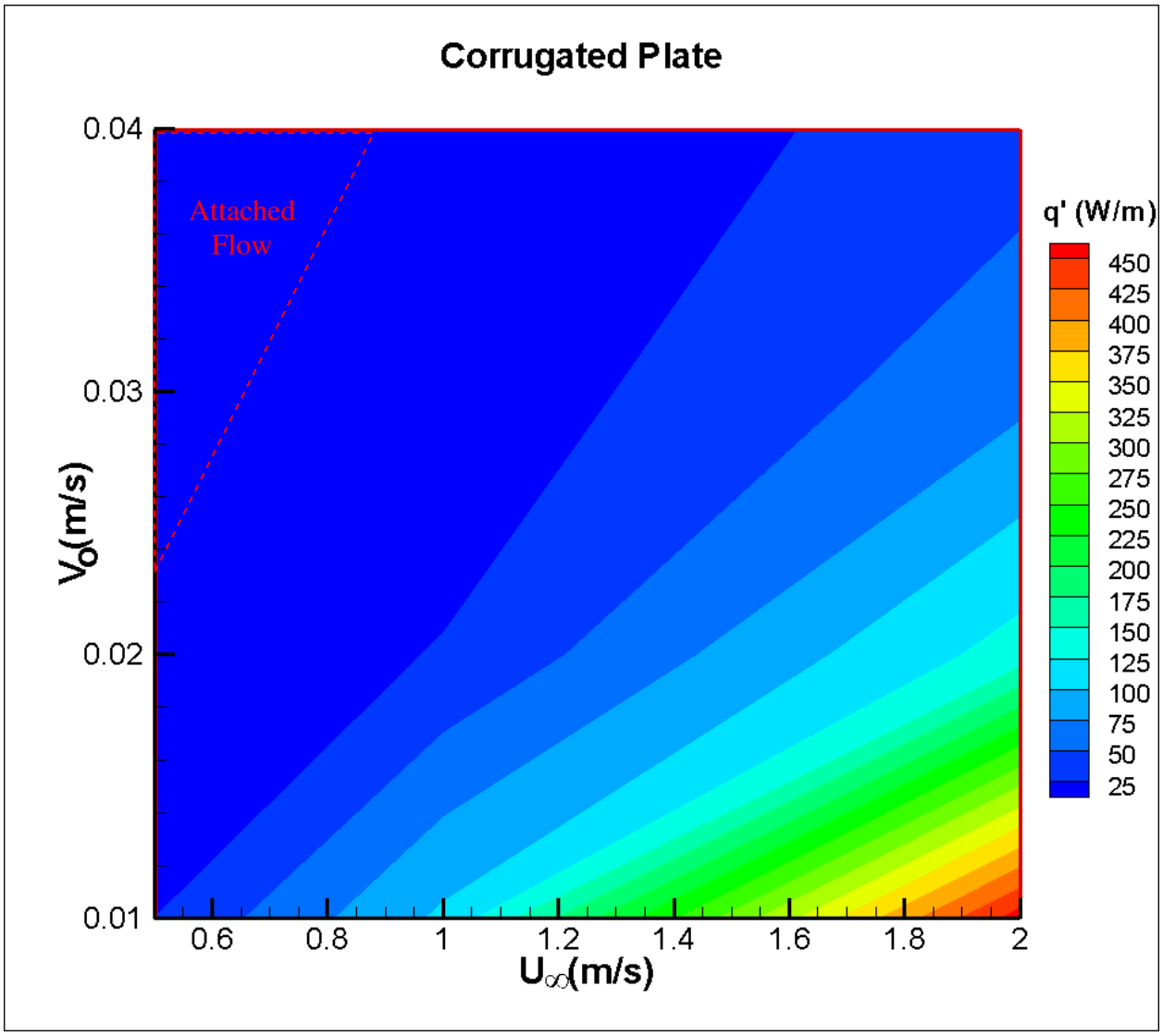

Figure 4.9: Contour Plot for Heat Loss from a Corrugated Perforated Plate in the Developing Region. The Approximate Location of the Attached Flow Region is Noted.

The difference in heat transfer rates exhibited in these plots is best described in terms of separated and attached flow behavior. For the flat perforated plate, all of the flow is attached. For the corrugated perforated plate, however, only the top left hand corner exhibits attached behavior. The heat transfer rate in this region is comparable between the two situations. For the corrugated plate, however, significant heat transfer enhancement occurs in the separated region.

Following the methodology of Gawlik and Kutscher (2002), discussed in Section 2.6.1, it is possible to build correlations that predict developing region heat loss for the specific absorber plate being considered.

Developing Region, Attached Flow: In terms of the Nusselt number, heat loss for flow over a flat plate is given by:

$$Nu_{flat} = \frac{q'_{dev,flat}}{\mathrm{k}\Delta\mathrm{T}} = \frac{\rho C_p \Delta T U_\infty}{\mathrm{k}\Delta T V_0}\left[\frac{v}{Pr+Pr^2}\right] \tag{4.5}$$

Gawlik and Kutscher (2002) developed their correlation after recognizing that, given attached flow behavior, surface geometry could be considered by simply scaling Eqn. 4.5 using least square linear regression. (see Eqn 2.22).

$$Nu_{att} = \mathrm{C}Nu_{flat} \tag{4.6}$$

In this situation, however, it is not productive to build a correlation for attached flow. Primarily, only 2 of the 12 cases examined exhibited attached flow behavior. Therefore, there are only two points on which to base a correlation. If developed, it would only be valid for suction velocities between 0.03 and 0.04 m/s, and for wind speeds of about 0.05 m/s. Furthermore, the attached flow region is approximate (see Table 4.1 and Figure 4.9), so it may be difficult to determine exactly when to apply any correlation that is developed. Instead, a single unified correlation will be based on the entire data set.

Developing Region, Separated Flow: Gawlik and Kutscher (2002) developed their correlation for heat loss in the developing region (see Eqn. 2.23) in terms of the suction parameter Re_s:

$$Re_s = \frac{U_\infty}{V_0} \tag{2.24}$$

In difference to their work, only a single geometry is being considered, and therefore a much simpler correlation can be produced. Using a least square power fit analysis to fit the numerical data, the Nusselt number correlation for separated flow becomes:

$$Nu_{sep} = 0.0081 Re_s^{\,2.0829} \tag{4.7}$$

This correlation is only valid for wind speeds ranging from 0.5 to 2 m/s, and suction velocities of 0.01 to 0.04 m/s.

Table 4.2 and Figure 4.10 compare the quality of the correlations to numerically predicted results.

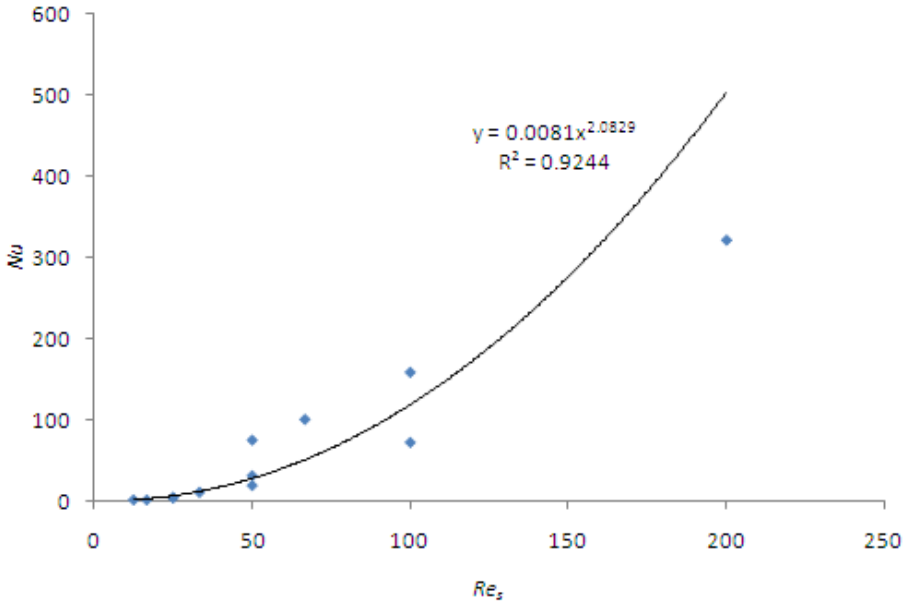

Figure 4.10: Comparison of Numerical Results with Correlation (Eqn. 4.7).

Table 4.2: Comparison between Numerical and Correlations Results for Nusselt Numbers in the Developing Region.

Wind Speed (m/s)	Suction Velocity (m/s)	ΔT (^{o}C)	Re_s	Numerical		Correlation	
				q'_{dev} (W/m)	Nu	Nu_{sep}	%err
0.5	0.01	48.3	50	25.1	19.8	28.0	8.3
	0.02	30.2	25	3.5	4.4	6.6	2.2
	0.03	23.1	17	1.2	2.0	2.8	0.9
	0.04	19.6	13	1.0	1.9	1.6	0.4
1.0	0.01	54.9	100	105.0	72.7	118.7	45.9
	0.02	31.9	50	26.7	31.8	28.0	3.8
	0.03	23.8	33	7.2	11.5	12.0	0.5
	0.04	19.6	25	2.7	5.2	6.6	1.4
2.0	0.01	54.7	200	463.0	321.8	502.7	180.9
	0.02	32.5	100	136.0	159.1	118.7	40.5
	0.03	25.3	67	67.3	101.1	51.0	50.2
	0.04	19.6	50	39.0	75.7	28.0	47.7

Fluid Properties at 300K: $\rho = 1.16$ kg/m^3, $\nu = 0.0000159$ m^2/s, Pr = 0.7, k = 0.0263 W/mK, and $C_p = 1007$ J/kgK
Grey represents attached flow. All others are separated.

It can be seen that the resulting correlation is not of great quality. Particularly, the assumption that the fit can be based on the form used by Gawlik and Kutscher (2002) does not appear to be adequate in that a secondary function of wind speed is not being represented. However, given that there are only 12 points on which to base the correlation, it was not deemed useful to attempt to produce a more detailed form of the fit equation. Furthermore, the required accuracy of the correlation is not stringent. In practice, the manufacturer needs heat loss information only for interests' sake, and it is understood that in reality, any correlation would only produce a 'ballpark' estimate. As such, it was decided to keep the equation developed.

4.4 Heat Exchanger Effectiveness

Before discussion can commence regarding absorber effectiveness, it is important to consider what we expect to see in the results (and why). The effectiveness is being determined in the asymptotic region, where it has been established that no convective losses are occurring. The model presented has been decoupled from radiative heat exchange, and therefore, solar input to the absorber must be captured entirely. In theory, wind speed should have no impact on the calculated heat exchanger effectiveness.

4.4.1 Numerical Results

4.4.1.1 No Wind Model

Using the no-wind model, air flow and heat transfer was modeled at suction velocities of 0.01, 0.02, 0.03, and 0.04 m/s. Figures 4.11 to 4.14 shows numerically obtained velocity vectors and temperature contours at these velocities. A Complete set of plots are contained in Appendix B.

In the absence of wind, flow structures are not appreciably altered by changes in suction velocity. In fact, the only significant difference between the cases is the temperatures experienced behind the absorber plate. As would be expected, the temperature behind the absorber drops as the suction velocity increases. This point should show up in the qualitative results. Lower temperatures (at higher suction velocities) should result in higher heat transfer rates behind the absorber, as well as lower effectiveness numbers for the absorber in general.

These points will be examined quantitatively in a later section.

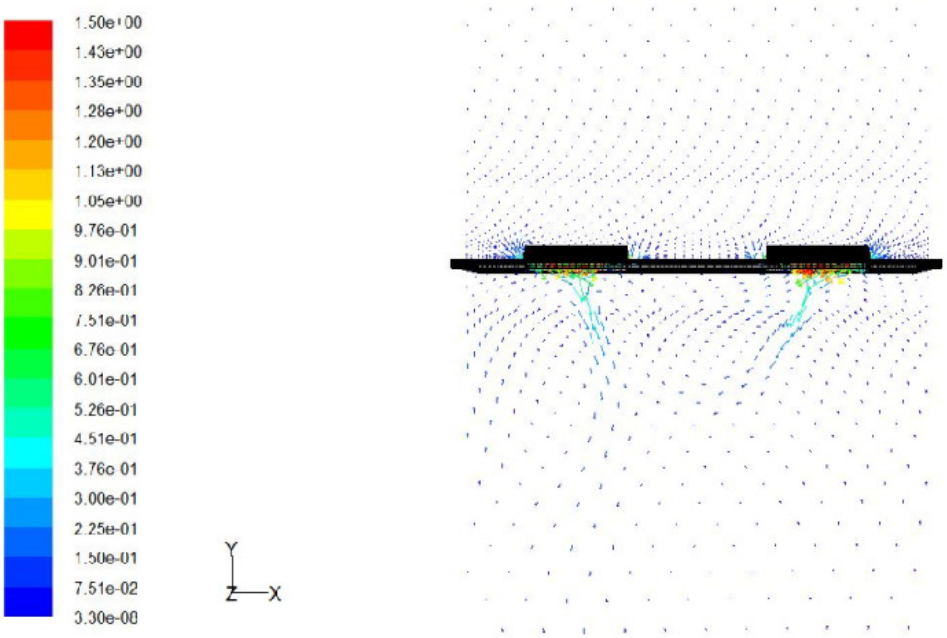

Figure 4.11: Velocity Vectors for the No Wind Case at a Suction Velocity of 0.01 m/s.

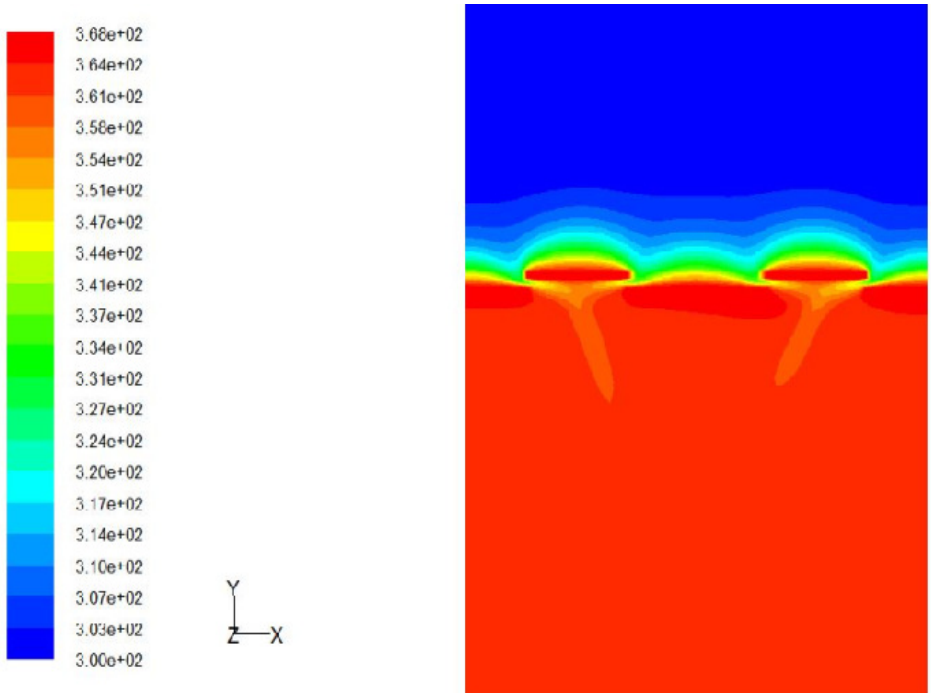

Figure 4.12: Temperature Contours for the No Wind Case at a Suction Velocity of 0.01 m/s.

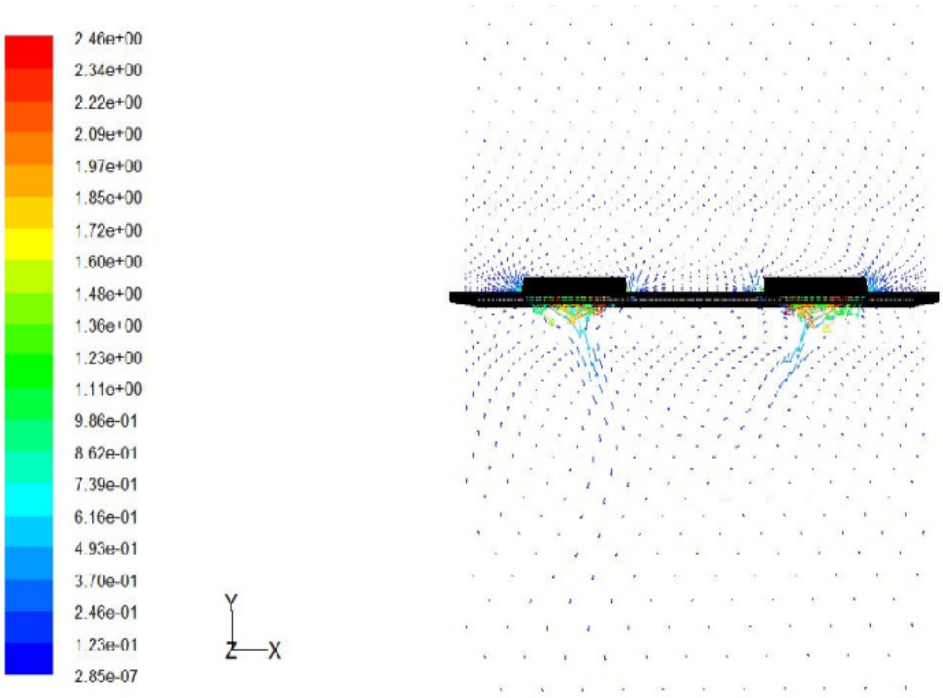

Figure 4.13: Velocity Vectors for the No Wind Case at a Suction Velocity of 0.04 m/s.

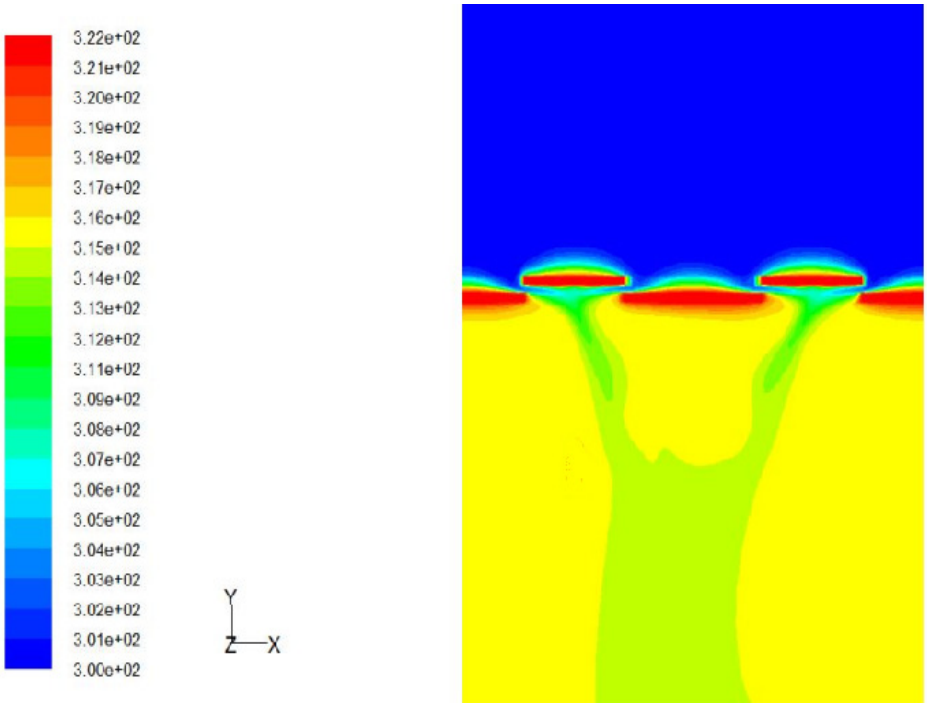

Figure 4.14: Temperature Contours for the No Wind Case at a Suction Velocity of 0.04 m/s.

4.4.1.2 Wind Effect Model

Using the full model, air flow and heat transfer was modeled at suction velocities of 0.01, 0.02, 0.03, and 0.04 m/s, and at wind speeds of 0.5, 1,0, and 2.0 m/s. Figures 4.15 to 4.20 show numerically obtained temperature contours at selected wind speeds and suction velocities. A Complete set of plots are contained in Appendix B.

Figures 4.15 and 4.19 represent cases were flow separation was seen to occur. The separation of flow is also clearly visible in the corresponding temperature contour plots (Figures 4.16 and 4.20). As was discussed in Section 4.2, the flow structures are seen to strengthen and grow with increased wind velocity. It is noted, however, that the temperature behind the absorber does not seem to have changed significantly between the two cases shown (0.5 and 2.0 m/s wind speed at 0.01 m/s suction velocity). This supports the premise that wind speed should play little or no role in the effectiveness. Where the heat transfer is occurring in these plots has obviously changed, but the magnitude of total heat transfer has essentially remained the same.

Figure 4.17 shows one of the two cases where attached flow was seen to occur. The corresponding temperature profile (Figure 4.18) suggests that the flow was near to separation. Comparing Figures 4.16 and 4.18, the temperature behind the absorber is seen to drop as suction velocity increases. As with the no wind analysis, this point should show up in the qualitative results. Lower temperatures (at higher suction velocities) should result in higher heat transfer rates behind the absorber, as well as lower effectiveness numbers for the absorber in general.

These points will be examined quantitatively in a later section.

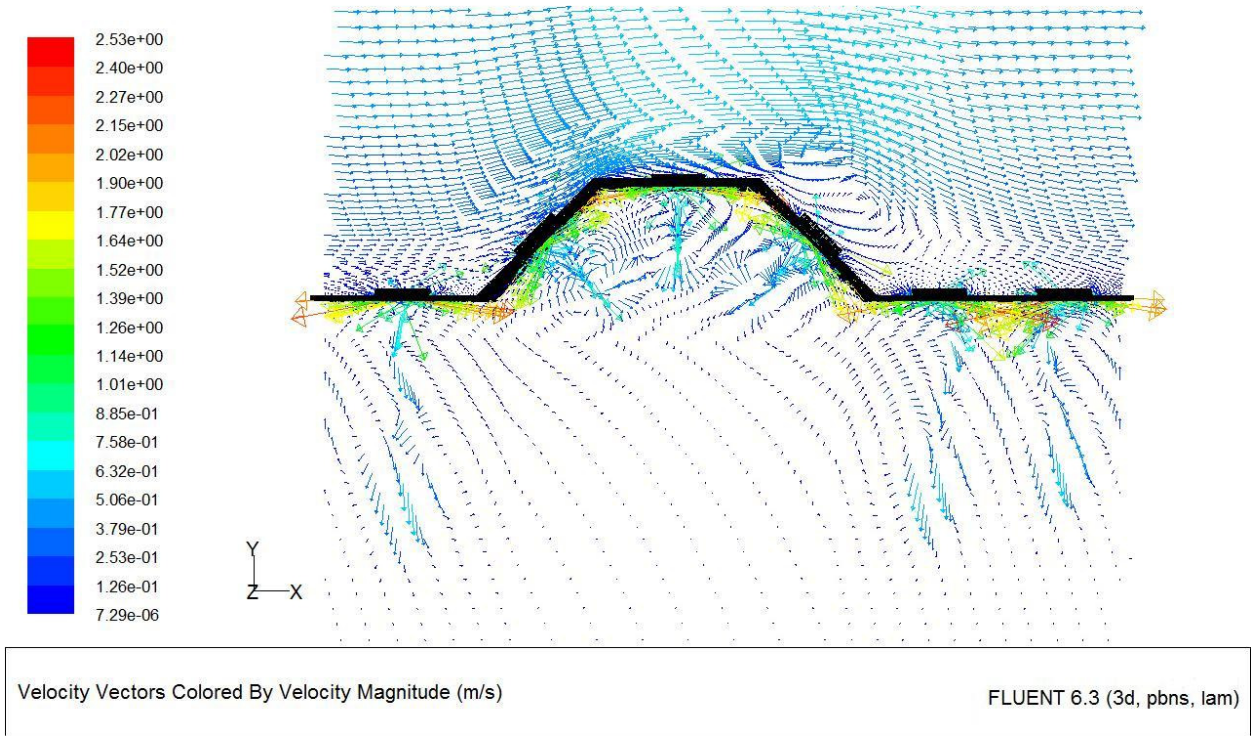

Figure 4.15: Velocity Vectors at a Wind Speed of 0.5 m/s and Suction Velocity of 0.01 m/s.

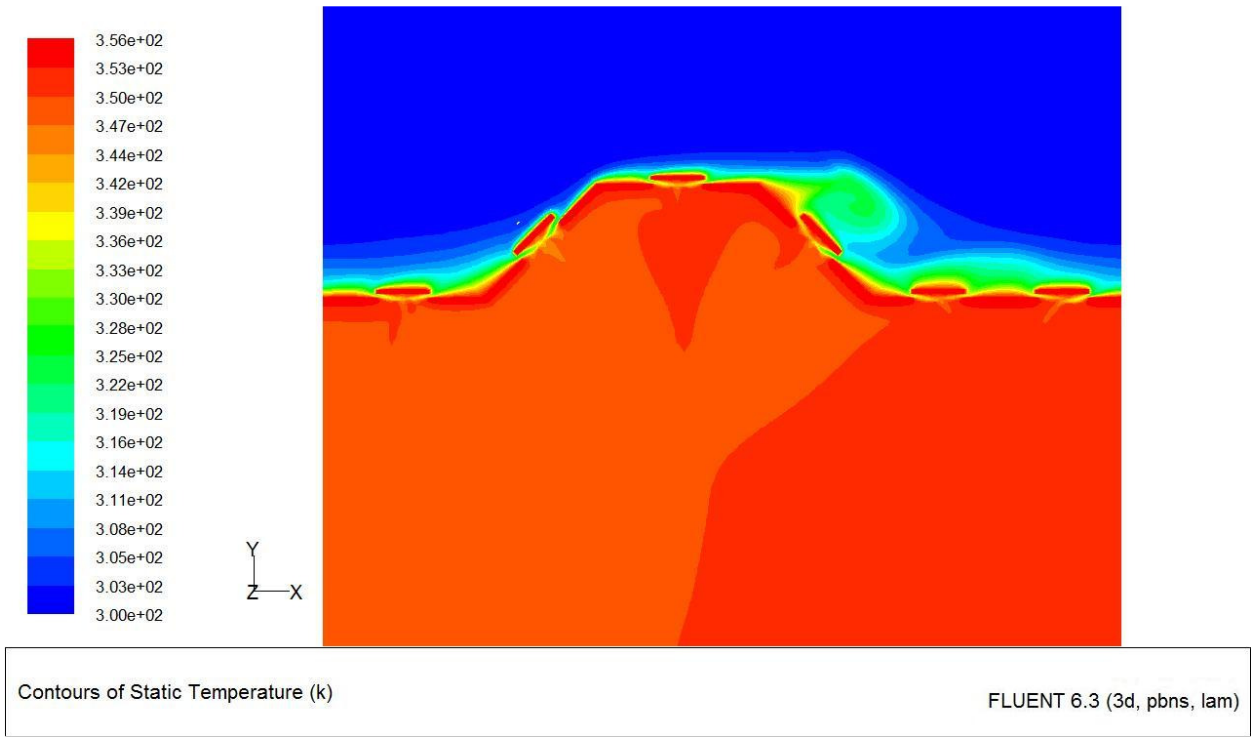

Figure 4.16: Temperature Contours at a Wind Speed of 0.5 m/s and Suction Velocity of 0.01 m/s.

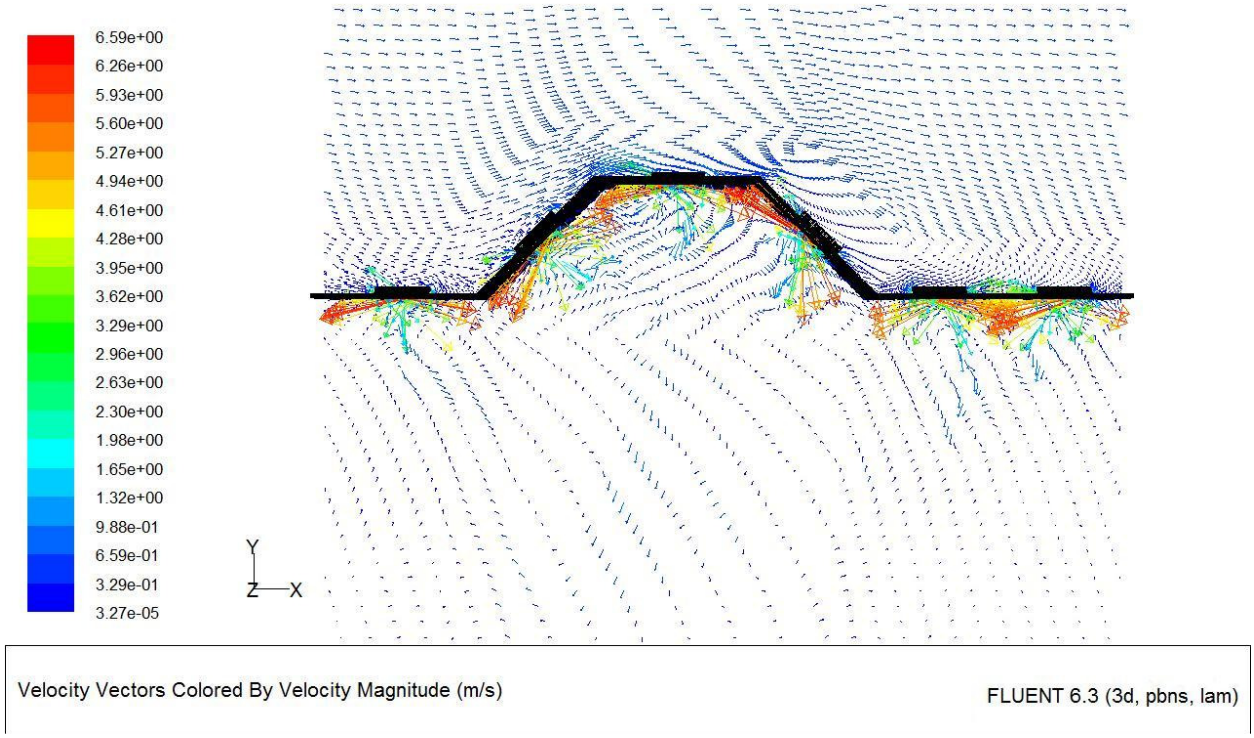

Figure 4.17: Velocity Vectors at a Wind Speed of 0.5 m/s and Suction Velocity of 0.04 m/s.

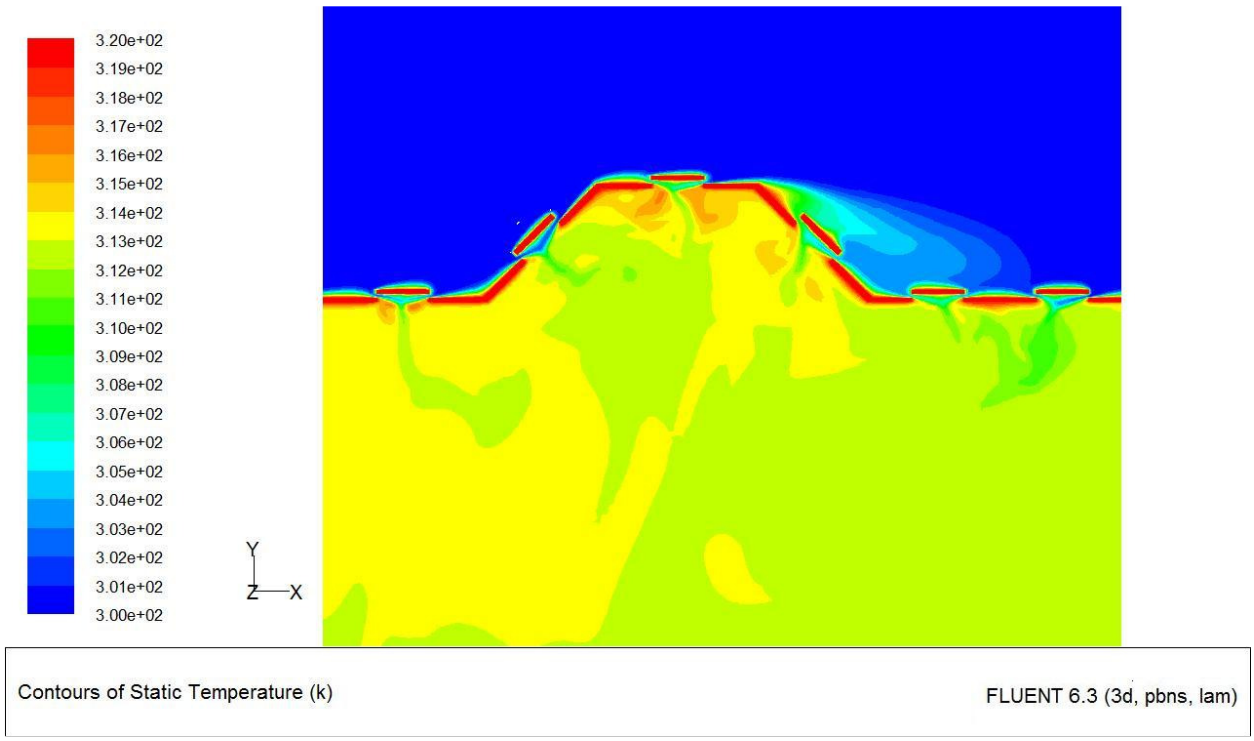

Figure 4.18: Temperature Contours at a Wind Speed of 0.5 m/s and Suction Velocity of 0.04 m/s.

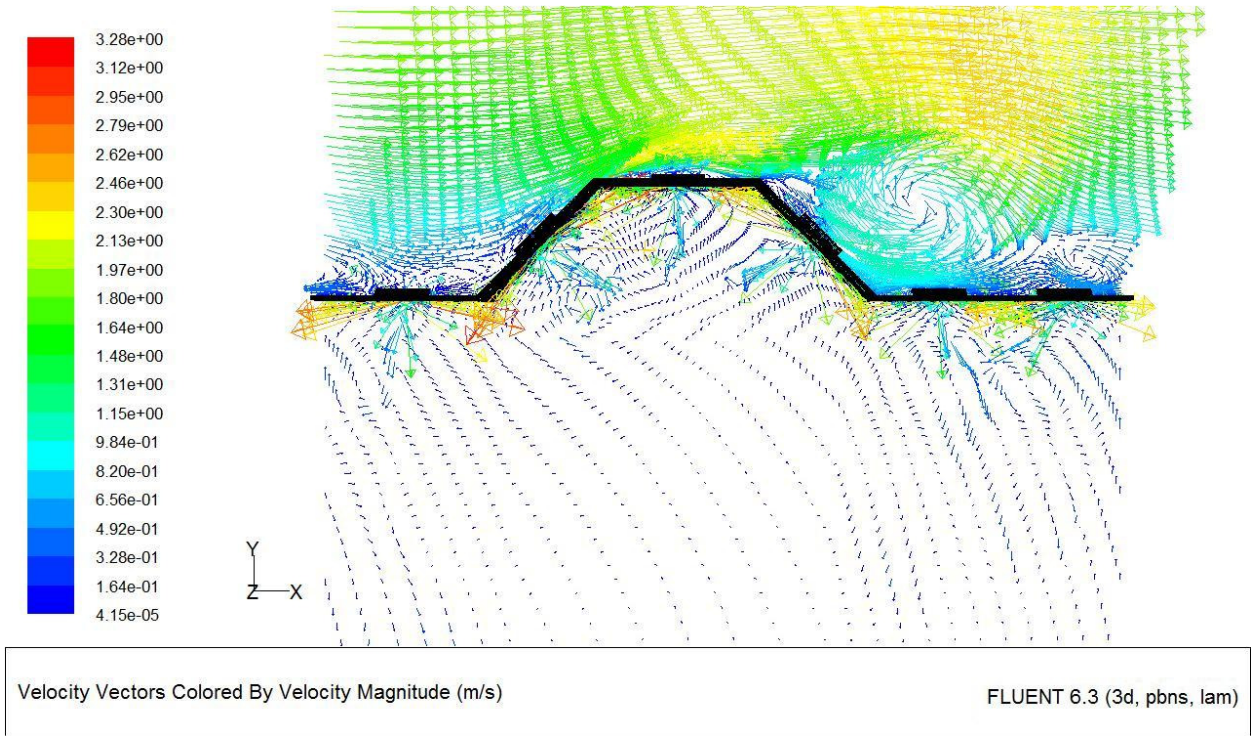

Figure 4.19: Velocity Vectors at a Wind Speed of 2.0 m/s and Suction Velocity of 0.01 m/s.

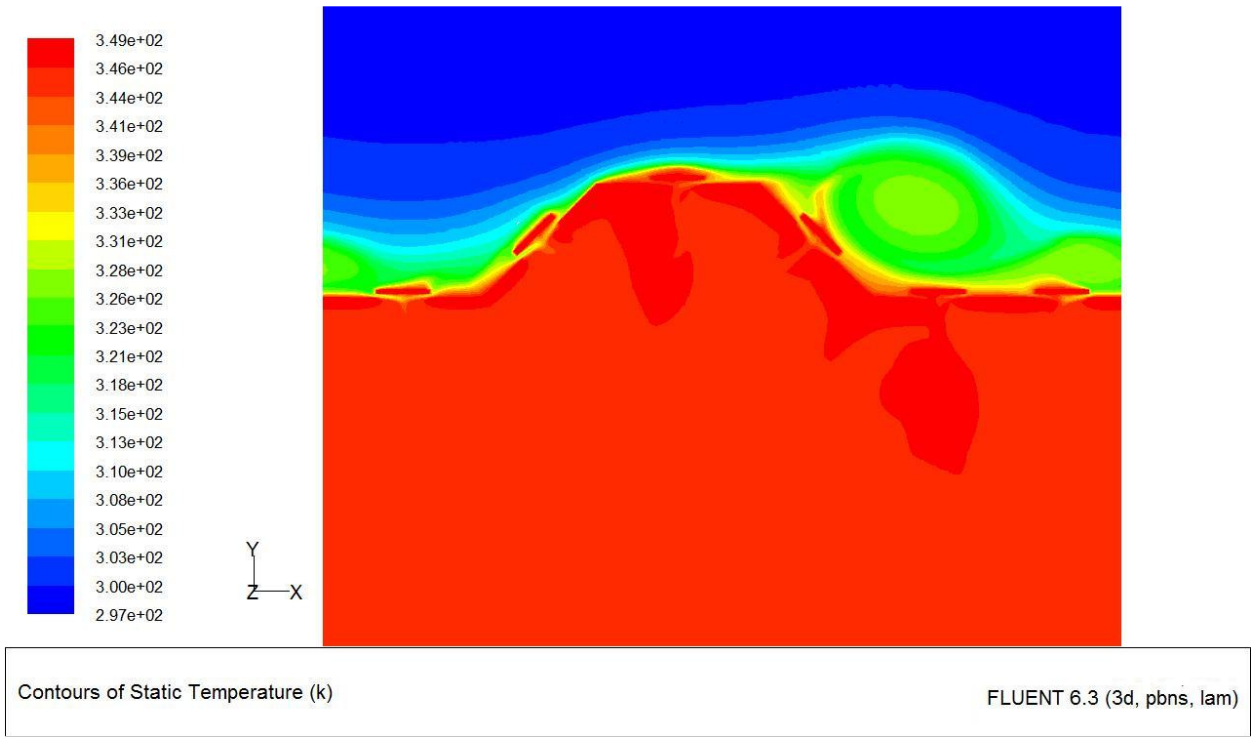

Figure 4.20: Temperature Contours at a Wind Speed of 2.0 m/s and Suction Velocity of 0.01 m/s.

4.4.2 Effectiveness

The main purpose of this work is to derive a correlation to predict the effectiveness of the Solarwall™ transpired solar air heater. In this section, the development of that correlation is described. The new effectiveness equation is compared to the results of the currently employed correlation from Van Decker et al. (2001).

4.4.2.1 Correlation Development

Using the numerical model, it is possible to calculate the effectiveness of the absorber directly from the free stream air temperature, T_∞, average absorber plate temperature, T_{abs}, and from the average temperature leaving the plenum, T_{in}, using:

$$\varepsilon = \frac{T_{\text{in}} - T_\infty}{T_{\text{abs}} - T_\infty} \tag{4.8}$$

where $0 < \varepsilon < 1$. To assess the proper form of the effectiveness correlation, however, a slightly more complex approach is followed.

The effectiveness correlation will be determined by first considering convective heat transfer from the absorber plate. It can be described using the general relation:

$$Nu_D = aRe_D^m \tag{4.9}$$

where

$$Nu_D = \frac{UD_h}{k} \tag{4.10}$$

$$Re_D = \frac{V_o D_h}{\nu} \tag{4.11}$$

In Eqns. 4.10 and 4.11, D_h, is the hydraulic diameter:

$$D_h = \frac{A_h}{p} \tag{4.12}$$

where A_h and p are the area and perimeter length of the perforations, respectively. For the absorber being studied here, $A_h = 0.000327$ m^2 and $p = 0.01$ m, giving $D_h = 0.0327\ m$.

In Eqn. 4.10, the thermal transmission, U, is based on the logarithmic mean temperature difference

$$UA\frac{T_{in}-T_\infty}{ln\left(\frac{T_{abs}-T_\infty}{T_{abs}-T_{in}}\right)} = \dot{m}C_p(T_{in} - T_\infty) \tag{4.13}$$

Here, $\dot{m} = \rho A_{abs} V_o$, and $\mathrm{A} = 2\mathrm{A_{abs}}$ to account for heat transfer from both sides of the absorber plate. Equation 4.13, therefore becomes

$$U = \frac{\rho V_o C_p}{2} \ln\left(\frac{T_{\mathrm{abs}}-T_\infty}{T_{\mathrm{abs}}-T_{\mathrm{in}}}\right) \tag{4.14}$$

By combining Eqn. 4.14 with Eqns. 4.9 to 4.12, we are now able to produce a plot of Nu_D vs Re_D. Coefficients a and m in Eqn. 4.9 can then be determined using least squares regression. The resulting correlation is:

$$Nu_D = 4.647\mathrm{Re_D^{0.4271}} \tag{4.15}$$

The results of this process are given in Table 4.3 and Figure 4.21. Fluid properties were determined at 300 K. Equation 4.15 is valid only for suction velocities between 0 and 0.04 m/s.

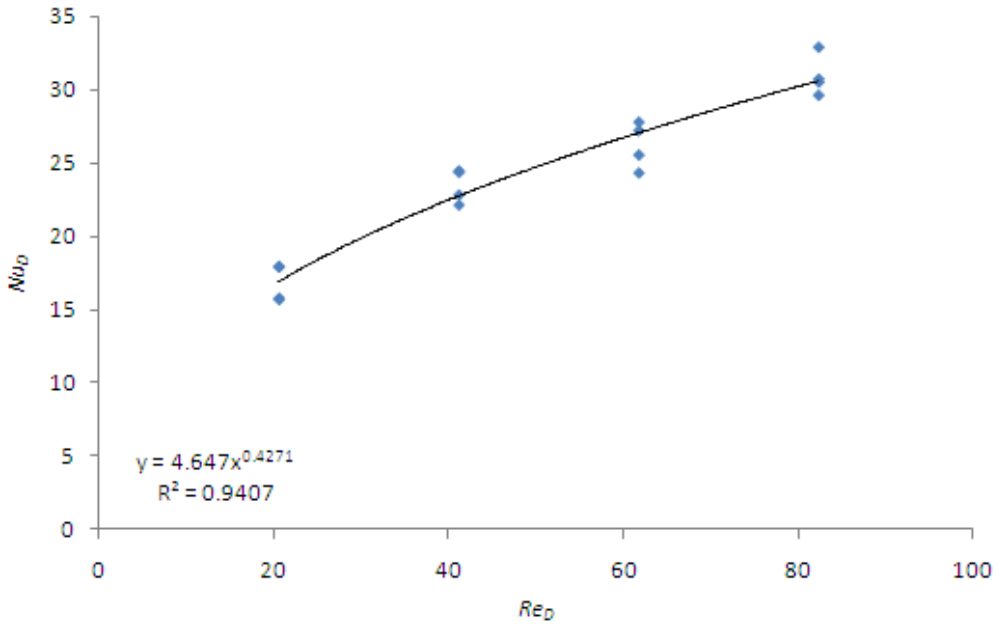

Figure 4.21: Nu_D vs Re_D based on Numerical Results.

Table 4.3: Comparison of Numerically Determined Heat Transfer Versus Correlation Predictions.

wind speed (m/s)	suction velocity (m/s)	T_∞ (K)	T_{mid} (K)	T_{in} (K)	T_{abs} (K)	U (W/m^2K)	Re_D	Nu_D Numerical	Nu_D Eqn 4.15	%error
0.0	0.01	300.0	350.2	362.0	367.8	14.4	20.6	17.9	16.9	5.7
	0.02	300.0	325.4	335.6	343.7	19.7	41.2	24.4	22.7	7.0
	0.03	300.0	312.8	319.7	328.5	20.5	61.7	25.5	27.0	5.9
	0.04	300.0	308.7	314.9	322.0	26.5	82.3	32.9	30.6	7.1
0.5	0.01	300.0	340.0	350.0	354.7	14.4	20.6	17.9	16.9	5.5
	0.02	300.0	318.0	325.4	332.5	17.8	41.2	22.1	22.7	2.8
	0.03	300.0	311.1	317.0	325.3	19.6	61.7	24.3	27.0	11.2
	0.04	300.0	308.7	312.7	319.6	24.5	82.3	30.5	30.6	0.2
1.0	0.01	300.0	341.8	348.6	354.9	12.7	20.6	15.8	16.9	7.3
	0.02	300.0	320.4	325.3	331.9	18.3	41.2	22.8	22.7	0.3
	0.03	300.0	312.5	317.0	323.8	21.9	61.7	27.2	27.0	0.6
	0.04	300.0	308.4	312.8	319.6	24.7	82.3	30.7	30.6	0.5
2.0	0.01	300.0	340.0	342.7	348.3	12.6	20.6	15.7	16.9	7.9
	0.02	300.0	320.5	324.5	330.2	19.6	41.2	24.3	22.7	6.6
	0.03	300.0	313.4	316.6	323.1	22.3	61.7	27.8	27.0	2.7
	0.04	300.0	309.8	312.5	319.6	23.8	82.3	29.6	30.6	3.2

Fluid Properties at 300K: $\rho = 1.16$ kg/m^3, $\nu = 0.0000159$ m^2/s, Pr = 0.7, k = 0.0263 W/mK, and $C_p = 1007$ J/kgK

In order to derive a correlation for absorber plate effectiveness, we start with the heat exchanger effectiveness equation:

$$\varepsilon = 1 - e^{\frac{-UA}{\dot{m} \cdot C_p}} \tag{4.16}$$

This particular equation is applicable because one side of the heat exchanger is a radiative process, thereby making the $\dot{m} \cdot C_p$ product of one side equal to infinity.

Combining Eqns. 4.10 and Eqn. 4.16, inserting the heat transfer correlation (Eqn. 4.15), and expanding the mass flow rate term, results in:

$$\varepsilon = 1 - e^{\frac{-9.294 Re_D^{0.4271} k}{\rho V_o D_h C_p}} \tag{4.17}$$

Finally, by recognizing that Eqn. 4.17 is to be applied to a specific absorber plate, and by assuming constant fluid properties at 300K, the effectiveness correlation can be reduced to a function of suction velocity only. Equation 4.17 reduces to:

$$\varepsilon = 1 - e^{-0.1662 V_o^{-0.5729}} \tag{4.18}$$

As was stated at the beginning of this section, Eqn. 4.8 allows for the calculation of effectiveness directly from the numerical results. As such, it is possible to test the quality of the effectiveness correlation (Eqn. 4.18). Figure 4.22 and Table 4.4 show the quality of the correlation. As can be seen, the fit is very good.

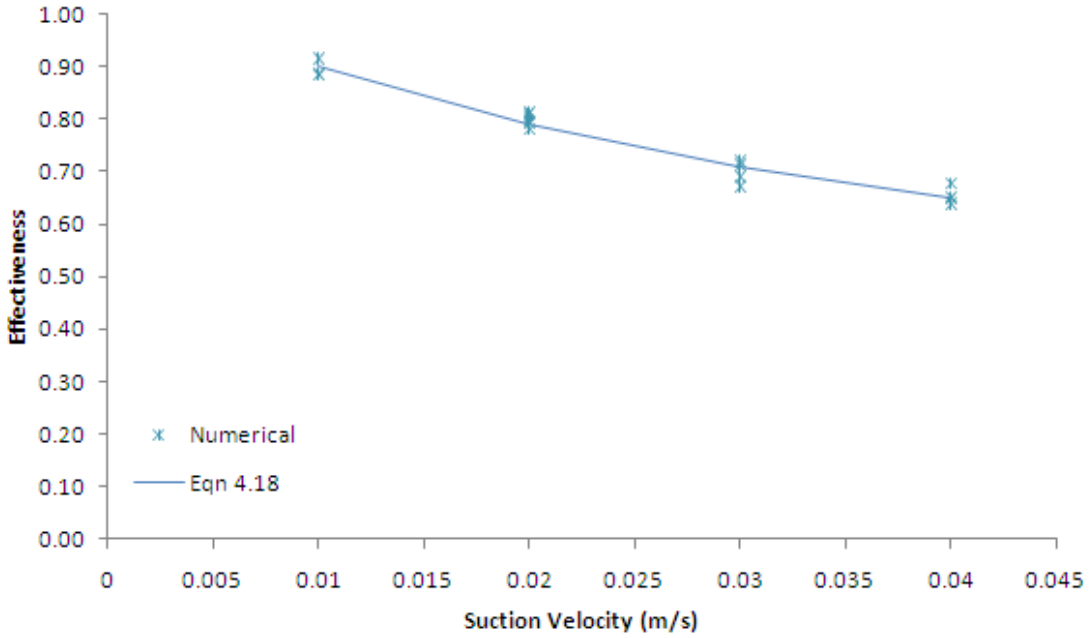

Figure 4.22: Comparison of Numerically Determined Effectiveness Values Versus Correlation.

Table 4.4: Comparison of Numerically Determined Effectiveness Versus Correlation Predictions.

Suction Velocity (m/s)	T_∞ (K)	T_{mid} (K)	T_{in} (K)	T_{abs} (K)	Numerical	Eqn 4.18	%error
0.01	300.0	350.2	362.0	367.8	0.92	0.90	1.41
	300.0	340.0	350.0	354.7	0.91	0.90	1.35
	300.0	341.8	348.6	354.9	0.89	0.90	1.88
	300.0	340.0	342.7	348.3	0.88	0.90	2.05
0.02	300.0	325.4	335.6	343.7	0.81	0.79	2.87
	300.0	318.0	325.4	332.5	0.78	0.79	1.15
	300.0	320.4	325.3	331.9	0.79	0.79	0.13
	300.0	320.5	324.5	330.2	0.81	0.79	2.72
0.03	300.0	312.8	319.7	328.5	0.69	0.71	2.97
	300.0	311.1	317.0	325.3	0.67	0.71	5.72
	300.0	312.5	317.0	323.8	0.71	0.71	0.32
	300.0	313.4	316.6	323.1	0.72	0.71	1.37
0.04	300.0	308.7	314.9	322.0	0.68	0.65	3.98
	300.0	308.7	312.7	319.6	0.65	0.65	0.10
	300.0	308.4	312.8	319.6	0.65	0.65	0.28
	300.0	309.8	312.5	319.6	0.64	0.65	1.81

4.4.2.2 Comparison to Van Decker et al. (2001)

Currently, the correlation produced experimentally by Van Decker et al. (2001) is used in industry standard software to determine solar absorber effectiveness. It is therefore useful to compare Eqn. 4.18 to Eqn. 2.27. Figure 4.23 shows the results of this comparison.

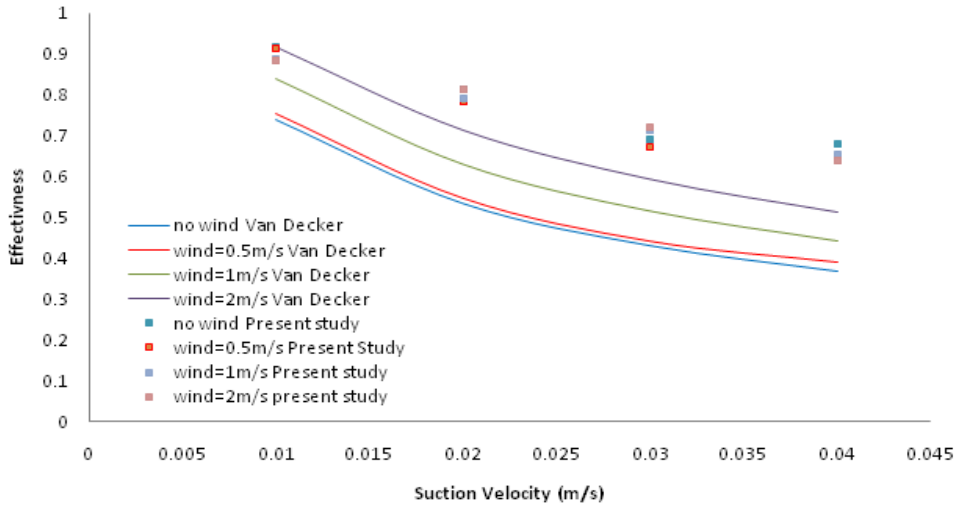

Figure 4.23: Overall Effectiveness of the Absorber Plate as a Function of Wind Speed and Suction Velocities. Present Study – Solid Lines. Van Decker et al. (2001) – Dashed Lines.

Van Decker et al.'s (2001) results are significantly different than those produced in the current study. There are a number of possible reasons for this. As was previously noted, for example, the absorber plate considered here is corrugated, while theirs was flat. The fact that their correlation is dependent on wind velocity, however, indicated the likely cause of the discrepancy. In the present study, the asymptotic region was considered. The experimental study of Van Decker et al. (2001), however, was conducted on a 2' by 2' absorber. His correlation is undoubtedly based on results obtained in the developing region. This, however, does not discredit their work. The correlation of Van Decker et al. (2001) is likely better suited to smaller installations, while the present work is more suited to larger ones. The two correlations can provide bounds on the expected performance of a system installation.

4.4.2.3 Heat Transfer

It was noted at the beginning of Section 4.4 that theory predicts that effectiveness (and therefore the total heat transfer) should not be a function of wind speed. Preliminary examination of temperature contours support this in that the average temperature behind the absorber seems to be similar for cases with the same suction velocity, but different wind speeds. Velocity vector and temperature contour plots, however, clearly suggest that the location at which the heat transfer is occurring moves more strongly to the outward side of the absorber as wind speed increases.

To gain a better understanding of the heat transfer that is taking place, it is convenient to determine the effectiveness of the outward or inward faces of the absorber. Using Eqn. 4.8, we define

$$\varepsilon_f = \frac{T_{\mathrm{mid}} - T_\infty}{T_{\mathrm{abs}} - T_\infty} \tag{4.19}$$

$$\varepsilon_b = \frac{T_{\mathrm{in}} - T_{\mathrm{mid}}}{T_{\mathrm{abs}} - T_\infty} \tag{4.20}$$

where ε_f and ε_b are the outward (front) and inward (back) effectiveness, respectively. The subscript *mid* indicated the fluid just after it has passed through the perforations.

Tables 4.5 and 4.6 shows the percentage of total effectiveness, and therefore heat transfer, occurring on the outward and inward faces of the absorber as a function of suction velocity.

Table 4.5: Percentage of Heat Transfer from the Outward Face of the Absorber at Different Suction Velocities and Wind Speeds. The Results of Van Decker et al. (2001) are in Brackets.

Suction Velocity (m/s)	Wind Speed (m/s)			
	0	0.5	1	2
0.01	81.0% (67.7%)	80.0% (69.8%)	85.9% (72.8%)	93.7% (75.1%)
0.02	71.7% (62.7%)	71.0% (65.5%)	80.7% (69.9%)	83.7% (73.4%)
0.03	65.4% (58.4%)	65.2% (61.9%)	73.4% (67.1%)	80.7% (71.6%)
0.04	58.1% (54.7%)	68.4% (56.9%)	65.9% (64.7%)	78.3% (69.8%)

Table 4.6: Percentage of Heat Transfer from the Inward Face of the Absorber at Different Suction Velocities and Wind Speeds. The Results of Van Decker et al. (2001) are in Brackets.

Suction Velocity (m/s)	Wind Speed (m/s)			
	0	0.5	1	2
0.01	19.0% (32.2%)	20.0% (30.2%)	14.1% (27.2%)	6.3% (24.9%)
0.02	28.3% (37.3%)	29.0% (34.5%)	19.3% (30.1%)	12.3% (26.5%)
0.03	34.6% (41.6%)	34.8% (38.1%)	26.6% (32.8%)	19.3% (28.4%)
0.04	41.9% (45.1%)	31.6% (43.1%)	34.1% (35.3%)	22.7% (30.3%)

As can be seen in the tables, the majority of heat transfer occurs from the outward face of the absorber. This is expected because this is where the greatest temperature difference between the fluid and absorber is experienced, and because the fluid motion is greater. Increasing the wind speed, therefore, results in better mixing at the surface and better effectiveness from the outward face of the absorber. As suction increases, however, the proportion of this heating begins to shift in favor of greater heating from the back side of the absorber. This is due to the fact that higher suction results in faster air flow, and colder temperatures behind the absorber.

It is noted that Van Decker et al. (2001) also noticed this trend. In fact, the correlation for effectiveness that was produced in their study actually considered heat transfer from the outward face, inward face, and perforation separately. The results of Van Decker et al. (2001) have been included in Tables 4.3 and 4.4 for comparison. His results confirm the same general trends discussed previously: increased wind speed increases heat transfer from the outward side, and increased suction increases it to the inward side. It is noted, however, that the geometry study in that work was different that what is considered in the present study. The reader is therefore cautioned from attempting to draw further parallels between these results.

Chapter 5

Conclusions and Recommendations

5.1 Conclusions

A 3-D CFD model was created to evaluate the effectiveness and heat loss of an unglazed transpired solar collector with a trapezoidal corrugation.

The model successfully predicted the occurrence of separated or attached flows. Attached flows were seen to occur only for low wind speeds (0.5 m/s) and high suction velocities (0.03 and 0.04 m/s).

Heat loss in the entry region was evaluated and a correlation was developed.

$$Nu_{sep} = 0.0081 {Re_s}^{2.0829} \quad (4.7)$$

where

$$Re_s = \frac{U_\infty}{V_0} \quad (2.24)$$

The correlation is valid for wind speeds from 0.5 to 2 m/s, and suction velocities between 0.01 and 0.04 m/s.

The heat loss correlation was not of great quality, largely due to the few points on which it was based. Given that the required accuracy of the correlation is not stringent, however, it was not deemed useful to attempt to produce a more detailed form of the fit equation. In practice, the manufacturer needs heat loss information only for interests' sake, and it is understood that in reality, any correlation would only produce a rough estimate.

Effectiveness in the asymptotic region was also examined, and correlations for heat transfer and effectiveness were produced. Heat transfer can be predicted using:

$$Nu_D = 4.647\mathrm{Re}_\mathrm{D}^{0.4271} \tag{4.15}$$

where

$$Nu_D = \frac{UD_h}{k} \tag{4.10}$$

$$Re_D = \frac{V_o D_h}{\nu} \tag{4.11}$$

$$U = \frac{\rho V_o C_p}{2} \ln\left(\frac{T_{\mathrm{abs}} - T_\infty}{T_{\mathrm{abs}} - T_{\mathrm{in}}}\right) \tag{4.14}$$

and D_h = 0.0327 m.

The correlation for effectiveness is:

$$\varepsilon = 1 - e^{-0.1662 V_o^{-0.5729}} \tag{4.18}$$

Equations 4.15 and 4.18 produce accurate estimates of heat transfer and effectiveness for suction velocities from 0.01 to 0.04 m/s.

It is noted that effectiveness and heat transfer were not a function of wind velocity. They were both determined in the asymptotic region, where it has been established that no convective losses are occurring. The numerical model has been decoupled from radiative heat exchange, and

therefore, solar input to the absorber must be captured entirely. In theory, wind speed should have no impact on the calculated heat exchanger effectiveness.

The effectiveness correlation was compared to the correlation produced by Van Decker et al. (2001). While the two were of the same order of magnitude, they did not show good agreement. It is noted that that correlation was based on experiments conducted on a 2' by 2' absorber plate. It is very likely that the effectiveness values determined in that study were in the developing region. This is supported by the fact that Van Decker et al.'s (2001) correlation is dependent on the wind speed. In this regard, the correlation of Van Decker et al. (2001) is likely better suited to smaller installations, while the present work is more suited to larger ones. The two correlations can likely provide bounds on the expected performance of a system installation.

5.2 Recommendations

A number of recommendations have been made for further study.

- A more accurae correlation of heat loss in the developing region would consist of separate relations for attached and separated flows. Unfortunately, too few situations were examined at which attached flow occurred. It is suggested that the numerical study by expanded to obtain more data points for attached flow, and to help assess exactly when the onset of separation can be predicted.
- The presented work was limited to numerical simulation. It is vital to extend this work to include experimental work which would permit better validation of the numerical model.
- Numerical software is limited in that either laminar or turbulent flow can be examined, but not both. While efforts were made to select a flow regime that replicated the flow

structures observed experimentally, this was far from definitive proof that the correct model was chosen. Direct numerical simulation (DNS) could be used model the system, but it is applicability is currently beyond computational abilities. Flow visualization would also assist in better defining the flow regime.

- The numerical model can be used as a tool to optimize the current Solarwall™ design. Modifications can be made to the model could result in a better effectiveness and lower heat loss. These modifications include the arrangement of the holes on the plate (triangular array instead of square array), the inclination angle of the corrugation, and the distance between the peak and the base of the corrugations. All these factors could be tested and optimized.

References

Abdulla, I. E., Yang, Z., and Cook, M. (2009). *Computational Analysis and Flow Structure of a Transitional Separated Reattached Flow over a Surface Mounted Obstacle and a Forward-Facing Step*. International Journal of Computational Fluid Dynamics. Vol. 23(1). pp. 25–57.

AltE Store (2010). Retrieved on November 25th, 2010, from www.altestore.com/store/Solar-Air-Heating/Your-Solar-Home-Solarsheat-Products/Your-Solar-Home-1500G-Glazed-Solar-Air-Heater/p2282/

Armaly, B.F., Durst F., Pereira F., and Schonung B. (1983). *Experimental and Theoretical Investigation of Backward-Facing Step Flow*, J. Fluid Mech. 127 pp.473–496

Arpaci, V. S., and Larsen, P. S. (1984). Convection Heat Transfer, Ed(2). Englewood Cliffs: Prentice Hall. Inc

Arulanandam, S. J., Hollands, K.G.T., and Brundrett, E. (1999). *A CFD Heat Transfer Analysis of the Transpired Solar Collector Under No-Wind Conditions*. Solar Energy. Vol. 67(1). pp. 93-100.

Bejan, A. (1984). Convective Heat Hransfer, Ed(1). New York: John Wiley & Sons.

BP Statistical Review of World Energy (2009). Retrieved on September 1st, 2010 from www.bp.com/productlanding.do?categoryId=6929&contentId=7044622

Cao, S., Hollands, K. G. T., and Brundrett, E. (1993). *Heat Exchange Effectiveness of Unglazed Transpired-Plate Solar Collector in 2D Flow*. Proceedings of the ISES World Congress. August 23-27. Budapest, Hungary. pp. 351-366.

Chaube, A, Sahoo, P.K. and Soanki, S.C. (2006). *Analysis of Heat Transfer Augmentation and Flow Characteristics Due to Rib Roughness Over Absorber Plate of a Solar Air Heater*. Renewable Energy 31. pp. 317–331.

Chen Y.T., Nie, J.H., Hsieh, H.T., and Sun L.J.(2006). *Three-Dimensional Convection Flow Adjacent to Inclined Backward-Facing Step*. International Journal of Heat and Mass Transfer 49 pp.4795–4803

Chiang, T.P., and Sheu T.W. (1999) *A Numerical Revisit of Backward-Facing Step Flow Problem*, Phys in Fluids 11 (4), pp.862–874.

Conserval Engineering Inc. (2010). SolarWall™. Retrieved on September 2010, from solarwall.com/en/products/solarwall-air-heating.php

Duffie, J. A., & Beckman, W.A. (2006). Solar Engineering of Thermal Processes, Ed.3. New York: John Wiley & Sons, Inc.

Dymond, C., and Kutscher, C. F. (1997). *Development of a Flow Distribution and Design Model for Transpired Solar Collectors*. Solar Energy. Vol. 60(5). pp. 291-300.

FLUENT. 2005. FLUENT 6.3 Manual my.fit.edu/itresources/manuals/fluent6.3/help/index.htm

Gambit. (2005). Gambit 2.3 Manual combust.hit.edu.cn:8080/fluent/Gambit13_help/gambit.htm

Garg, H. P. (1982). Treatise on Solar Energy. Vol.1, Fundamentals of Solar Energy Research. New York: John Wiley & Sons, Inc.

Gawlik, K. M., & Kutscher C. (2002). *Wind Heat Loss from Corrugated, Transpired Solar Collectors*. Transactions of the ASME. Vol. 124(3), pp. 256-261.

Gawlik, G., Christensen C., and Kutscher C. (2005). *A Numerical and Experimental Investigation of Low-Conductivity Unglazed, Transpired Solar Air Heaters*. Journal of Solar Energy Engineering Transactions of the ASME, Vol. 127(1), pp. 153-155.

Golneshan, A. A. (1994). *Forced Convection Heat Transfer From Low Porosity Slotted Transpired Plates*. Ph.D. Thesis. University of Waterloo, Waterloo

Goswami, Y., and Kreider J. (2000). Principles of Solar Engineering, Ed(2). Philadelphia: Taylor and Francis, Inc.

Green Terra Firma (2007). Retrieved on November 25th, 2010 from greenterrafirma.com/evacuated_tube_collector.html

Gunnewiek, L. H., Brundrett E., & Hollands K.G.T. (1996). *Flow Distribution in Unglazed Transpired Plate Solar Air Heaters of Large Area*. Solar Energy Vol. 58(4-6), pp. 227-237.

Gunnewiek, L.H., Hollands K.G.T., & Brundrett E. (2002). Effect of Wind on Flow Distribution in Unglazed Transpired-Plate Collectors. Solar Energy, Vol. 72(4), pp. 317-325.

Hamza, A. H. (2002). *Experimental Study on Laminar Flow Forced-Convection in a Channel with Upper V-Corrugated Plate Heated by Radiation*. International Journal of Heat and Mass Transfer. Vol. 45. pp. 2107–2117.

Iglisch, R. (1944). *Exact Calculation of Laminar Boundary Layer in Longitudinal Flow Over a Flat Plate with Homogeneous Suction*, Tech. Memo. No.1205, National Advisory Committee for Aeronautics, Washington, D.C.

Incropera, F.P., & DeWitt D.P. (2002). Fundamentals of Heat and Mass Transfer, Ed. 5. New York: John Wiley & Sons, Inc.

International Panel on Climate Change (IPCC) (2007). Synthesis Report.

Karwa, R., Solanki, S.E., and Saini, J.S. (1999). *Heat Transfer Coefficient and Friction Factor Correlations for the Transitional Flow Regime in Rib-Roughened Rectangular Ducts*. International Journal of Heat and Mass Transfer. Vol. (42). pp. 1597-1615.

Karwa, R., Solanki, S.E., and Saini, J.S. (2001). *Thermo-Hydraulic Performance of Solar Air Heaters Having Integral Chamfered Rib Roughness on Absorber Plates*. Energy. Vol. (26). pp. 161–176.

Kutscher, C. F., Christensen C., & Barker G. (1991). *Unglazed Transpired Solar Collectors: An Analytical Model and Test Results*. Solar World Congress. Vol. 2(2). pp.1245-1250.

Kutscher, C. F. (1992). *An Investigation of Heat Transfer for Air Flow Through Low Porosity Perforated Plates*, Ph.D. Thesis, Univ. of Colorado,Dept. of Mech. Eng.

Kutscher, C. F., Christensen C., and Barker G. (1993). *Unglazed Transpired Solar Collectors: Heat Loss Theory*. Journal of Solar Energy Engineering, Transactions of the ASME. Vol. 115(3). pp. 182-188.

Kutscher, C. F. (1994). *Heat Exchange Effectiveness and Pressure Drop for Air Flow through Perforated Plates with and without Crosswind.* Journal of Heat Transfer, Transactions of the ASME Vol 116(2), pp. 391-399.

Lee, C. K. and Abdelmoneim (2001). *Componential Analysis of Heat Transfer in Turbulent Flow Past a Horizontal Surface with Two Dimensional Ribs*. International Communication of Heat and Mass Transfer. Vol. 28(2). pp. 161-170.

Maddaeus A. D. (1983). *The Three-Dimensional Laminar Asymptotic Boundary Layer with Suction*. Journal of Engineering Mathematics. Vol. 17. pp. 73-91.

Natural Resources Canada (NRCan) (2009). *Finding SolarWall Success at 3M Perth*, Retrieved on November 25th, 2010 from oee.nrcan-rncan.gc.ca/industrial/technical-info/library/newsletter/archives-2007/Vol-XI-no-10-may15.cfm?attr=20

Prasad (1983). *Heat Transfer Characteristics of a Solar Air Heater used for Drying Purposes.* Journal of Applied Energy. Vol.(13). pp. 83-93.

Prasad B. and Saini J. (1988). *Effect of Artificial Roughness on Heat Transfer and Friction Factor in a Solar Air Heater.* Journal of Solar Eng. Vol.(41). pp. 555-560.

Ramlow B. & Nusz B (2006). Solar Water Heating. Ed(1). Canada: Edward Cad well Inc

Sandia (2007). *Sandia Invention to Make Parabolic Trough Solar Collector Systems More Energy Efficient*, National Nuclear Security Administration News Release.

Schlichting, H. (1979). Boundary Layer Theory, Seventh Edition, McGraw-Hill, Book Co., New York, pp. 392–393.

Sigmaplot 2009, Sigmaplot 11 manual

Solar Energy Laboratory (SEL) (2005). TRNSYS 16 — A Transient System Simulation Program. Version 16. University of Wisconsin, Madison.

Solar Panels Plus (2007). Retrieved on November 25th, 2010 from www.solarpanelsplus.com/solar-panel-types/

Sunden, B., and Trollheden, S. (1989). Periodic Laminar Flow and Heat Transfer in a Corrugated Two-Dimensional Channel. International Communications in Heat and Mass Transfer, Vol. 16. p.215-225

Sparrow, E. M., and Ortiz, C. (1982). *Heat Transfer Coefficients for the Upstream Face of a Perforated Plate Positioned Normal to an Oncoming Flow*. International Journal of Heat and Mass Transfer. Vol. 25(1). pp. 127-135.

Statistics Canada (2010) Retrieved on November 25th, 2010 from www.statcan.gc.ca/start-debut-eng.html

Summers, D. (1995). *Thermal Simulation and Economic Assessment of Unglazed Transpired Collector Systems*. MASc Thesis. University of Wisconsin, Madison.

Sustainable Design Update (2008), *Transpired Solar Collector*, Retrieved on November 25th, 2010 from sustainabledesignupdate.com/2008/03/simple-solar-air-heater/

The New York Times (2007). *As China Roars, Pollution Reaches Deadly Extremes*.

Van Decker, G.W.E., Hollands, K.G.T and Brunger, A.P. (2001). *Heat Exchange Effectiveness of Unglazed Transpired-Plate Solar Collector in 3D Flow*. Solar Energy 71(1), 33-45.

Appendix A

Description of the Computational Code

In this section, a general description of the numerical software Fluent will be discussed which solve the governing equations used for describing the fluids flow. The software developer, ANSYS Inc, is the world's largest provider of CFD software.

Fluent is based on a control volume approach, which discetizes the solution domain into control volumes. It is based on using the cell centered method. The general scalar transport equation is given by the following formula:

$$\int_v \frac{\partial \rho \phi}{\partial t}\, dV + \oint \rho \phi \vec{v} \cdot d\vec{A} = \oint \Gamma_\phi \nabla \phi \cdot d\vec{A} + \int_v S_\phi dV \qquad \text{(A.1)}$$

where

$\rho =$ density

$\vec{v} =$ velocity vector$(= u\hat{\imath} + v\hat{\jmath}$ in 2D)

$\vec{A} =$ surface area vector

$\Gamma_\phi =$ diffusion coefficient of ϕ

$\nabla\phi =$ gradiant of ϕ $\left(= \frac{\partial \phi}{\partial x}\hat{\imath} + \frac{\partial \phi}{\partial y}\hat{\jmath}$ in 2D$\right)$

$S_\phi =$ source of ϕ per unit volume

Then, Eqn. (A.1) is applied at each control volume as follows:

$$\frac{\partial \rho \phi}{\partial t} V + \sum_f^{N_{faces}} \rho_f \vec{v}_f \phi_f \cdot \vec{A}_f = \sum_f^{N_{faces}} \Gamma_\phi \nabla \phi_f \cdot \vec{A}_f + S_\phi V \quad \text{(A.2)}$$

where

N_{faces} = number of faces enclosing cells

ϕ_f = value of ϕ convicted at face f

$\rho_f \vec{v}_f \cdot \vec{A}_f$ = mass flux through the face

$\vec{A}_f$ = area of face f, $|A|$ $\left(= \left|A_x \hat{\imath} + A_y \hat{\jmath}\right| \text{ in 2D}\right)$

$\nabla \phi_f$ = gradient of ϕ at face f

V = cell volume

This equation has an unknown scalar ϕ at the cell center and the surrounding neighbor cells. This equation will be linearized and written in the following form

$$ap\phi = \sum_{nb} a_{nb} \phi_{nb} + b \quad \text{(A.3)}$$

Where the subscript nb refers to neighbor cells and ap and a_{nb} are the linerized form for ϕ and ϕ_{nb}.

After applying the linearized equation to each cell, a set of equations are arranged in a matrix. Fluent solves these set of equations by Gauss Seidel method in conjunction with algebraic multi grid method (AMG). The residual is defined as the imbalance of the componential domain, and it is defined by the following equation

$$R = \sum_{Cell\ p} \left| \sum_{nb} a_{nb} \phi_{nb} + b - ap\phi p \right| \quad \text{(A.4)}$$

it is difficult to judge the convergence by Equation (A.4) since there is no scaling is employed. Therefore, a scaled residual is used to judge the convergence as follows

$$R = \frac{\sum_{cells\ p} \left| \sum_{nb} a_{nb} \phi_{nb} + b - ap\phi p \right|}{\sum_{cells\ p} |ap\phi p|} \quad \text{(A.5)}$$

Appendix B

Numerical Results

B.1 Examination of Flow Separation and Reattachment

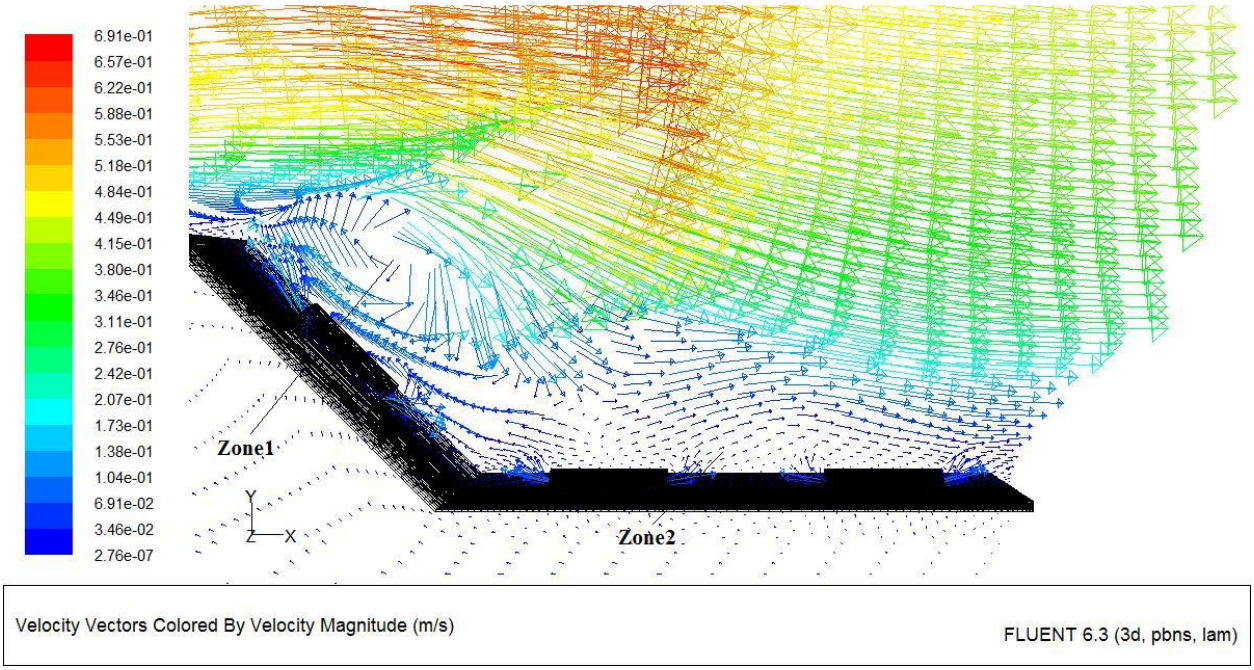

Figure B.1: Flow Behavior at a Wind Speed of 0.5 m/s with No Suction.

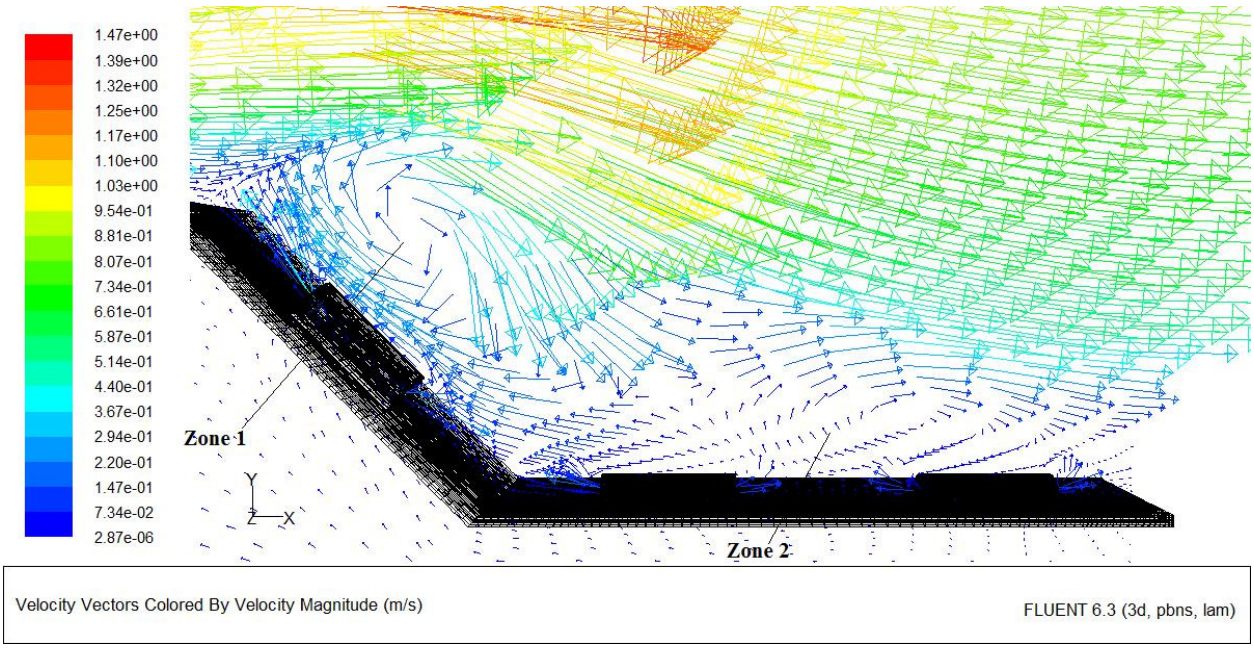

Figure B.2: Flow Behavior at a Wind Speed of 1.0 m/s with No Suction.

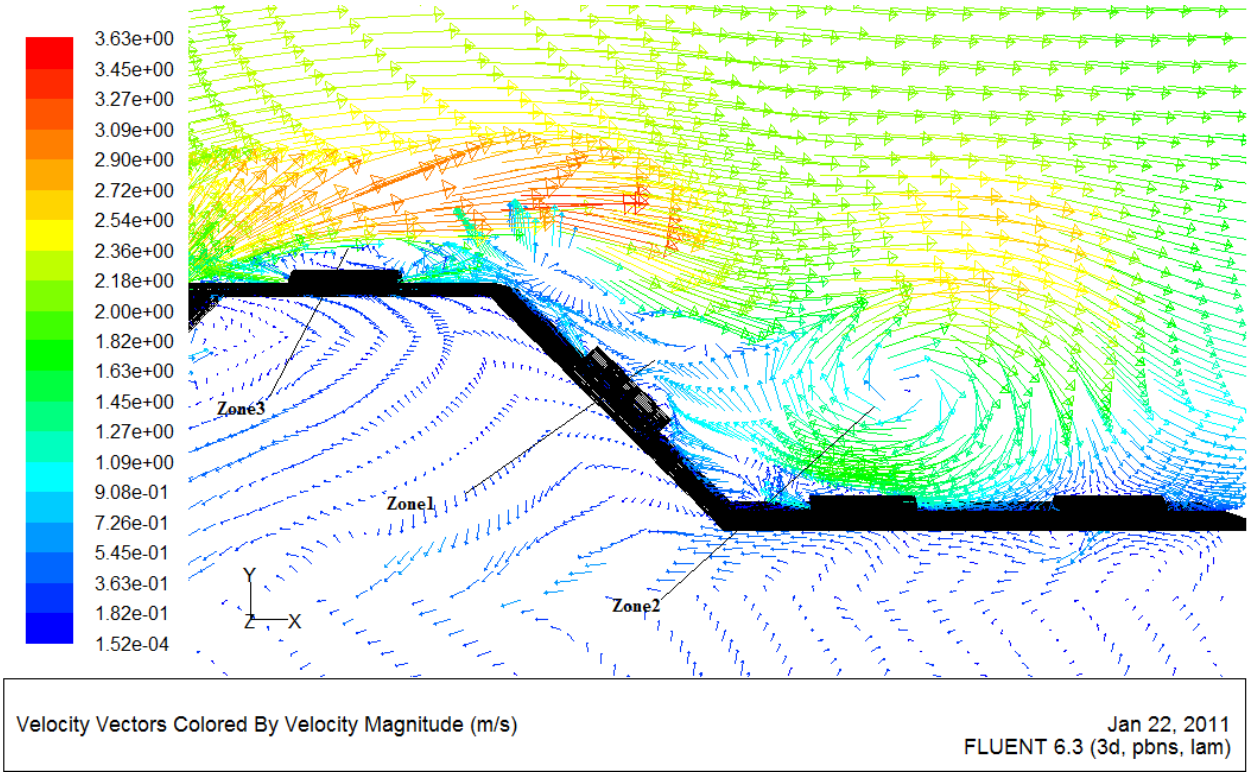

Figure B.3: Flow Behavior at a Wind Speed of 2.0 m/s with No Suction.

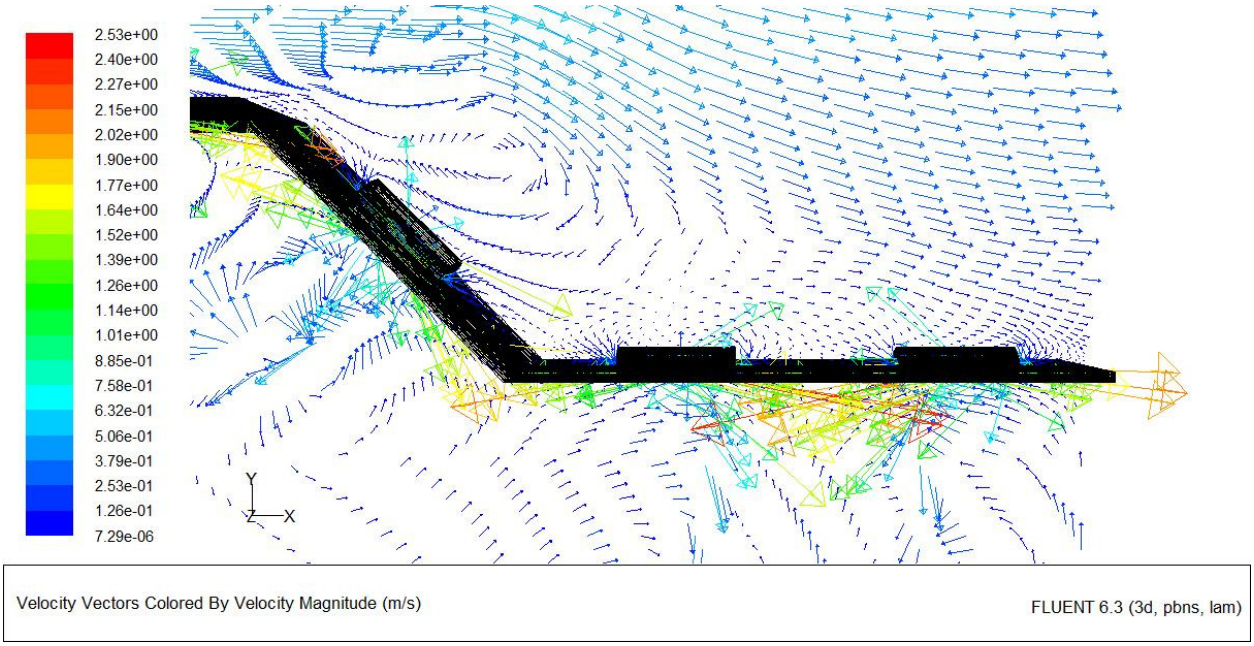

Figure B.4: Flow Behavior at a Wind Speed of 0.5 m/s and Suction Velocity of 0.01 m/s.

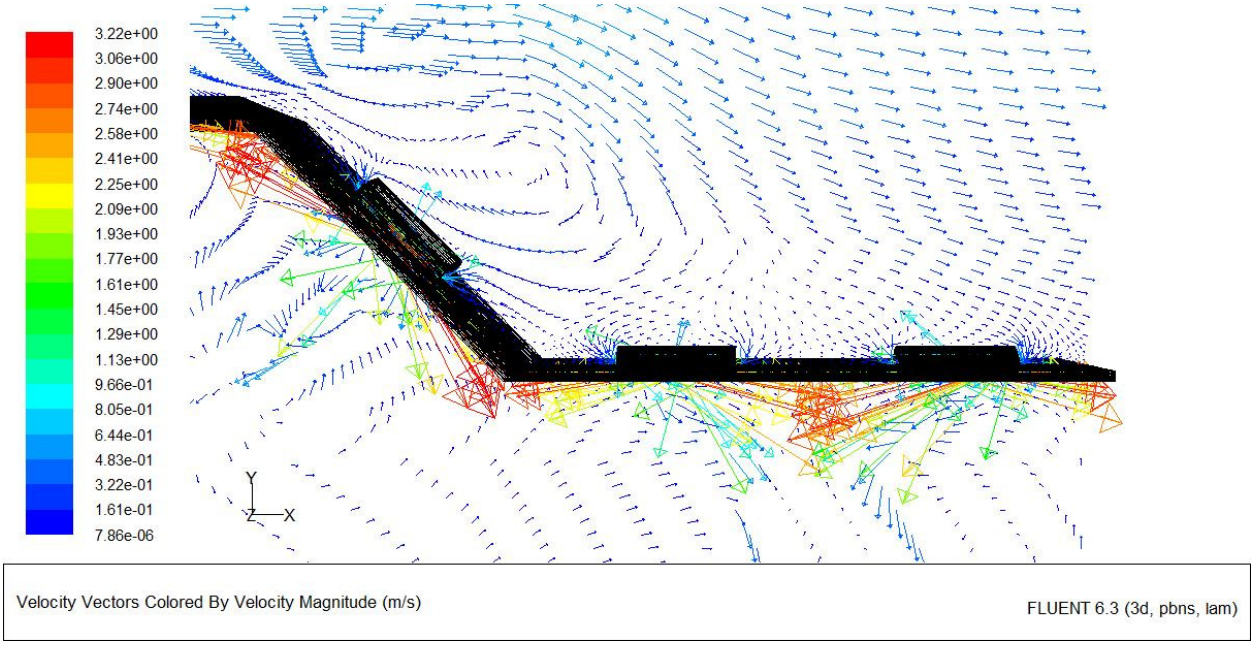

Figure B.5: Flow Behavior at a Wind Speed of 0.5 m/s and Suction Velocity of 0.02 m/s.

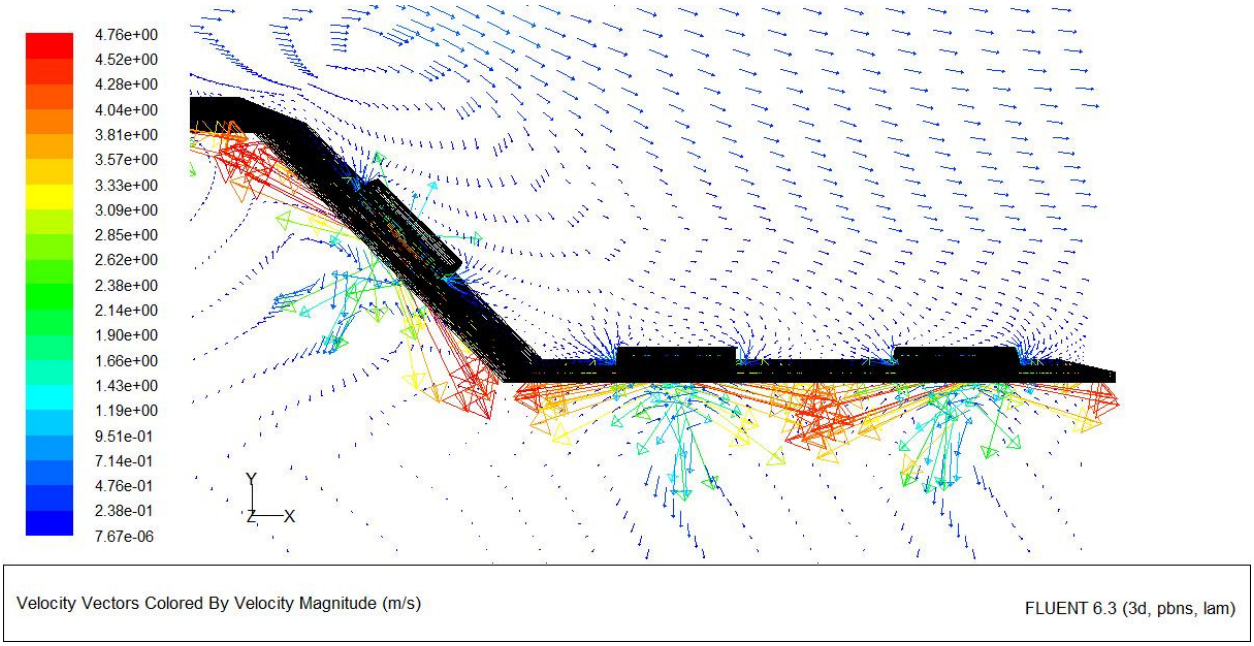

Figure B.6: Flow Behavior at a Wind Speed of 0.5 m/s and Suction Velocity of 0.03 m/s.

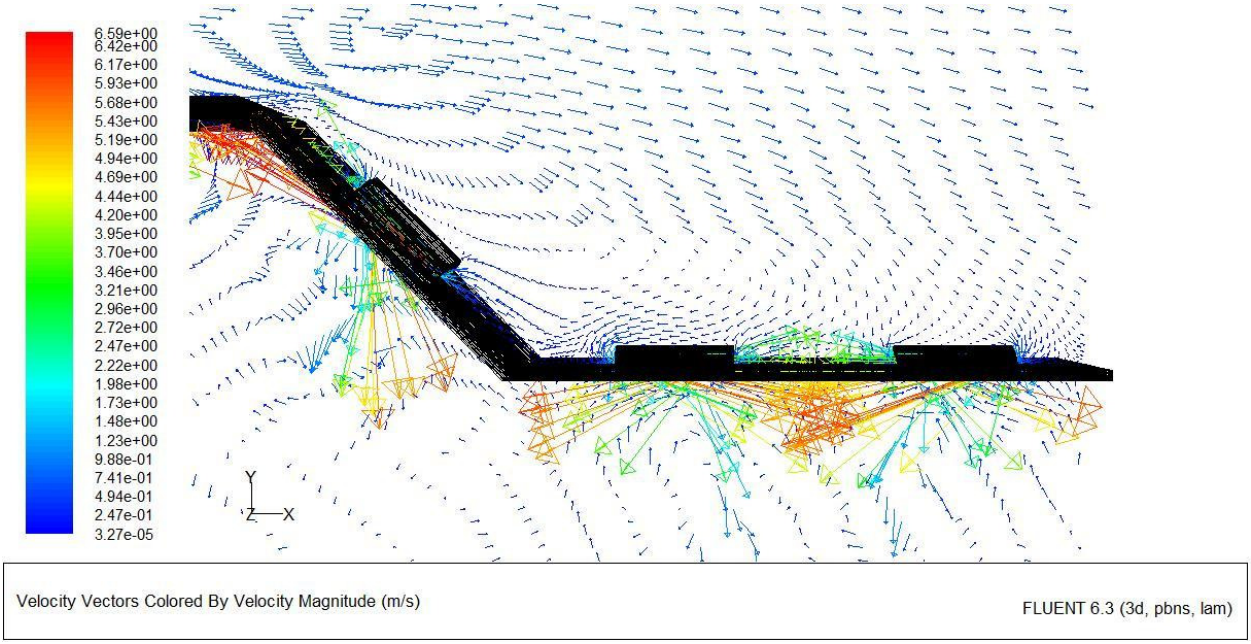

Figure B.7: Flow Behavior at a Wind Speed of 0.5 m/s and Suction Velocity of 0.04 m/s.

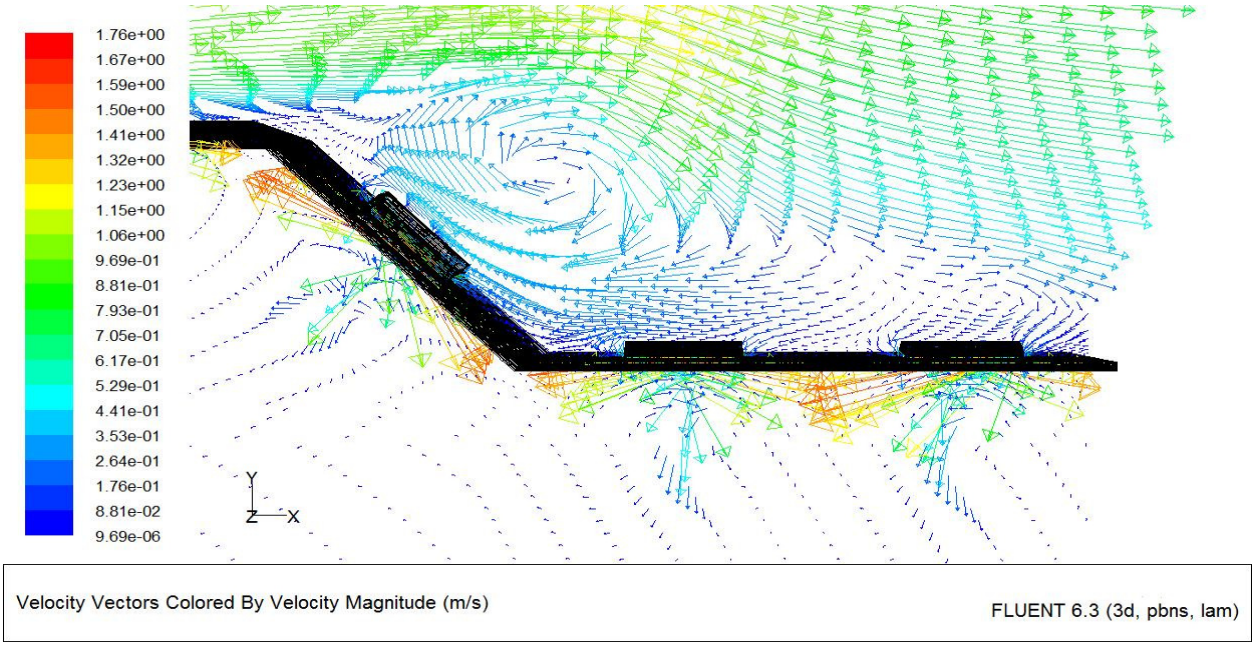

Figure B.8: Flow Behavior at a Wind Speed of 1.0 m/s and Suction Velocity of 0.01 m/s.

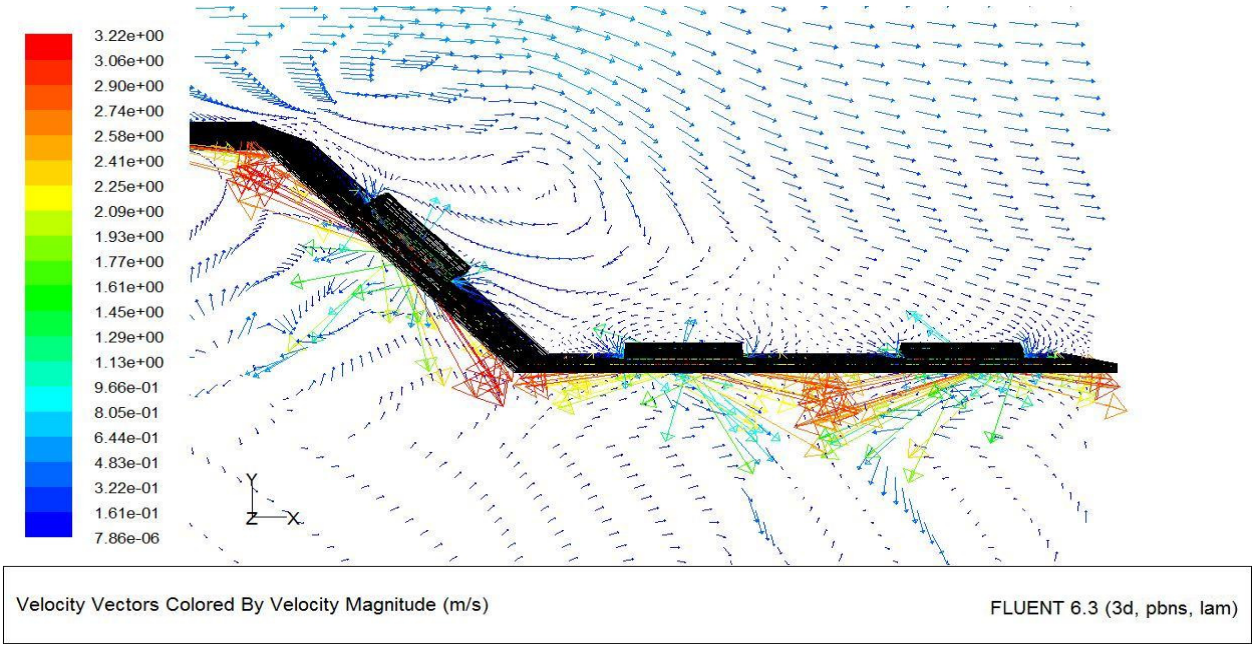

Figure B.9: Flow Behavior at a Wind Speed of 1.0 m/s and Suction Velocity of 0.02 m/s.

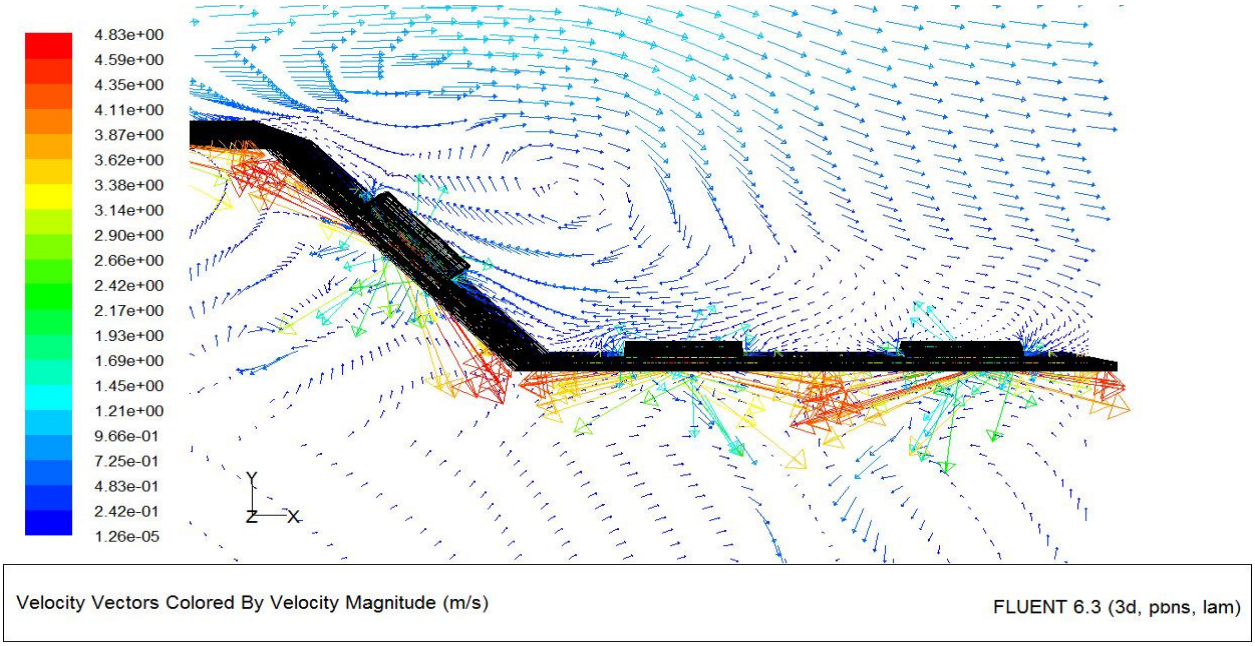

Figure B.10: Flow Behavior at a Wind Speed of 1.0 m/s and Suction Velocity of 0.03 m/s.

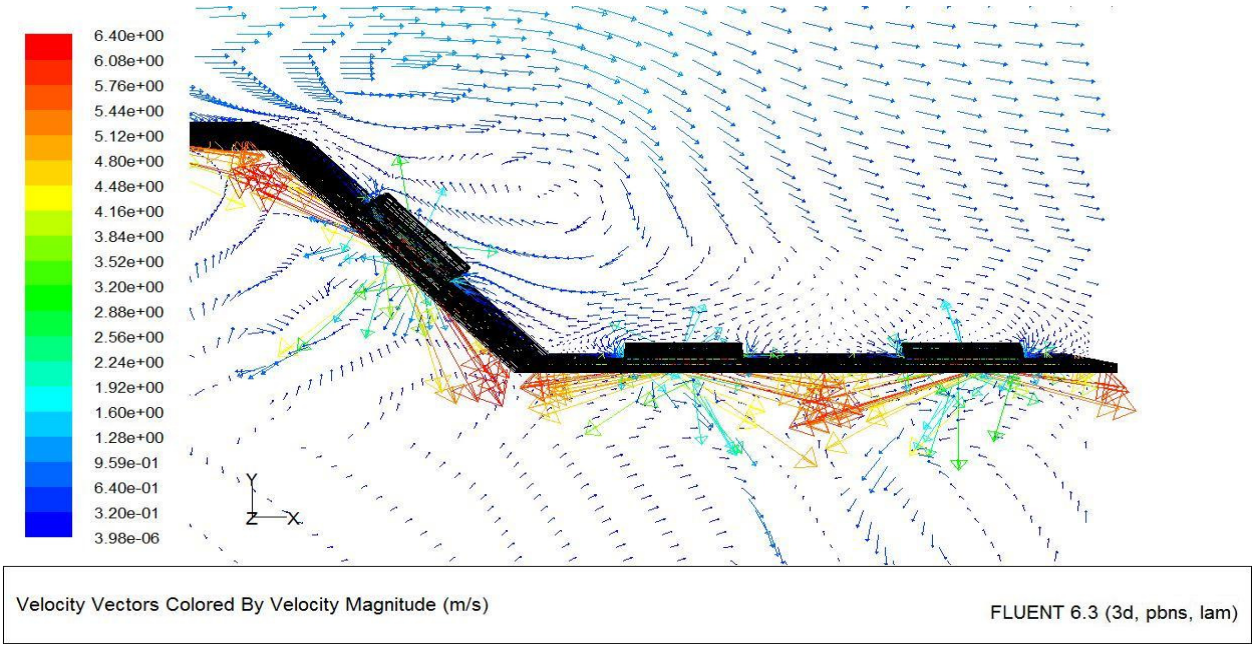

Figure B.11: Flow Behavior at a Wind Speed of 1.0 m/s and Suction Velocity of 0.04 m/s.

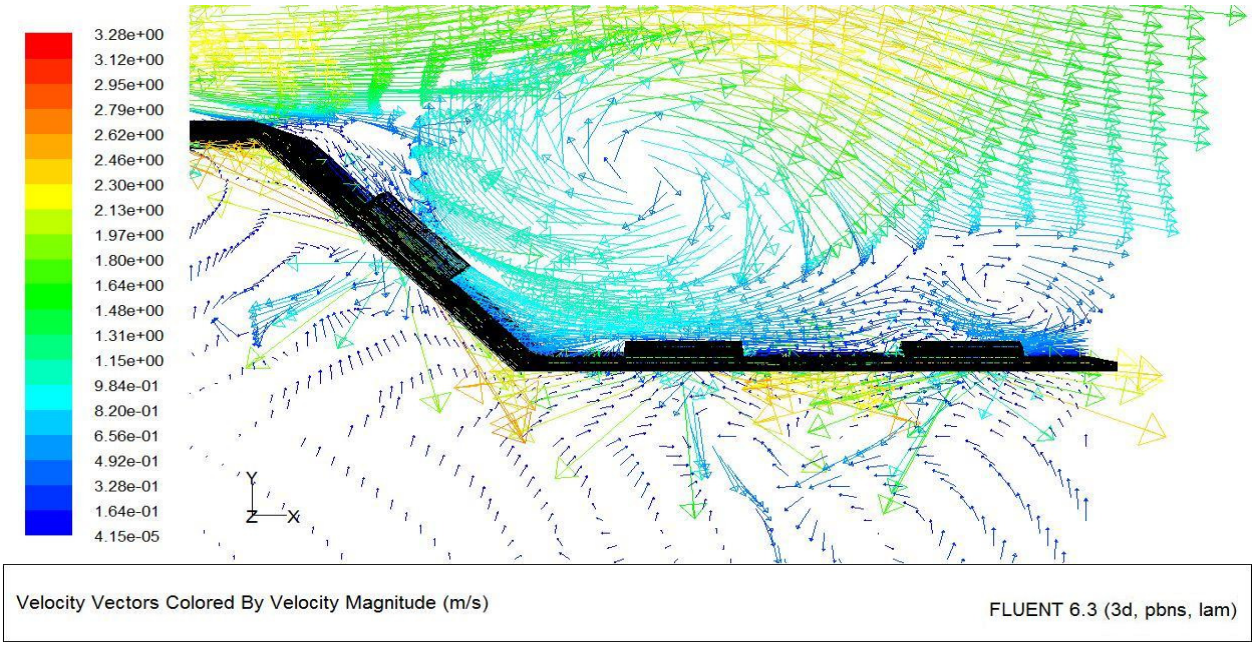

Figure B.12: Flow Behavior at a Wind Speed of 2.0 m/s and Suction Velocity of 0.01 m/s.

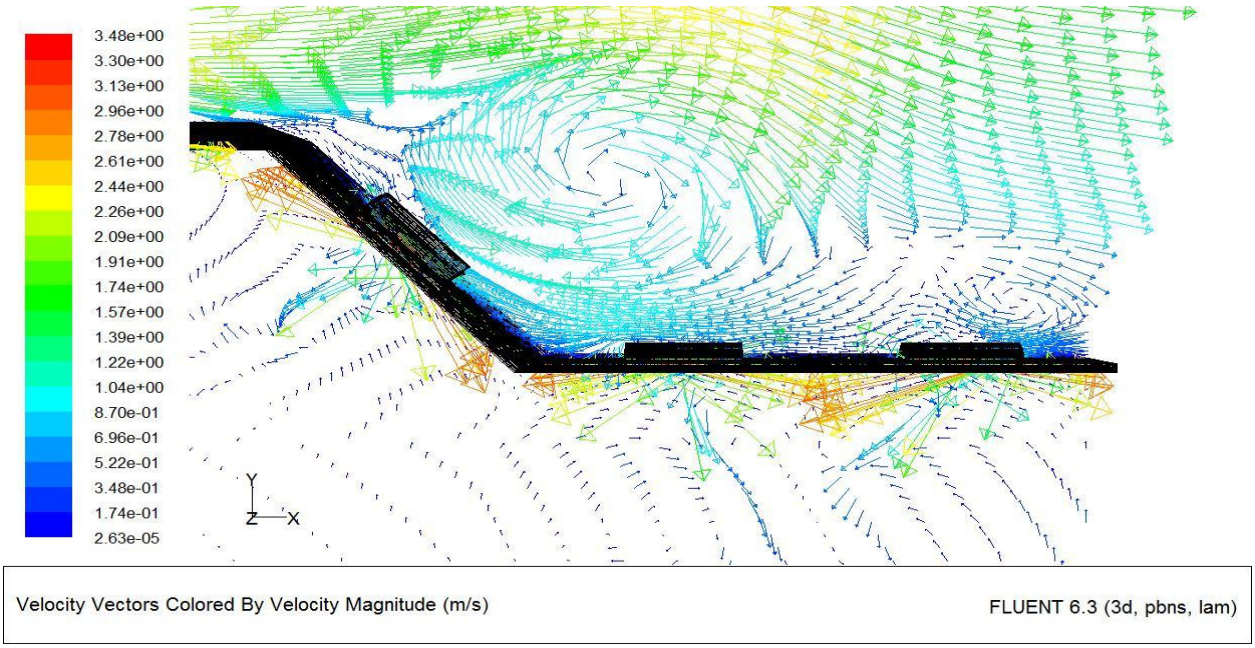

Figure B.13: Flow Behavior at a Wind Speed of 2.0 m/s and Suction Velocity of 0.02 m/s.

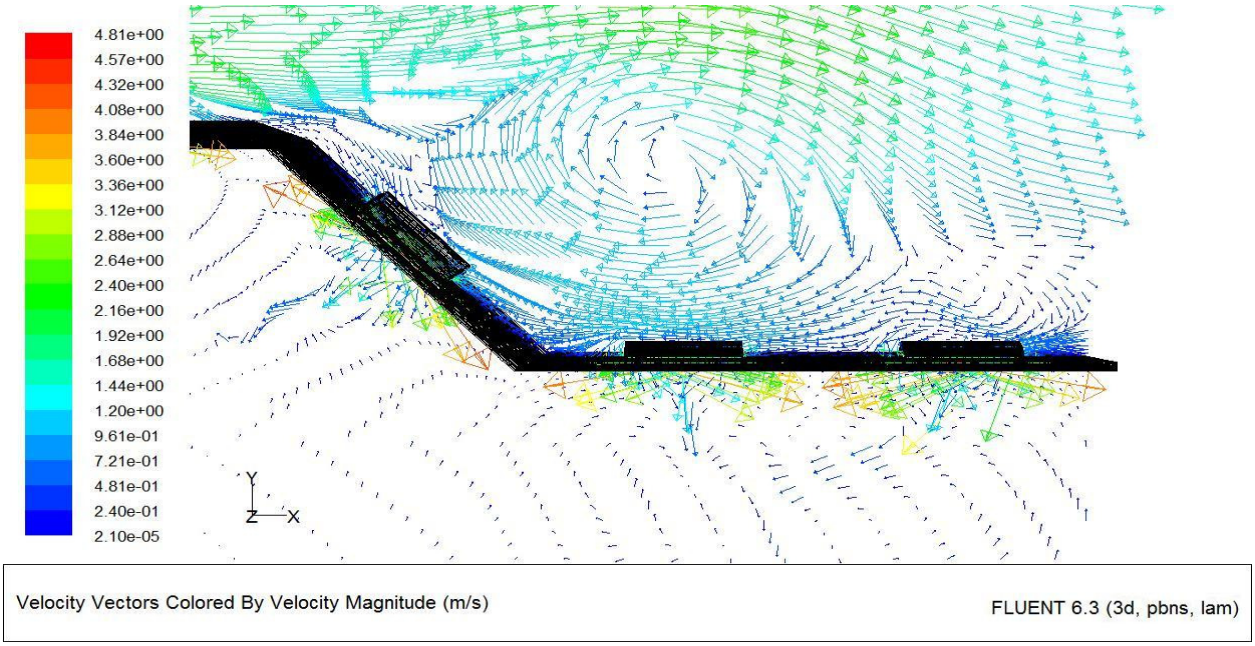

Figure B.14: Flow Behavior at a Wind Speed of 2.0 m/s and Suction Velocity of 0.03 m/s.

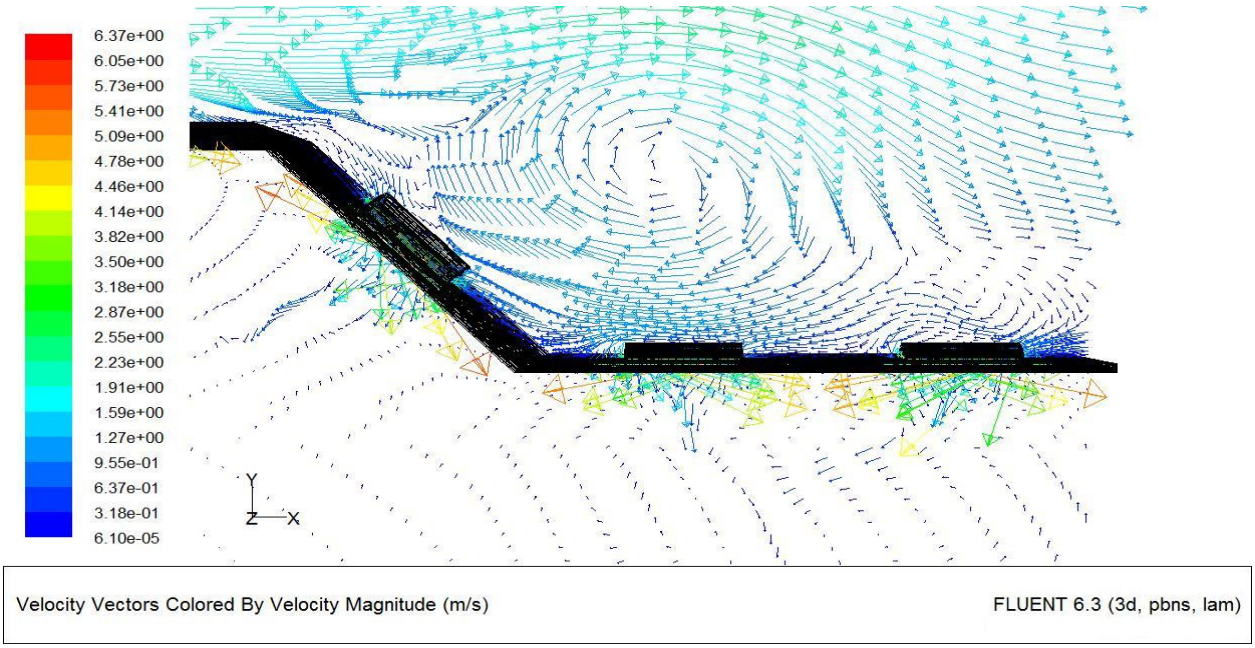

Figure B.15: Flow Behavior at a Wind Speed of 2.0 m/s and Suction Velocity of 0.04 m/s.

B.2 Vector Plots and Temperature Contours for No-Wind Models

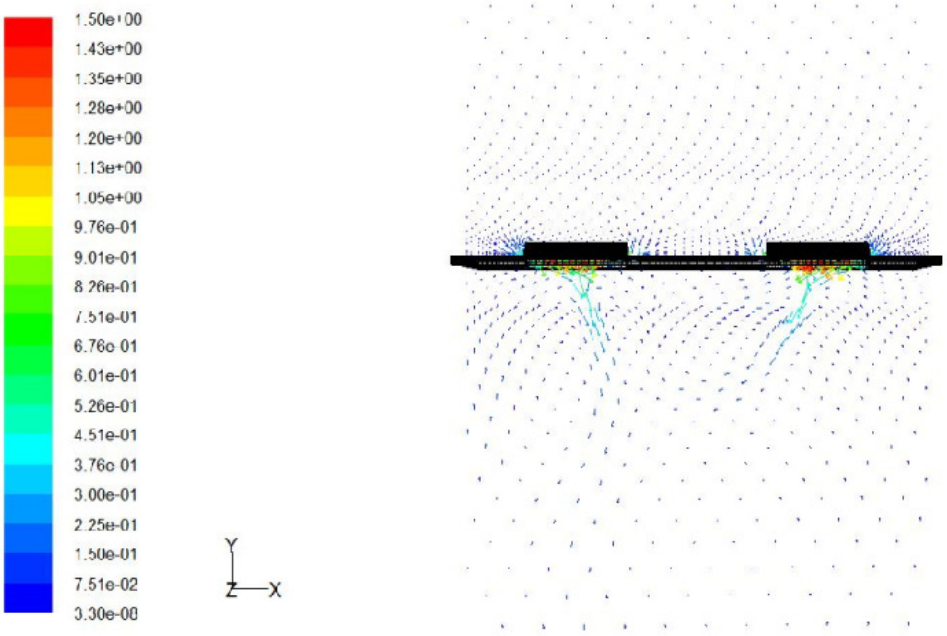

Figure B.16: Velocity Vectors for the No Wind Case at a Suction Velocity of 0.01 m/s.

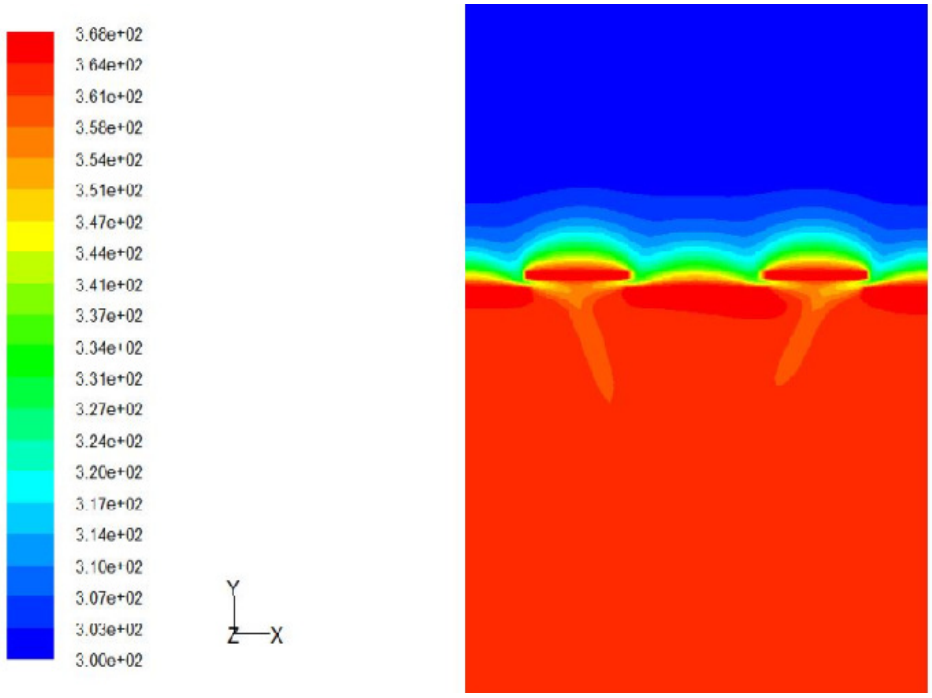

Figure B.17: Temperature Contours for the No Wind Case at a Suction Velocity of 0.01 m/s.

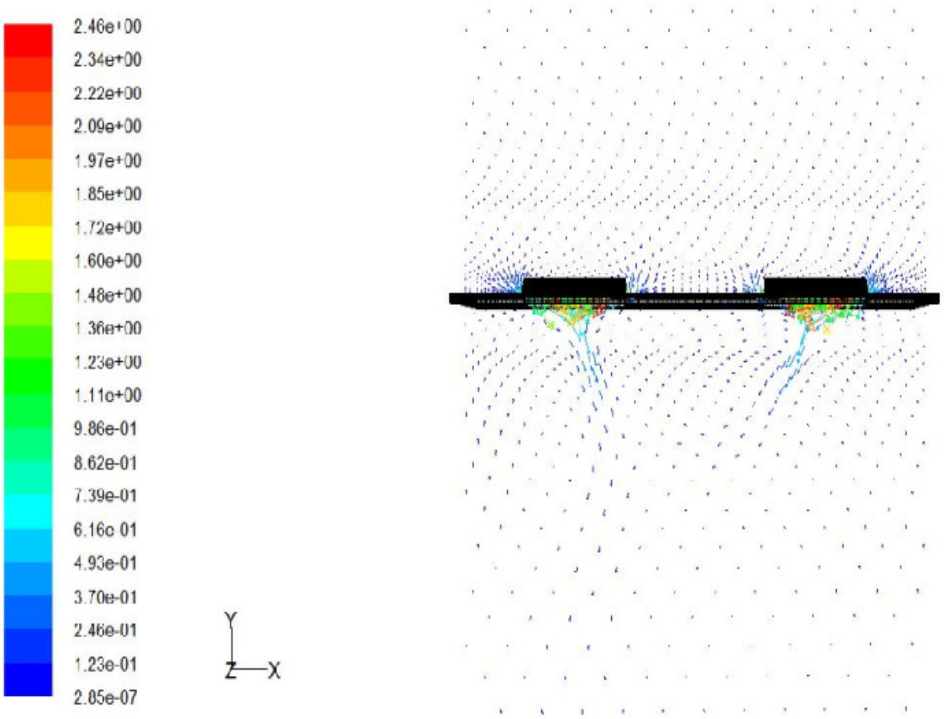

Figure B.18: Velocity Vectors for the No Wind Case at a Suction Velocity of 0.02 m/s.

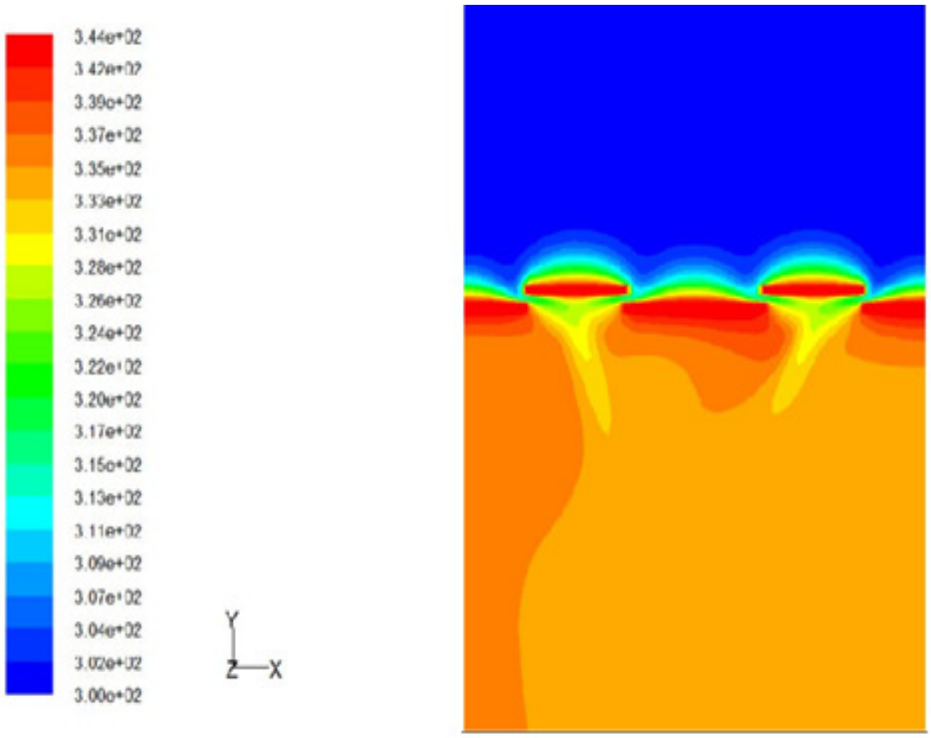

Figure B.19: Temperature Contours for the No Wind Case at a Suction Velocity of 0.02 m/s.

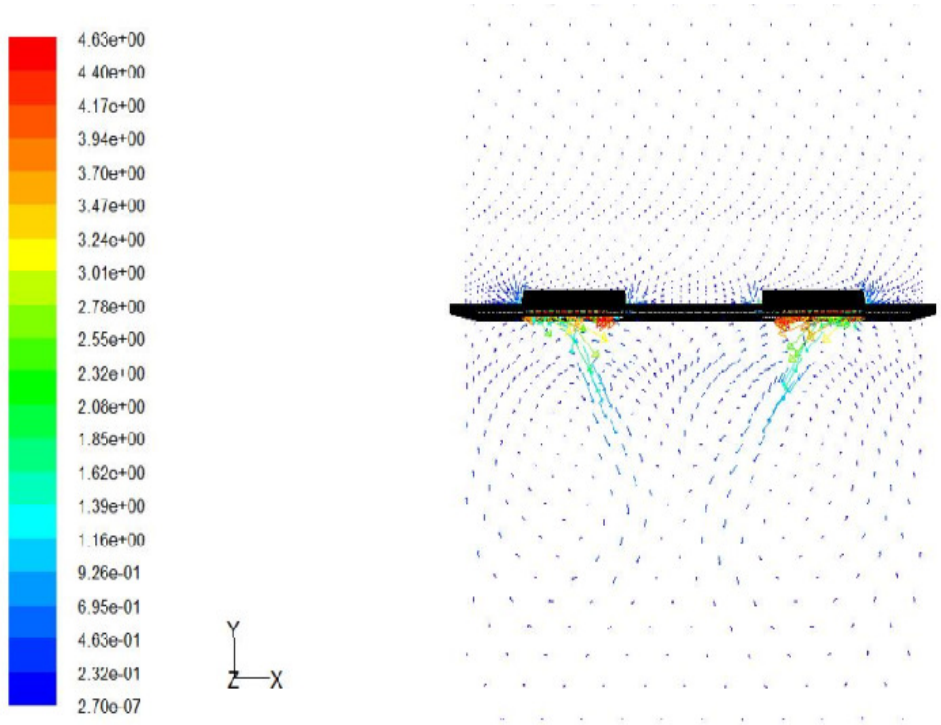

Figure B.20: Velocity Vectors for the No Wind Case at a Suction Velocity of 0.03 m/s.

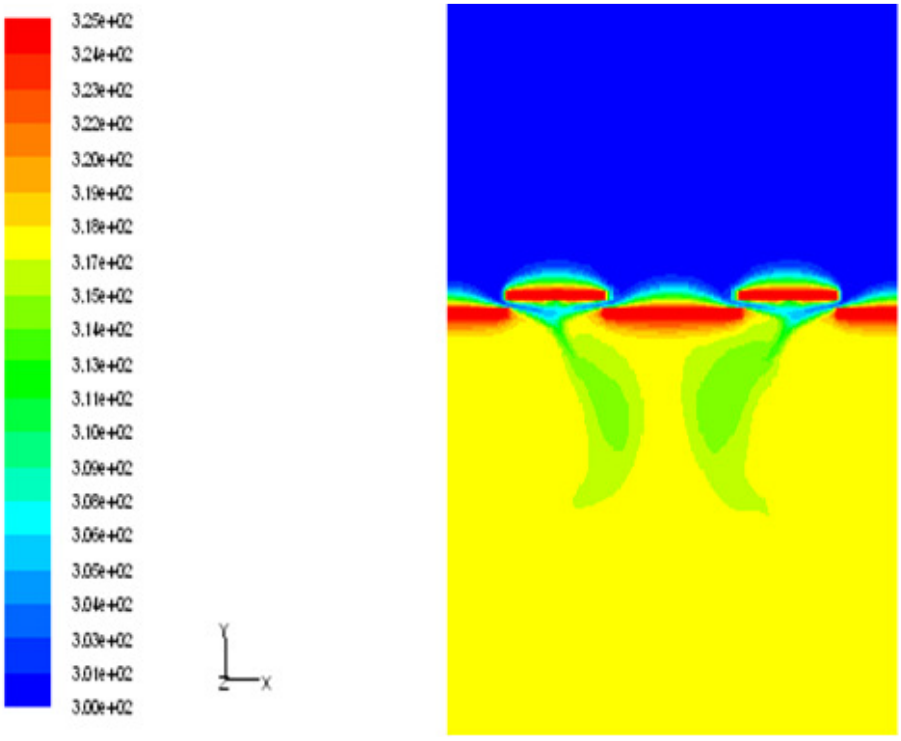

Figure B.21: Temperature Contours for the No Wind Case at a Suction Velocity of 0.03 m/s.

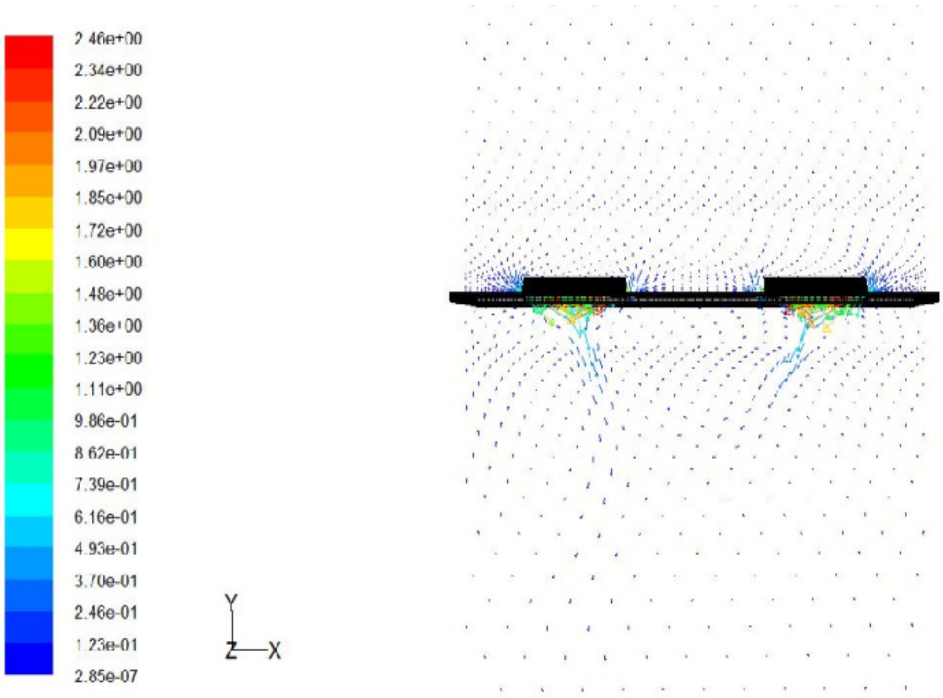

Figure B.22: Velocity Vectors for the No Wind Case at a Suction Velocity of 0.04 m/s.

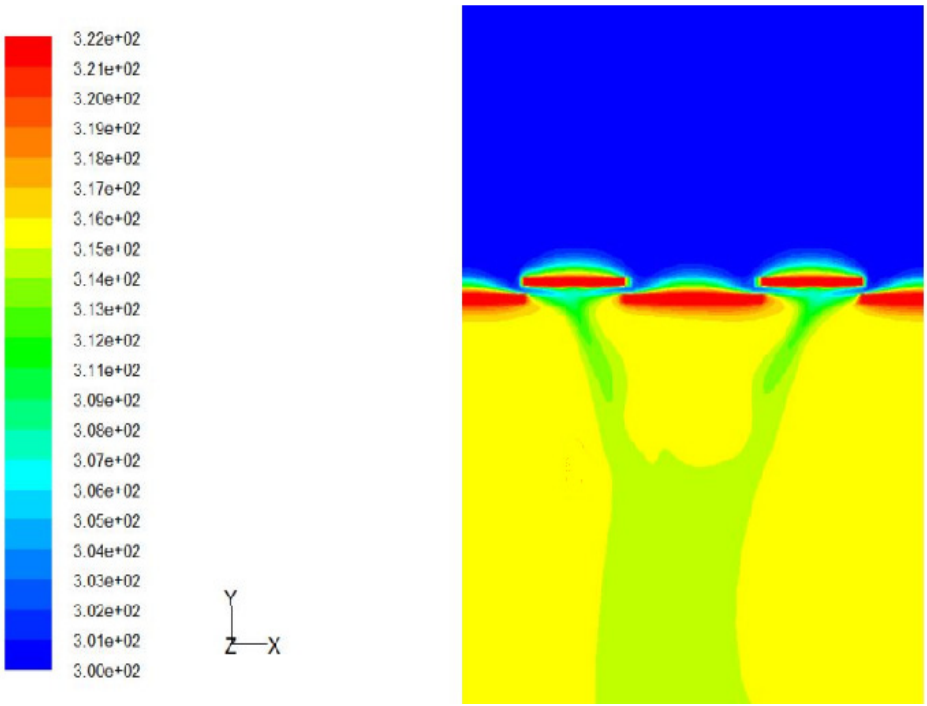

Figure B.23: Temperature Contours for the No Wind Case at a Suction Velocity of 0.04 m/s.

B.3 Vector Plots and Temperature Contours for Wind Models

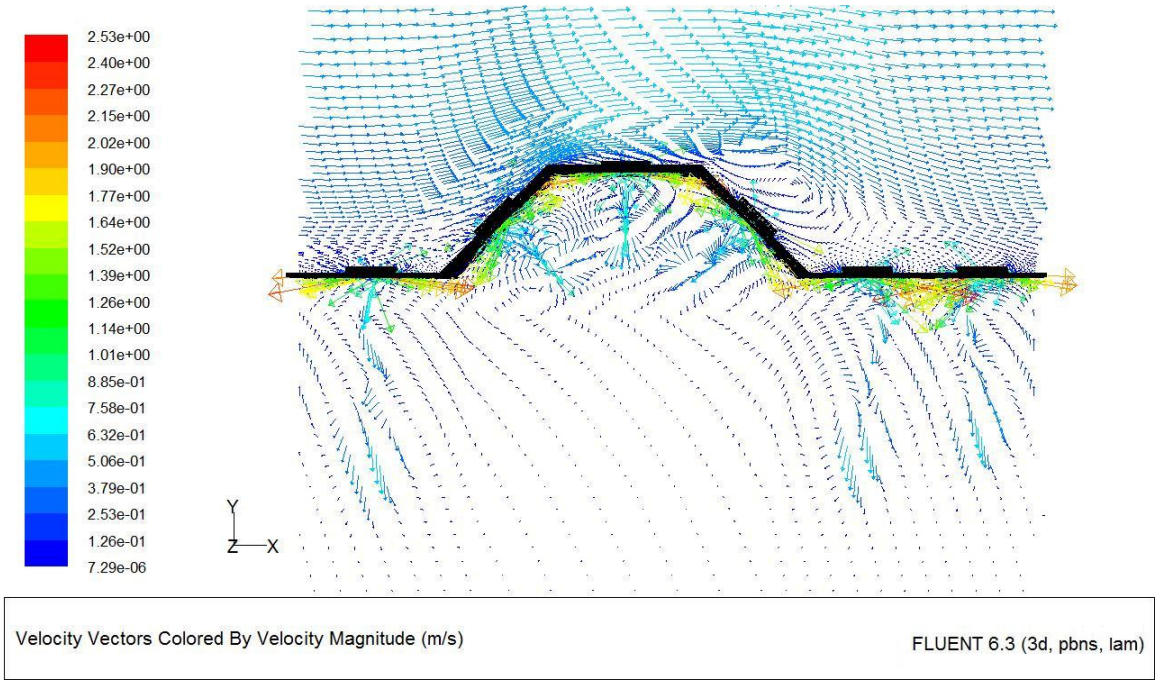

Figure B.24: Velocity Vectors at a Wind Speed of 0.5 m/s and Suction Velocity of 0.01 m/s.

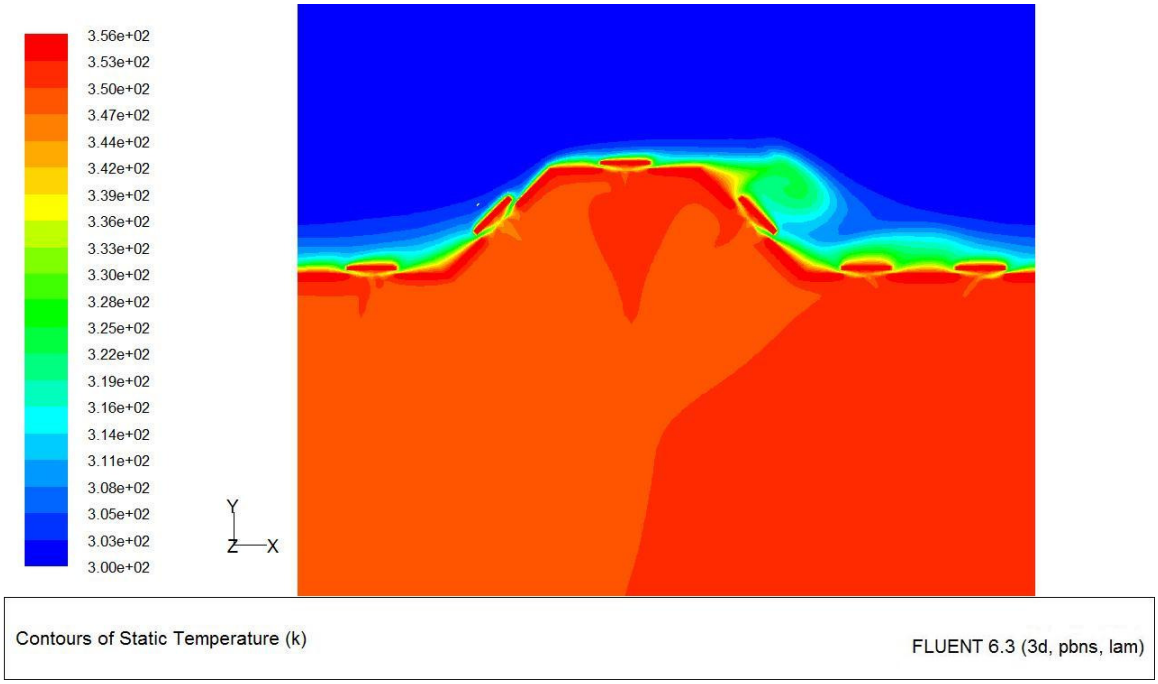

Figure B.25: Temperature Contours at a Wind Speed of 0.5 m/s and Suction Velocity of 0.01 m/s.

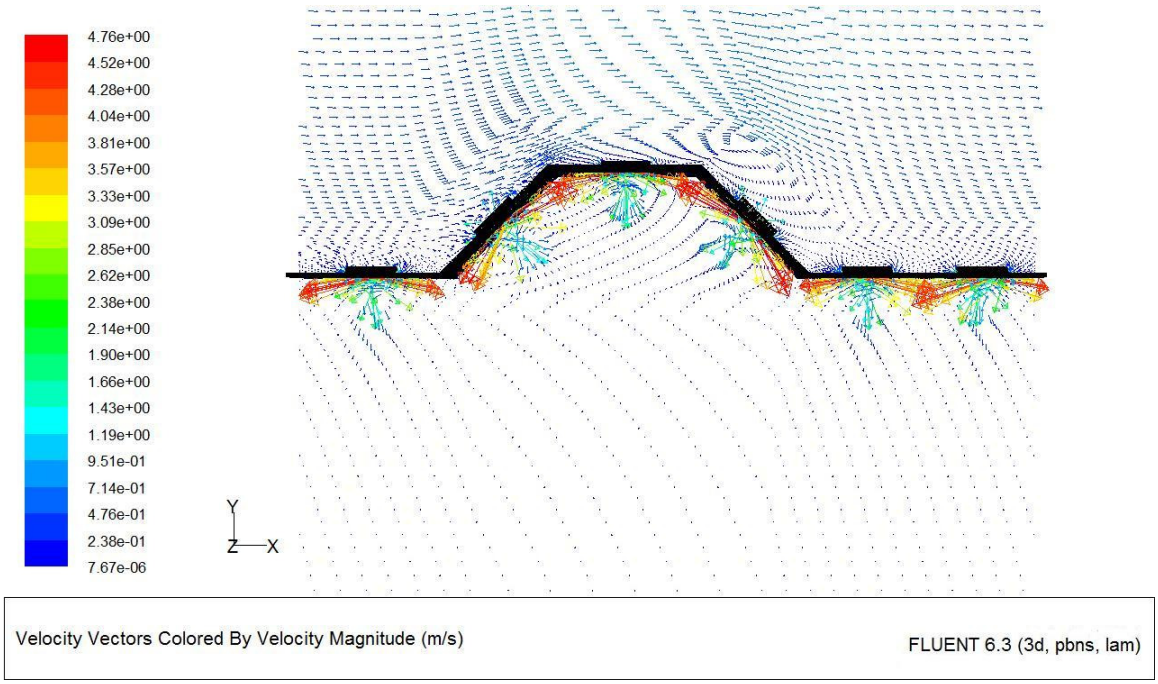

Figure B.26: Velocity Vectors at a Wind Speed of 0.5 m/s and Suction Velocity of 0.02 m/s.

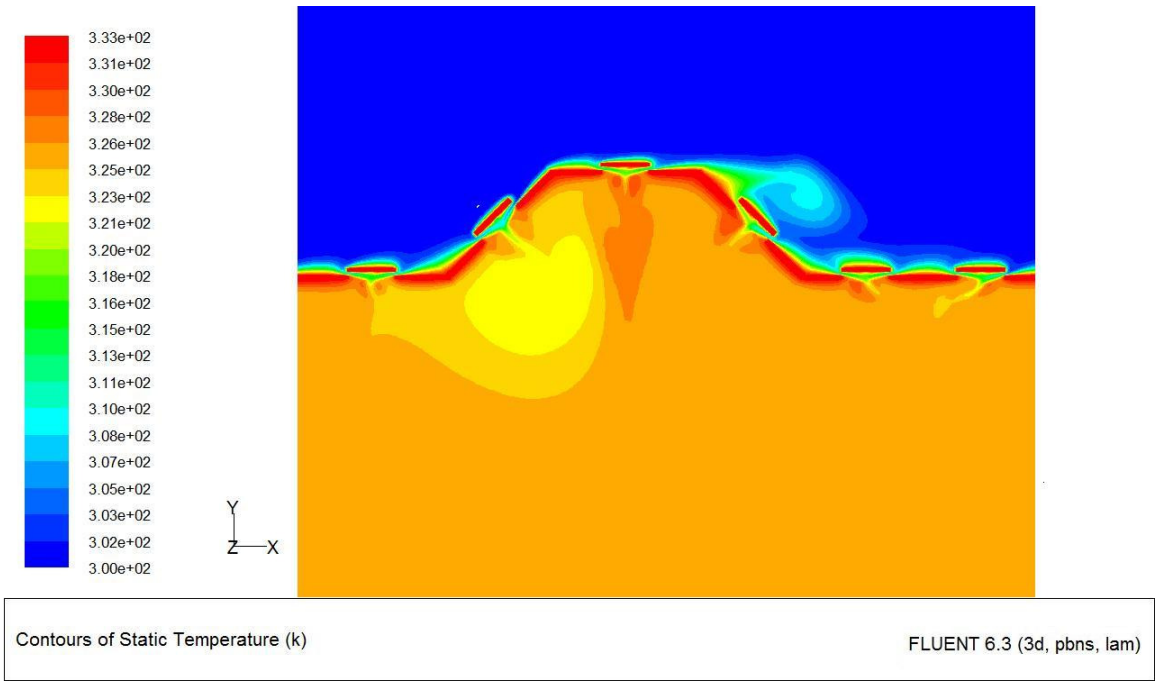

Figure B.27: Temperature Contours at a Wind Speed of 0.5 m/s and Suction Velocity of 0.02 m/s.

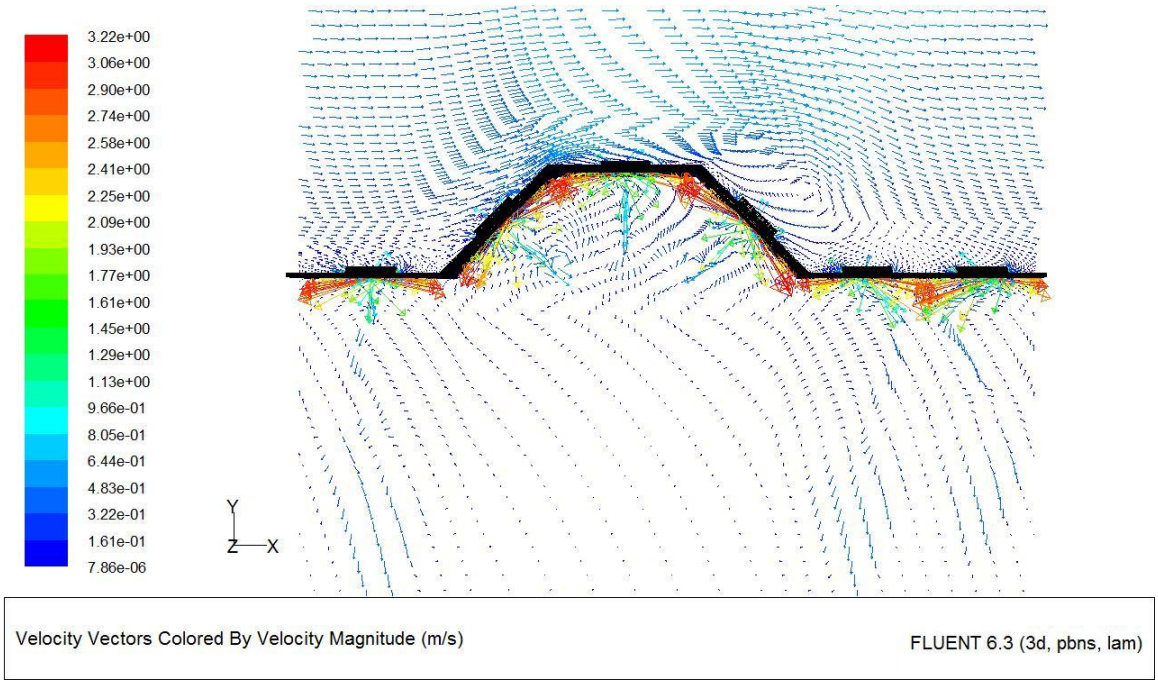

Figure B.28: Velocity Vectors at a Wind Speed of 0.5 m/s and Suction Velocity of 0.03 m/s.

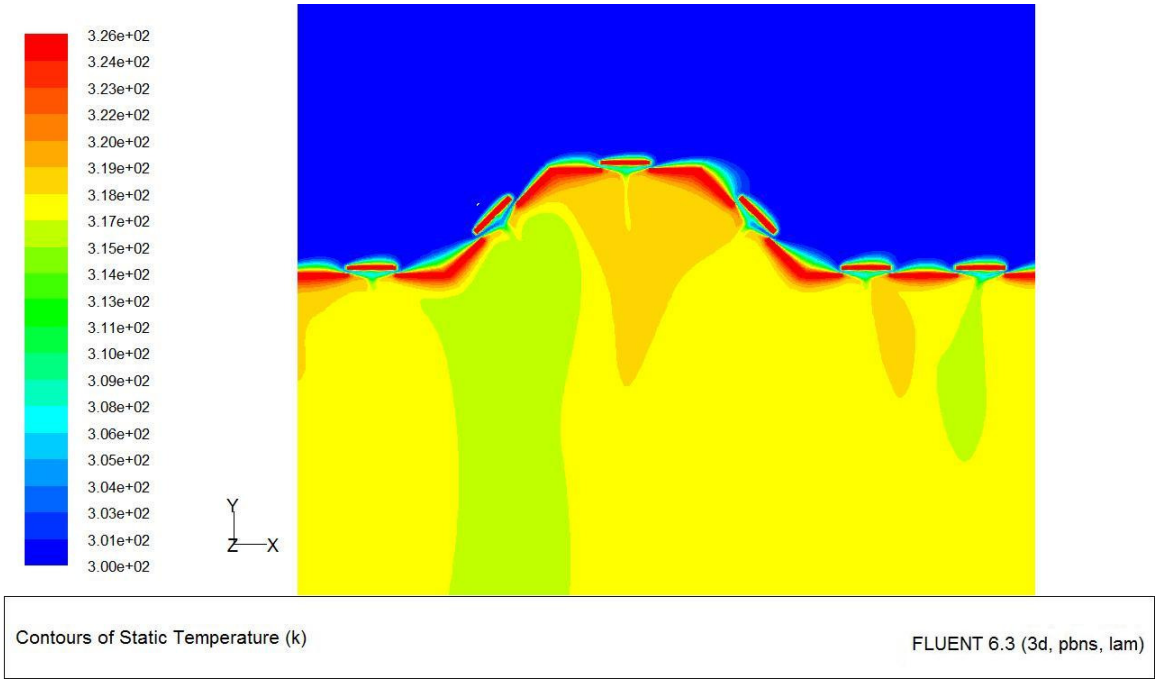

Figure B.29: Temperature Contours at a Wind Speed of 0.5 m/s and Suction Velocity of 0.03 m/s.

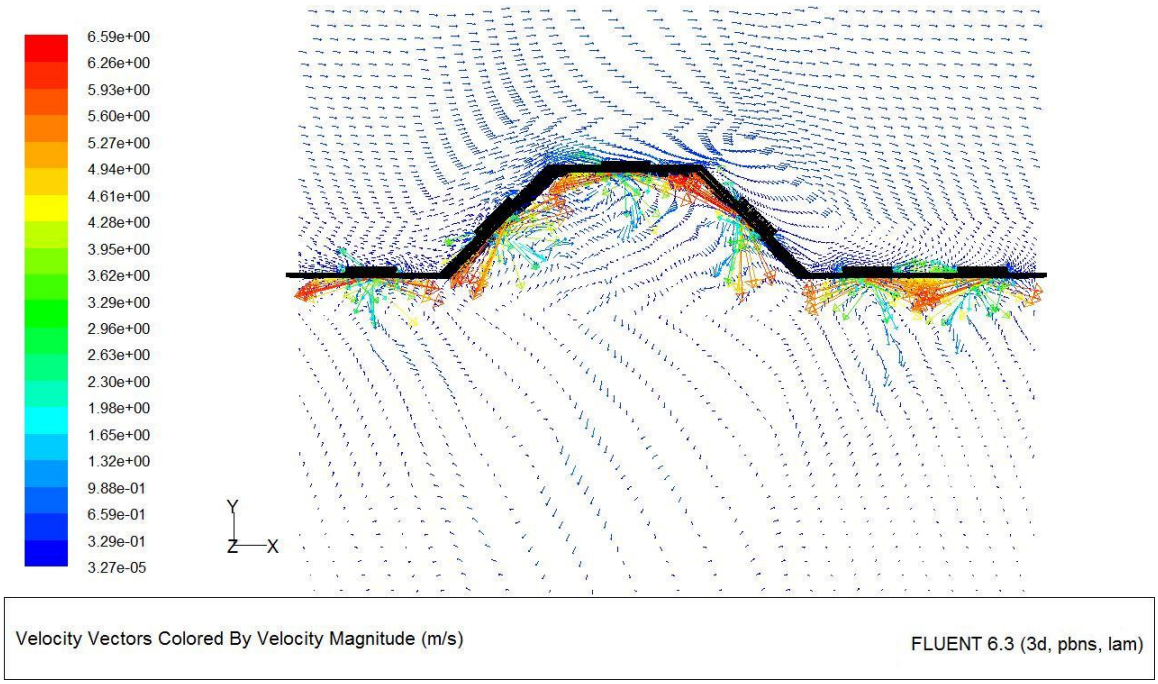

Figure B.30: Velocity Vectors at a Wind Speed of 0.5 m/s and Suction Velocity of 0.04 m/s.

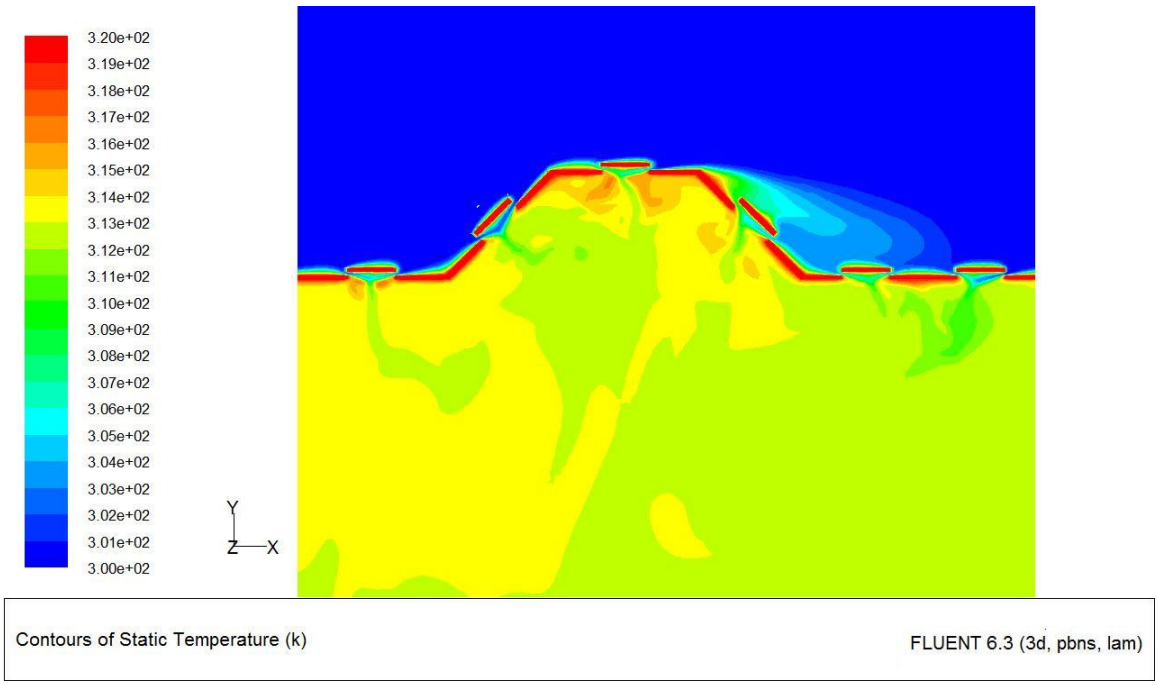

Figure B.31: Temperature Contours at a Wind Speed of 0.5 m/s and Suction Velocity of 0.04 m/s.

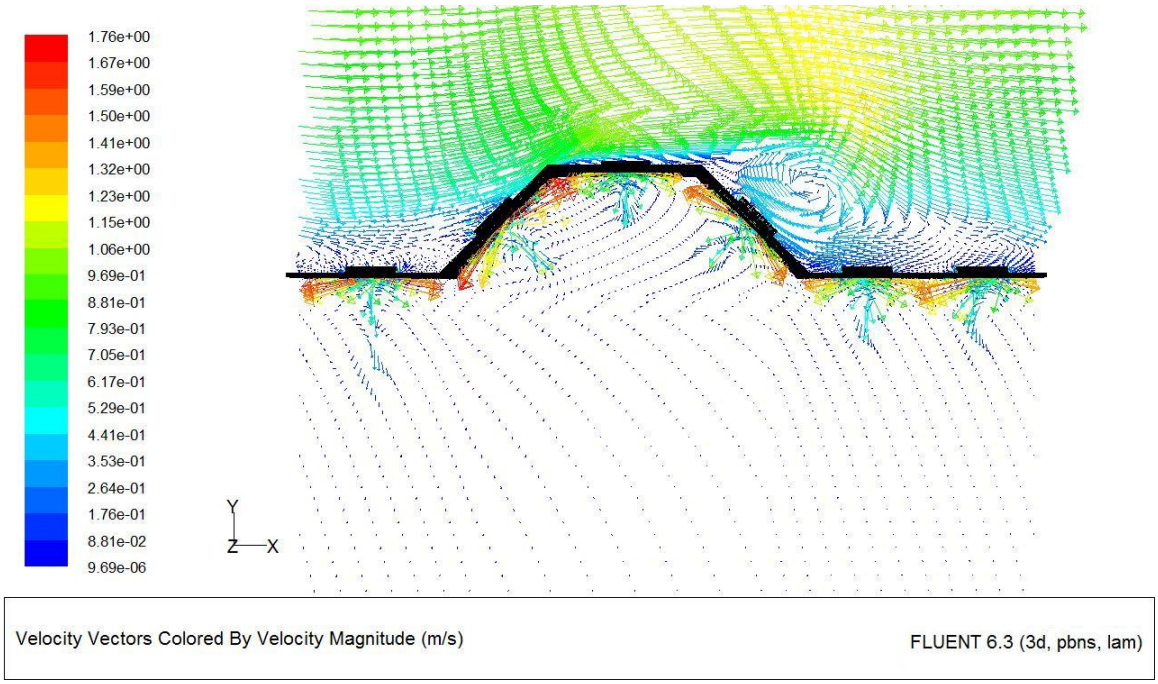

Figure B.32: Velocity Vectors at a Wind Speed of 1.0 m/s and Suction Velocity of 0.01 m/s.

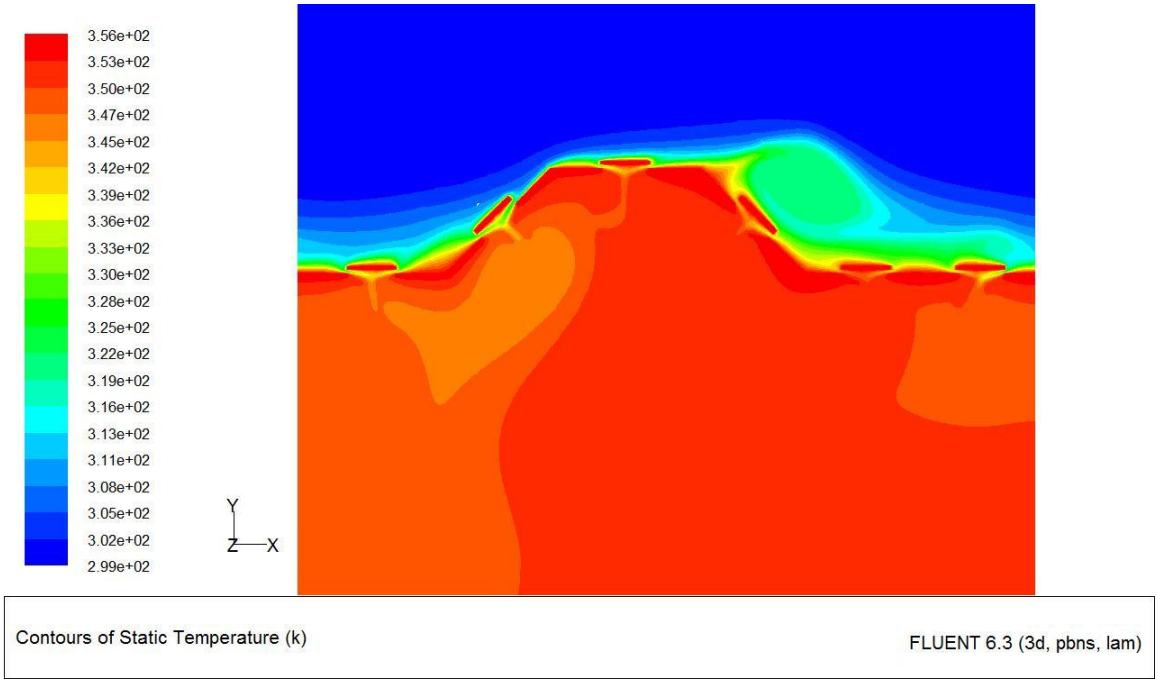

Figure B.33: Temperature Contours at a Wind Speed of 1.0 m/s and Suction Velocity of 0.01 m/s.

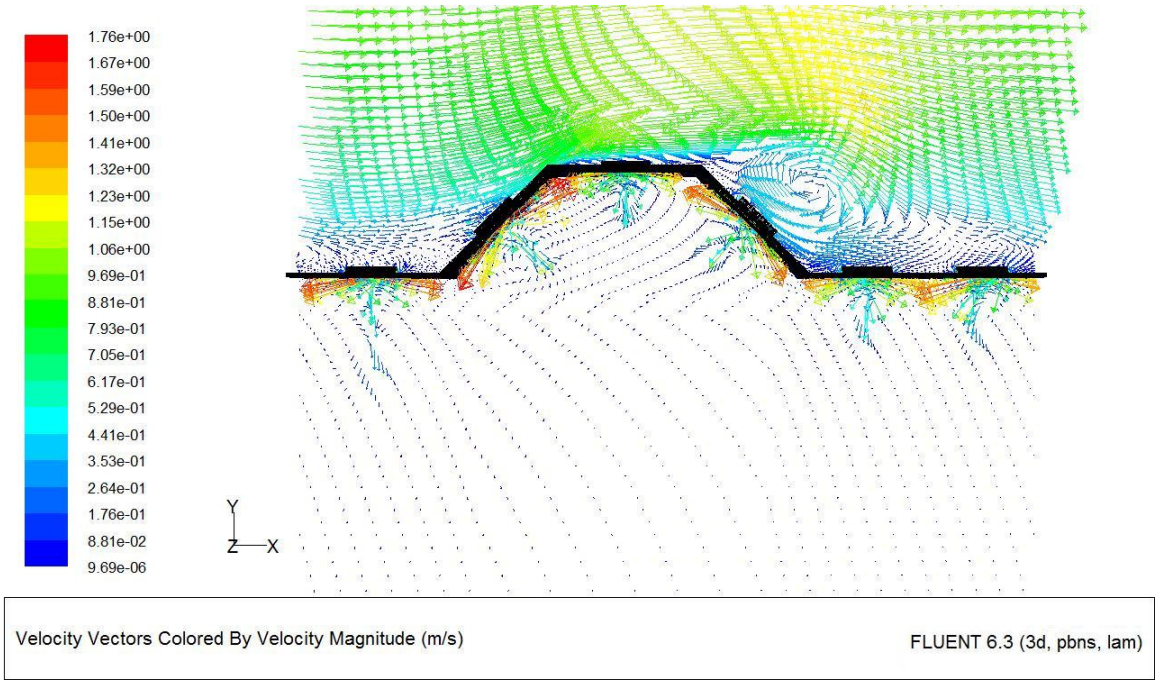

Figure B.34: Velocity Vectors at a Wind Speed of 1.0 m/s and Suction Velocity of 0.02 m/s.

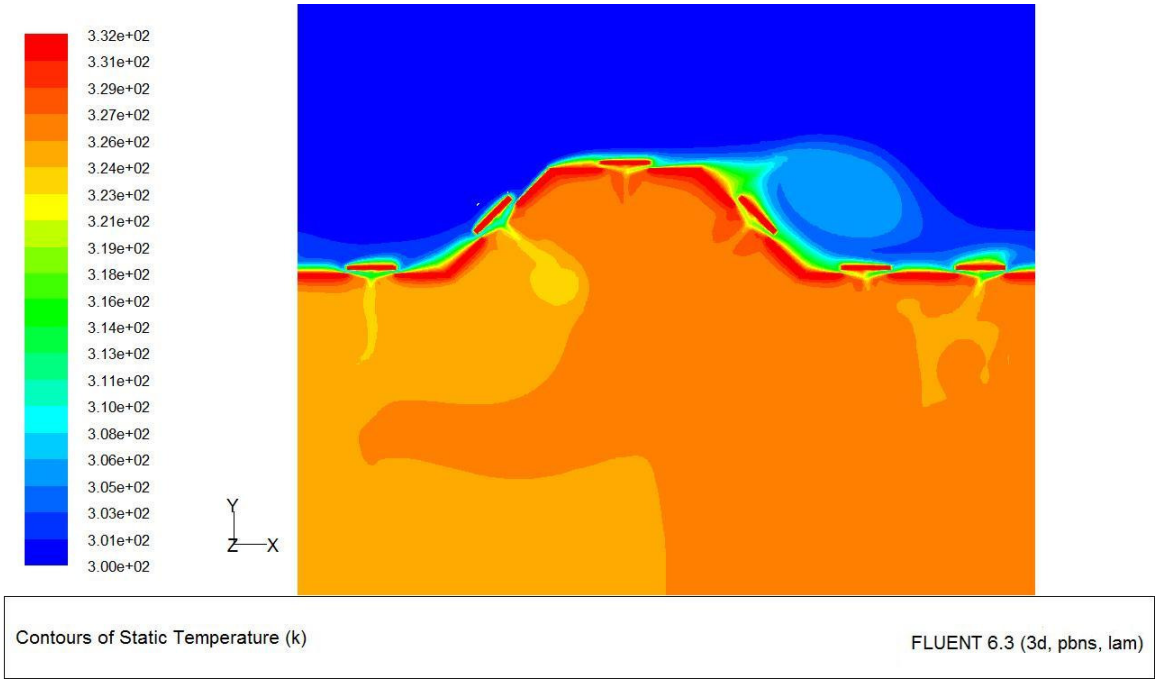

Figure B.35: Temperature Contours at a Wind Speed of 1.0 m/s and Suction Velocity of 0.02 m/s.

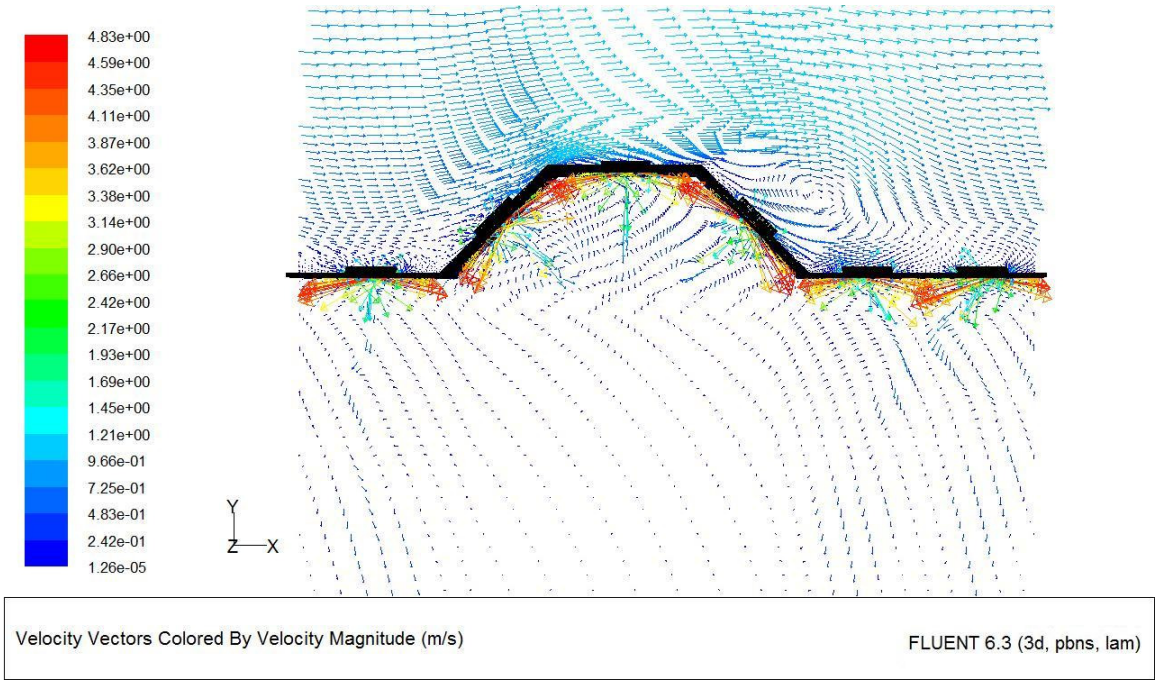

Figure B.36: Velocity Vectors at a Wind Speed of 1.0 m/s and Suction Velocity of 0.03 m/s.

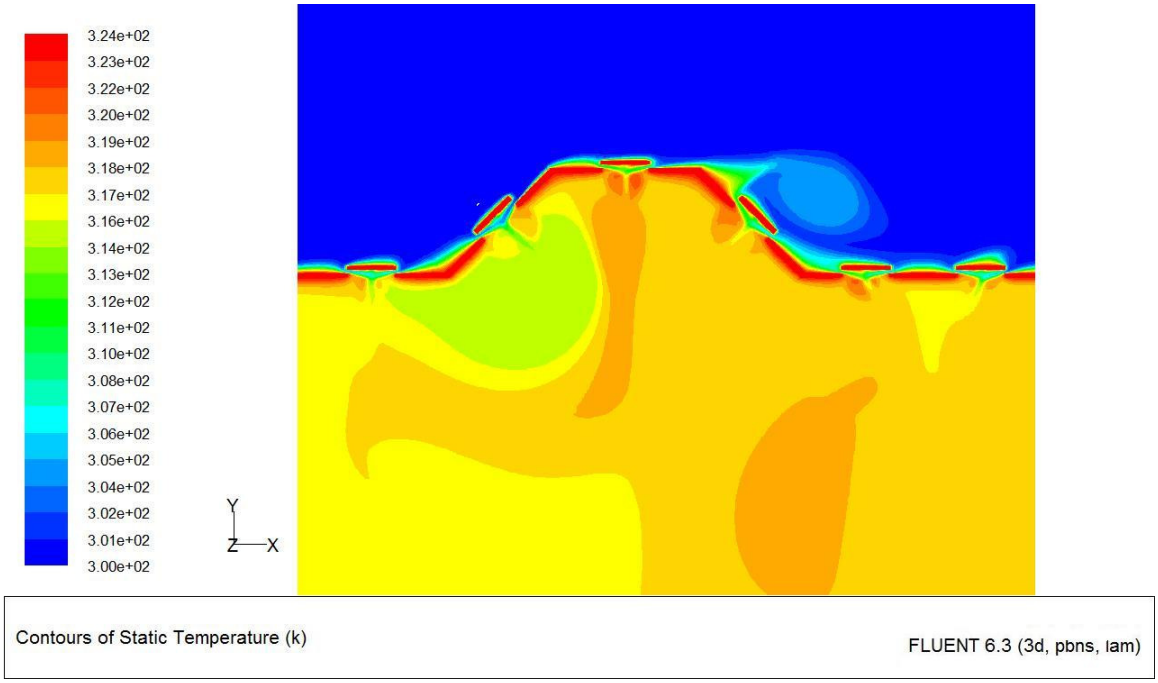

Figure B.37: Temperature Contours at a Wind Speed of 1.0 m/s and Suction Velocity of 0.03 m/s.

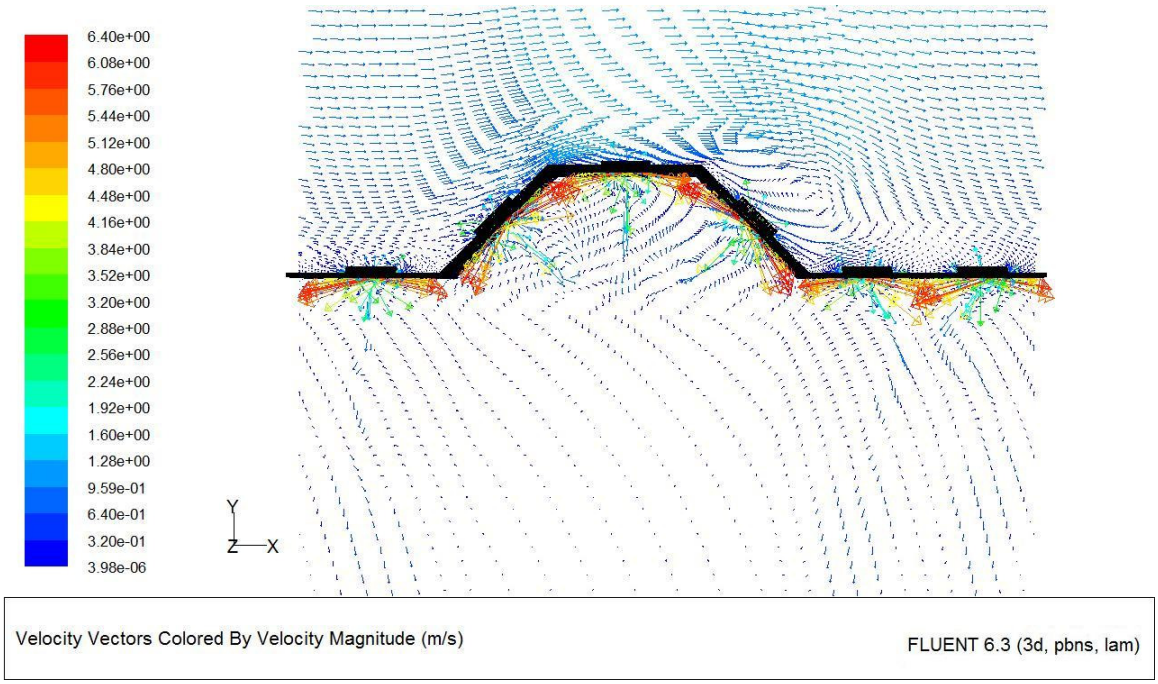

Figure B.38: Velocity Vectors at a Wind Speed of 1.0 m/s and Suction Velocity of 0.04 m/s.

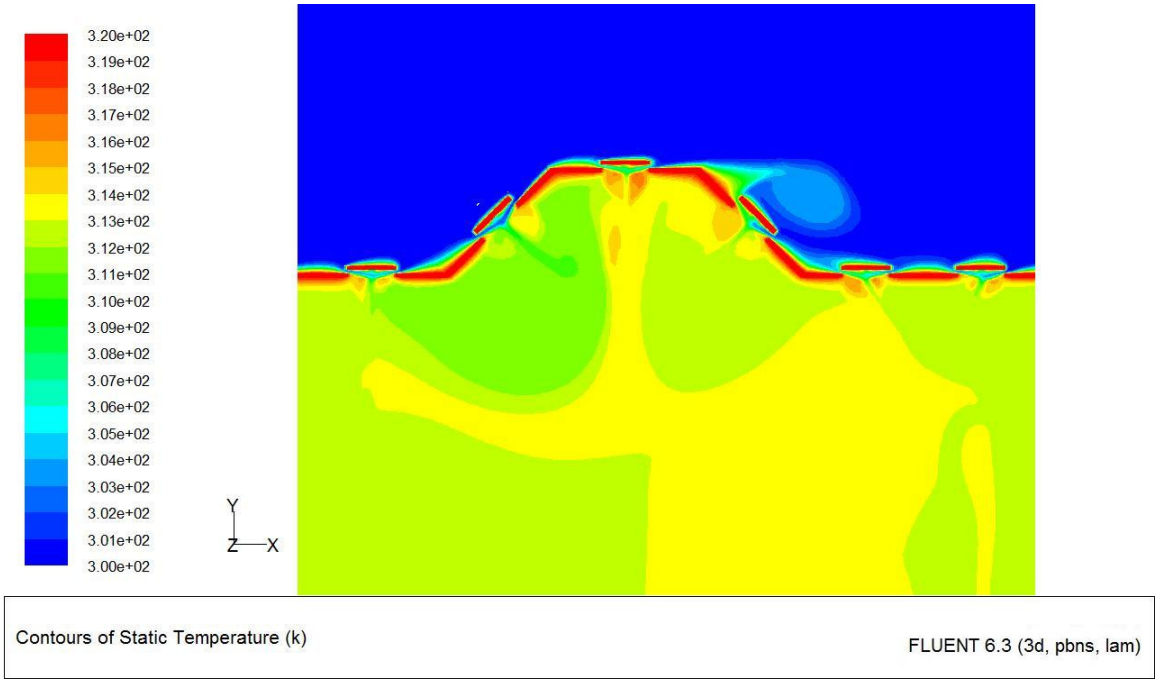

Figure B.39: Temperature Contours at a Wind Speed of 1.0 m/s and Suction Velocity of 0.04 m/s.

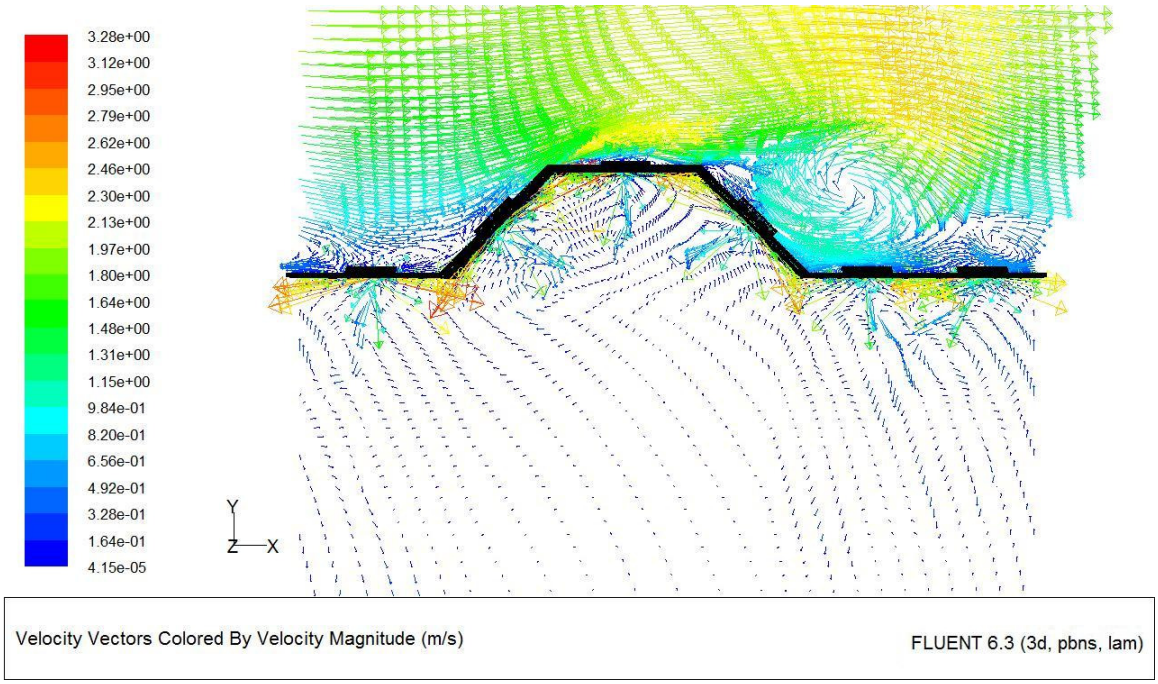

Figure B.40: Velocity Vectors at a Wind Speed of 2.0 m/s and Suction Velocity of 0.01 m/s.

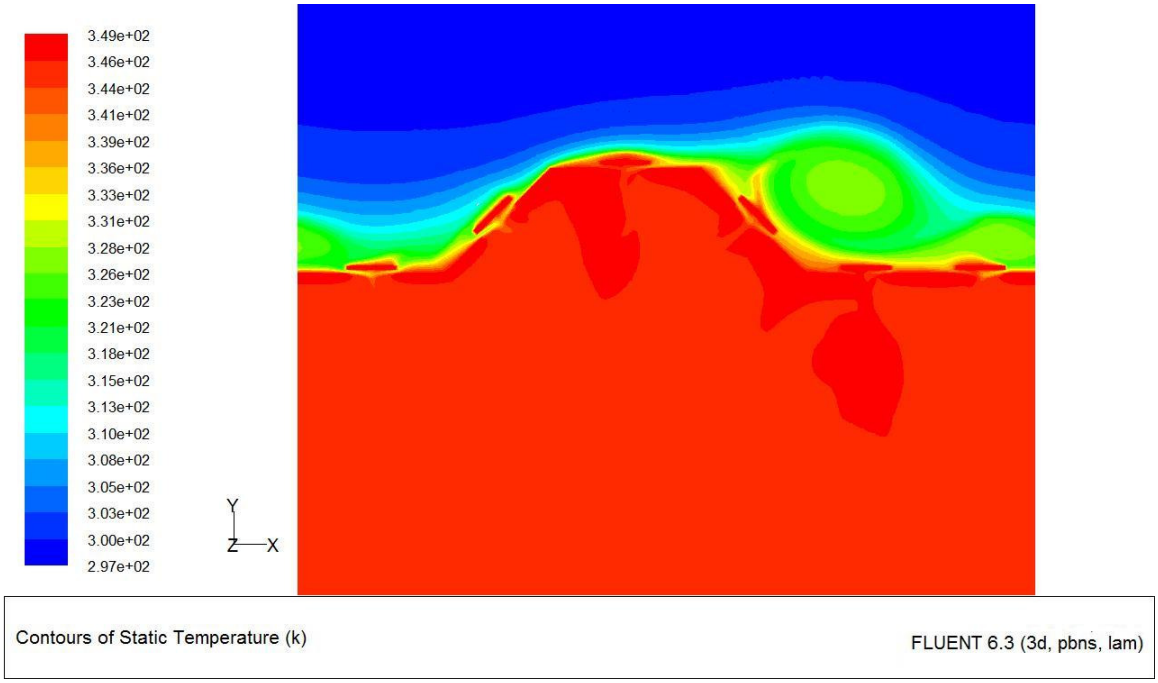

Figure B.41: Temperature Contours at a Wind Speed of 2.0 m/s and Suction Velocity of 0.01 m/s.

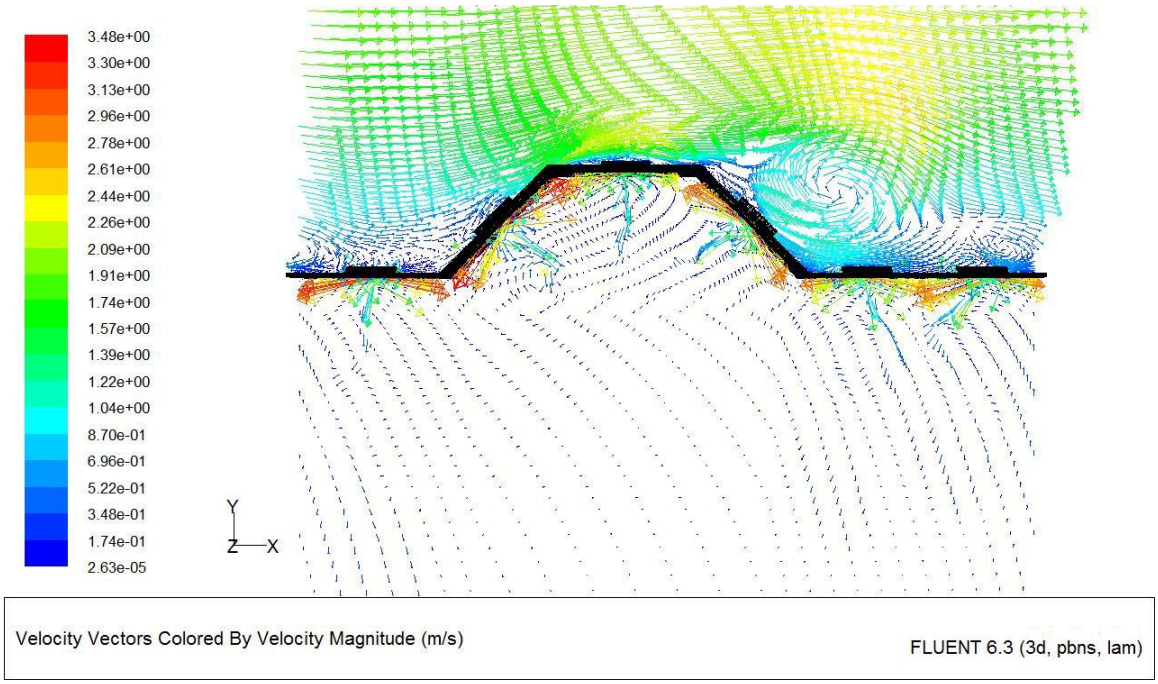

Figure B.42: Velocity Vectors at a Wind Speed of 2.0 m/s and Suction Velocity of 0.02 m/s.

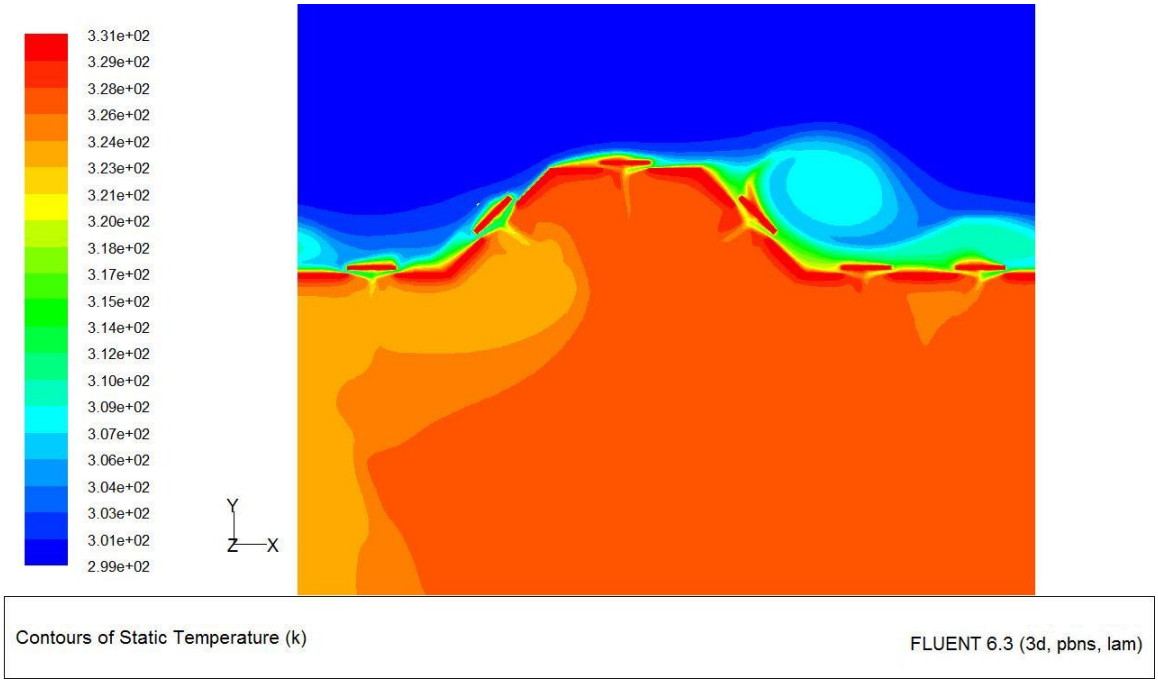

Figure B.43: Temperature Contours at a Wind Speed of 2.0 m/s and Suction Velocity of 0.02 m/s.

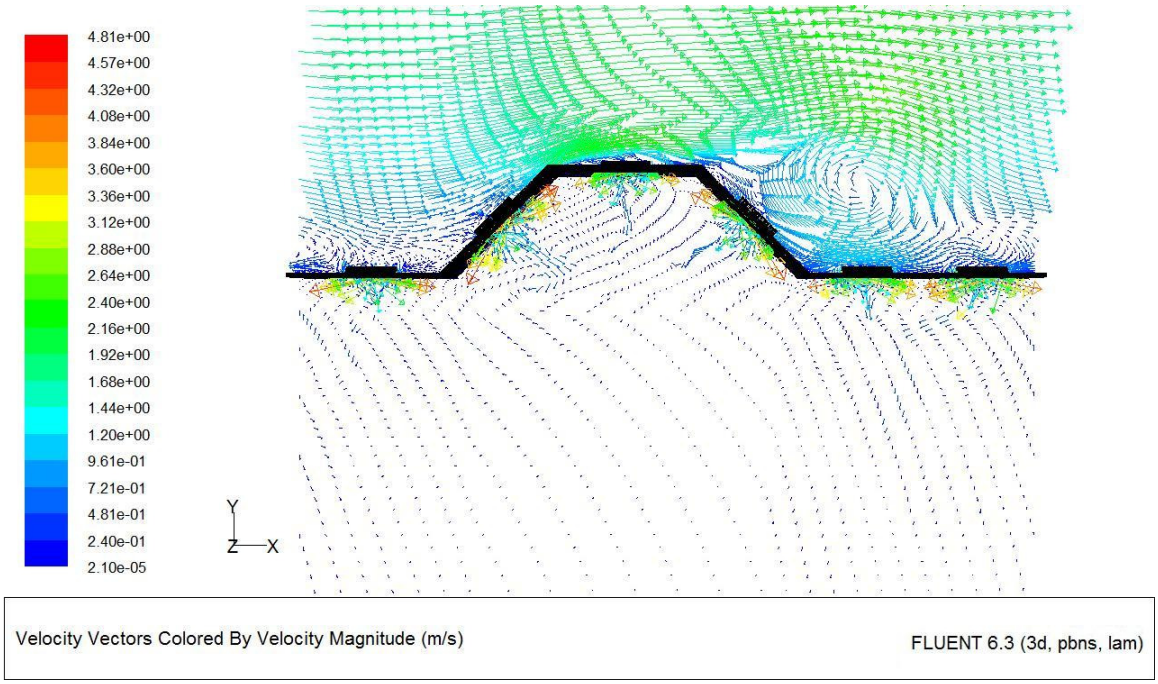

Figure B.44: Velocity Vectors at a Wind Speed of 2.0 m/s and Suction Velocity of 0.03 m/s.

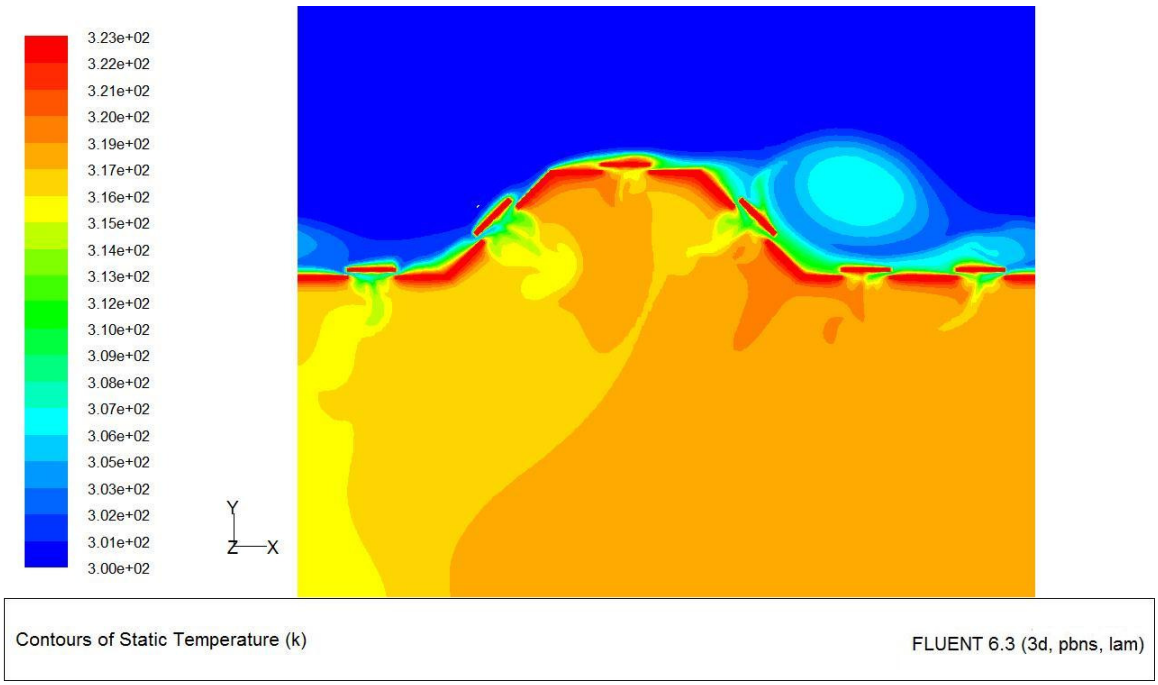

Figure B.45: Temperature Contours at a Wind Speed of 2.0 m/s and Suction Velocity of 0.03 m/s.

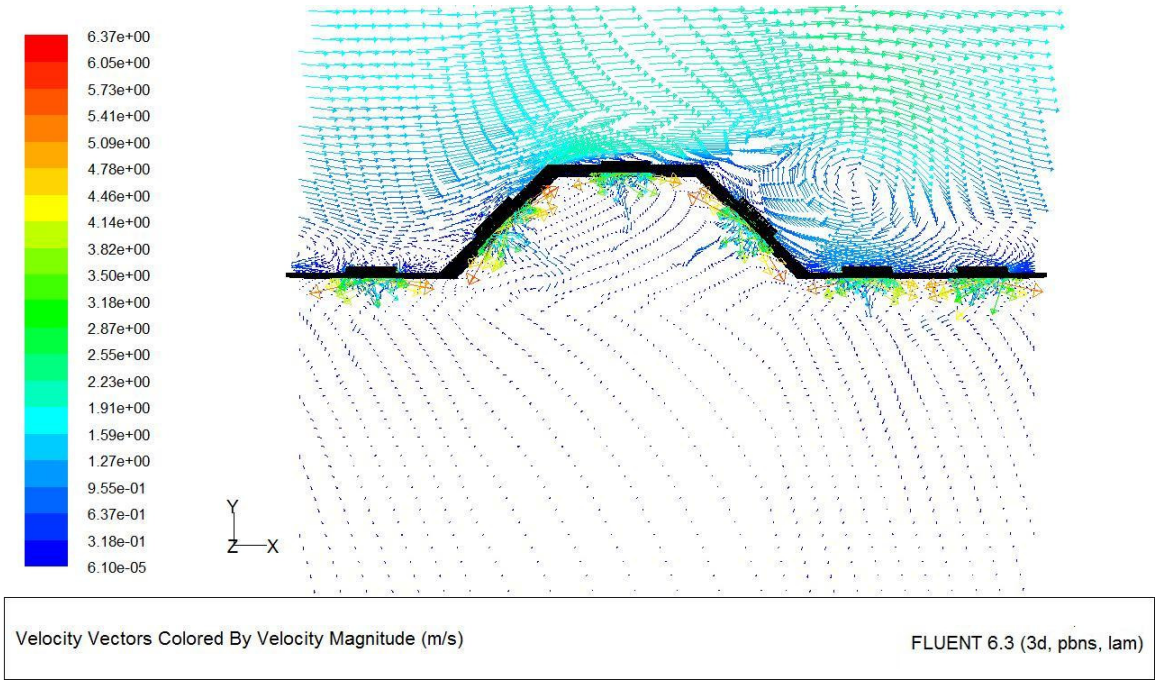

Figure B.46: Velocity Vectors at a Wind Speed of 2.0 m/s and Suction Velocity of 0.04 m/s.

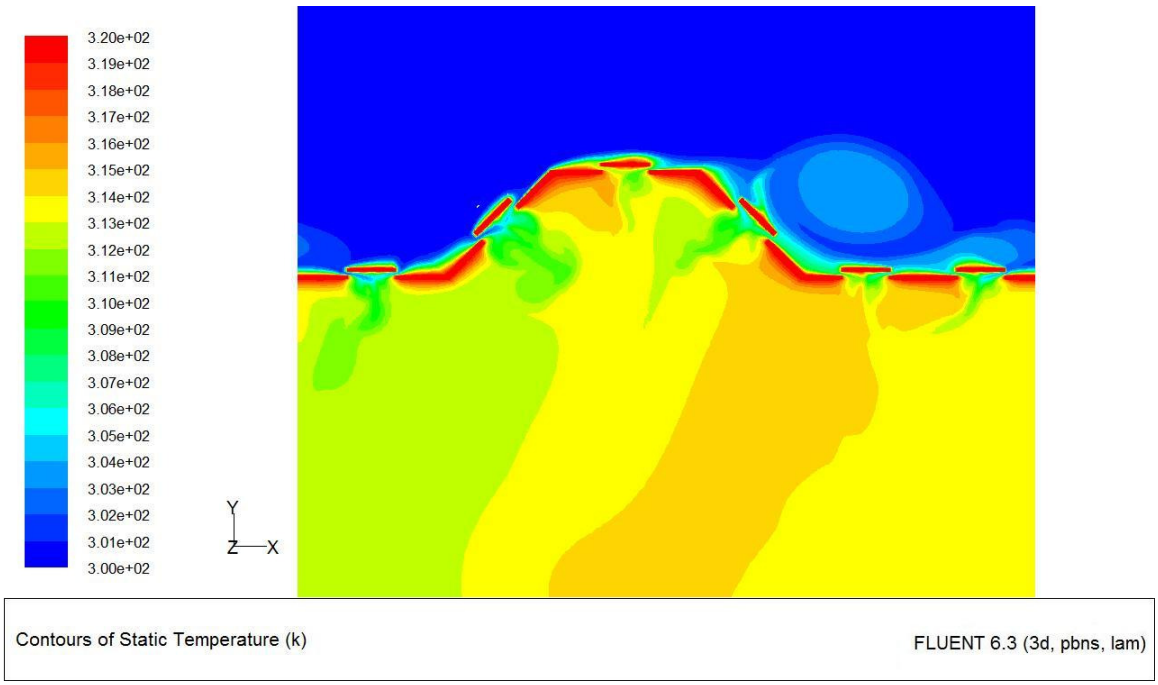

Figure B.47: Temperature Contours at a Wind Speed of 2.0 m/s and Suction Velocity of 0.04 m/s.